The Possible Role of the Petroleum System in the Metallogenesis of Gold in Meguma Metaturbidites: Geochemical Investigation in the Touquoy Deposit, Moose River, Nova Scotia

Ian Borg

Supervisor: Dr. Marcos Zentilli

2014-03-17

Thesis submitted as partial fulfilment for the degree of BSc (Honours)

Department of Earth Sciences, Dalhousie University.

Halifax, Nova Scotia, B3H 4R2, Canada

Distribution License

DalSpace requires agreement to this non-exclusive distribution license before your item can appear on DalSpace.

NON-EXCLUSIVE DISTRIBUTION LICENSE

You (the author(s) or copyright owner) grant to Dalhousie University the non-exclusive right to reproduce and distribute your submission worldwide in any medium.

You agree that Dalhousie University may, without changing the content, reformat the submission for the purpose of preservation.

You also agree that Dalhousie University may keep more than one copy of this submission for purposes of security, back-up and preservation.

You agree that the submission is your original work, and that you have the right to grant the rights contained in this license. You also agree that your submission does not, to the best of your knowledge, infringe upon anyone's copyright.

If the submission contains material for which you do not hold copyright, you agree that you have obtained the unrestricted permission of the copyright owner to grant Dalhousie University the rights required by this license, and that such third-party owned material is clearly identified and acknowledged within the text or content of the submission.

If the submission is based upon work that has been sponsored or supported by an agency or organization other than Dalhousie University, you assert that you have fulfilled any right of review or other obligations required by such contract or agreement.

Dalhousie University will clearly identify your name(s) as the author(s) or owner(s) of the submission, and will not make any alteration to the content of the files that you have submitted.

If you have questions regarding this license please contact the repository manager at dalspace@dal.ca.

Grant the distribution license by signing and dating below.

_____   _____

Name of signatory   Date

Department of Earth Sciences
Halifax, Nova Scotia
(902) 494-2358
Fax (902) 494-6889

DATE: April 27th, 2013

AUTHOR: Ian Borg

TITLE: The Possible Role of the Petroleum System in the Metallogenesis of Gold in
           Meguma Metaturbidites: Geochemical Investigation in the Touquoy Deposit,
           Moose River, Nova Scotia

Degree: B.Sc. Hons.   Convocation: May   Year: 2014

Table of contents

List of Figures

Chapter 6: Discussion & Conclusions

Abstract

The Possible Role of the Petroleum System in the Metallogenesis of Gold in Meguma Metaturbidites: Geochemical Investigation in the Touquoy Deposit, Moose River, Nova Scotia

Metaturbidite-hosted orogenic gold deposits of the Meguma Supergroup, in Nova Scotia, Canada, are currently being developed as the increase in metal prices makes formerly uneconomic, bulk-minable, disseminated prospects such as the Touquoy deposit more feasible. Recent research suggests that there may be relationships between mineralization and organic carbon in certain regions. The purpose of this study is to explore the relationship between organic carbon and metal deposits in a prominent example of orogenic-type gold in Nova Scotia.

For this study, 11 core samples and 12 ground pulp samples selected from the ore zone of the Touquoy deposit for further analysis. Procedures include geochemical analysis, spot analysis with an electron microprobe, and reflected light microscopy. The literature surrounding organic carbon and metal deposits was also explored, and the findings were applied to the Touquoy deposit. Finally, the data set from this study was combined with two others to supplement the findings, and for the purposes of comparison.

The geochemistry of the Touquoy samples, in addition to samples from other data sets, show that there is a positive correlation between gold and carbon at the deposit scale, but a negative correlation at the metre scale. Additionally there is a weak positive correlation between arsenic and carbon. Other results support a previous interpretation that sericite alteration is the main hydrothermal alteration product.

The data suggest that Meguma sediments were deposited off an Andean-type arc setting, rather than a passive margin as previously suggested. Additionally, there is also between one and two orders of magnitude more carbon in mineralized zones, than in barren Goldenville rocks. The presence of monoclinic pyrrhotite within the deposit, in addition to gold's close spatial association with arsenopyrite suggests there is a relationship between the two sulfides and warrants further study.

In conclusion, though sample size, and use of homogenized pulp samples prevented a clear relationship with carbon being laid out, the data of this study support the proposal of an ore deposit model which includes the interaction with organic carbon in the form of petroleum.

Keywords: organic carbon, gold, meguma, orogenic, arsenopyrite, petroleum

Acknowledgements

CHAPTER 1: INTRODUCTION

1.1 Statement of Purpose

Nova Scotia has a variety of ore occurrences, ranging from the large East Kemptville tin deposit of southwest Nova Scotia, to small uneconomic showings throughout the province. These deposits have been exploited since the arrival of the first Europeans, and have produced ores and industrial minerals ever since. Depending on the economic climate, some ores have become too expensive to extract, but the deposits remain as mining prospects until the price of raw materials rises again. The best examples of this dependence are the "orogenic-type" gold deposits (also called syn-orogenic, turbidite-hosted, or mesothermal gold deposits; e.g. Groves et al., 1998) of southern Nova Scotia, which have been mined on and off for more than 150 years, and are currently the focus of active development due to increased metal prices. Typically, past exploitation was focused on narrow gold-bearing veins, which were mined underground with labour intensive methods. Recently, economic feasibility relies on bulk surface mining of lower grade, disseminated deposits, in addition to stricter compliance with more environmental restrictions than the past.

In recent decades the field of geochemistry has advanced significantly, particularly where organic components are involved, as in the field of biogeochemistry (e.g. Southam and Saunders, 2005), which is advancing rapidly as technology increases. With such advances, more thorough studies of the isotopic components of ore deposits have become more common-place. Many of the larger economic deposits of lead, zinc and gold in Nova Scotia are known to have a spatial association with organic carbon in one of its many forms (e.g. Kontak, 1995; Kontak and Kerrich, 1995; Fallara et al., 1998).

Recent research suggests that organic carbon could play a more active and significant role in ore genesis than previously thought, either directly or indirectly by contributing reservoirs of sulfur, such as in some Andean manto-type copper deposits (e.g. Wilson and Zentilli, 1999; Carrillo-Rousa et al., 2013) which were traditionally exclusively linked with igneous processes. Many authors recommend further research to determine the degree of connection of organic matter and its potential value in exploration (e.g. Coveney and Pasava, 2004).

The aim of this thesis was to explore the literature and investigate, through geochemical means, whether there could be a causal relationship, either direct or indirect, between organic carbon and the concentration of gold in a prominent example of an orogenic-type, disseminated gold deposit in Nova Scotia.

1.2 Study Area

The focus of the study is the Touquoy gold deposit in Moose River, southeastern Nova Scotia, shown in Fig. 1.1, currently being developed by Atlantic Gold NL. The Touquoy area was selected because it is one of the most significant gold deposits amenable to bulk surface mining methods, and it is known to be spatially related with black (carbon rich) argillites (e.g. Bierlein and Smith, 2003).

The province of Nova Scotia is broadly divided into two regions; the Meguma Terrane of the southern part of the province and the Avalon Terrane in the northern part as shown in the inset map of Fig. 1.1. The two terranes are separated by the Cobequid-Chedabucto fault zone, which trends east-west across the province (e.g. White, 2010).

The Avalon Terrane in mainland Nova Scotia consists of Ordovician to Lower Devonian rocks, which rest unconformably on Neoproterozoic and Cambrian rocks (Murphy and Keppie,

2005). In the Avalon Terrane, Ordovician consists of volcanic rocks with interbedded red sediments that are disconformably overlain by approximately 1800 m of a continuous sedimentary sequence which varies from shallow marine to continental rocks.
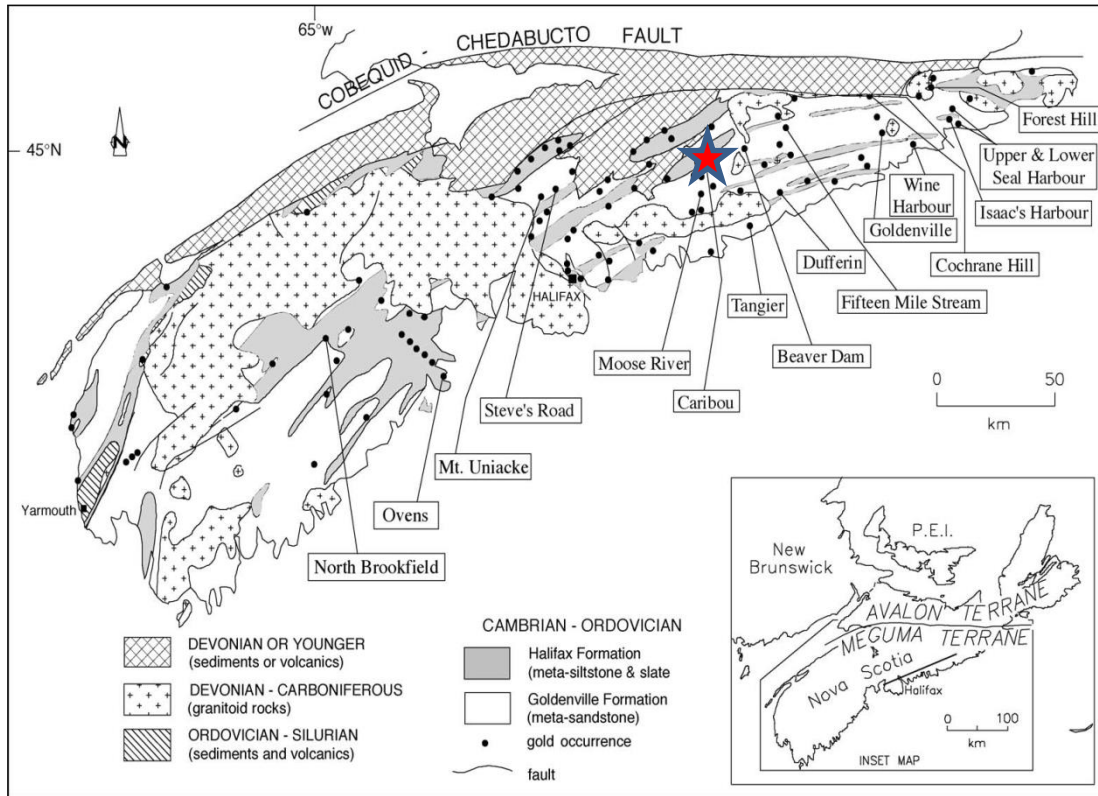
Figure 1.1: A simplified geologic map of southern Nova Scotia showing selected gold deposits. The red star is the location of the Touquoy deposit. The relationship between the Meguma and Avalon Terranes is shown in the inset map. From Ryan and Smith (1998).

Beginning in the Middle Devonian, interbedded basalts and continental rocks were laid down, which has been interpreted as the result of the Acadian Orogeny (Murphy and Keppie, 2005).

3

The Meguma Terrane of southern Nova Scotia consists of the overarching Meguma Supergroup which contains the Goldenville Group, which is dominated by metasandstones, and the overlying Halifax Group, which is composed primarily of slate (e.g. White, 2010). Volcanic rocks are present in overlying Silurian (White Rock) strata. These units were then intruded by the granitic South Mountain Batholith which is Devonian in age (e.g. Reynolds et al., 2004).). The Goldenville Group has been dated to at least Early-Cambrian; as the basement is not exposed, the lower most strata could be older (Waldron et al., 2009). The youngest units of the Halifax Group have been dated to approximately Lower Devonian (Schenk, 1997).

1.3 Previous Knowledge

Work within the 60 known Nova Scotia gold districts has been ongoing since the initial discovery of bedrock-hosted gold by Captain C. L'Estrange in 1858 during a moose-hunting trip along the Tangier River (Sangster and Smith, 2007). After the initial discovery, Canada's first gold rush led to the discovery of many more gold occurrences throughout the province. The relationship between anticline or dome structures has been noted by many authors since the 19th century (e.g. Faribault 1899; Douglas, 1948; Graves and Zentilli, 1982; Henderson et al., 1986; Ryan and Smith; 1998). With recent advances in geochemistry, many authors are taking a closer look at how organics are involved in the genesis of ore deposits. Traditionally, organic carbon was not thought to be important in these processes, but recent advances show that not only do organic molecules interact significantly with metals (e.g. Zentilli et al., 1997; Coveney and Pasava, 2004), but that organisms such as bacteria (Amend and Teske, 2005) also interact with metals in previously unidentified ways. Large et al. (2011) have put forth a model that suggests a close relationship between organic carbon in Carlin-type and, more relevant to this thesis, orogenic-type gold deposits.

In a review of some of the world's largest metal deposits, Coveney and Pasava (2004) have noted the spatial association between organic matter, such as hydrocarbons, and the deposits themselves as shown in Fig. 1.2. Though liquid petroleum is not present within Meguma gold deposits (the greenschist facies metamorphism would determine that carbon remains in the form of graphite or pyrobitumen), their anticline and dome structures can be interpreted as sites of former hydrocarbon reservoirs.

Figure 1.2: The locations of major metal deposits which are associated with organic matter. From Coveney and Pasava, 2004.

This is supported by the fact that more than 90% of gold deposits in the Meguma Terrane are located in the hinges of anticlines; in contrast, synclinal structures with similar lithologies lack any gold in economic quantities. Additionally, the isotopic signature of carbon found in calcite and ankerite, in sampled veins from the Moose River area, is very light (e.g. Kontack and Kerrich, 1997), which suggests a biogenic origin. Finally, in their detailed study of the Touquoy

deposit in the Moose River gold district, Bierlein and Smith (2003) found a strong correlation between gold mineralization and ankerite, whose carbon isotopes have an organic petroleum signature.

1.4 Project Objectives

The objectives of this study are to investigate, on the basis of a literature review and a geochemical and mineralogical study of the Touquoy deposit, whether and how organic carbon could have been involved in the processes responsible for its genesis.

Some questions to tackle are:

1. Are there carbon species associated with gold at Touquoy and how are they distributed and related to gold and other phases?

2. What does the literature say about gold transport and precipitation with regards to the stability of organic matter, and does this knowledge apply to Touquoy?

3. Does the fact that mineralized black (carbon rich) argillites at Touquoy, shown as an anomaly in aeromagnetic maps, have implications for genesis, exploration and environmental effects? Is the pyrrhotite in the Touquoy deposit responsible for this magnetic anomaly?

4. Can the geochemistry of metasedimentary rocks of the host Meguma Supergroup help in ascertaining the possible source of gold in the dozens of gold districts, or should one look for a source in granitoids on the sub-Meguma basement?

5. Is there a genetic model for Touquoy gold that is compatible with the current opinions in the literature, and with the data gathered in this thesis?

1.5 Methods, Approach and Limitations

This project was started in September 2013 extending a preliminary literature review carried out during summer employment with the Nova Scotia Department of Natural Resources. Sampling of the Touquoy deposit was carried out November 29th. Pulp samples from equivalent segments in the sampled drill core were sent for analysis at ACTLABS, and the analytical results were received on January 2nd. Rock samples were sectioned and prepared for petrographic study and polished thin sections were received from the Thin Section Lab at the Department of Earth Science on January 24th. Six of the polished thin sections were carbon coated, and analyzed in the electron microprobe on March 4th, and the analytical results were received on March 5th. NOTE: An additional microprobe session scheduled for March 14th (days before the submission deadline) was cancelled due to reasons out of the author's control.

The restricted number of samples studied, and the fact they all came from a rich ore zone within the Touquoy deposit precluded coming to any far reaching conclusions, but comparisons with relevant databases by other authors increase the usefulness of this project.

1.6 Format of Thesis

The thesis begins with Chapter 1 which introduces the topic to be studied and the rationale behind why it is important. Chapter 2 focuses on the background geology of the region and the geology of the Touquoy deposit. Chapter 4 discusses the methods used for selecting, examining and analyzing samples. Chapter 5 is an overview of the results obtained from the geochemical analysis, petrographic descriptions, and microprobe analysis. Chapter 6 is a discussion of the results and a discussion of the findings and finally presents conclusions of the study along with recommendations for future work.

CHAPTER 2: STRATIGRAPHY OF TOUQUOY WITHIN THE MEGUMA TERRANE

2.1 General Statement

The Meguma Terrane, in terms of what is relevant for this thesis, is the fault bounded domain south of the Cobequid-Chedabucto fault zone, (Fig. 1.1) is comprised of the Meguma Supergroup with metamorphic rocks as young as Emsian (Lower Devonian) and the Devonian South Mountain Batholith. The rocks deposited after the Acadian Orogeny, which include Devono-Carboniferous to Jurassic formations, are not discussed here, except for structural features that affected the gold deposits after their genesis.

2.2 Goldenville Group

The literature on the Meguma stratigraphy is vast and complex; for simplification this chapter draws heavily on the latest review by White (2010) as simplified in Fig 2.1. The Goldenville Group consists of the Bloomfield and Church Point formations in the northwestern part of the Meguma Terrane; the Moshers Island, Government Point, Green Harbour, and Moses Lake formations in the southeastern part (White, 2010), and the Moose River (host of the Touquoy deposit), Tangier, Taylors Head, and Beaverbank formations in the northeastern part (Horne and Pelly, 2007). Beginning in the northwestern part, the basal unit is the Church Point Formation, which consists of grey, medium- to thick-bedded metasandstone and green, cleaved metasiltstone, with rare black slate (White, 2010). Overlying the Church Point Formation in the Bloomfield Formation; it is dominated by green and maroon, thin- to medium-bedded metasiltsone, and is between 200 m and 400 m thick, increasing in thickness to 1000 m in the northwestern limb of the Black Point anticline (White, 2010).
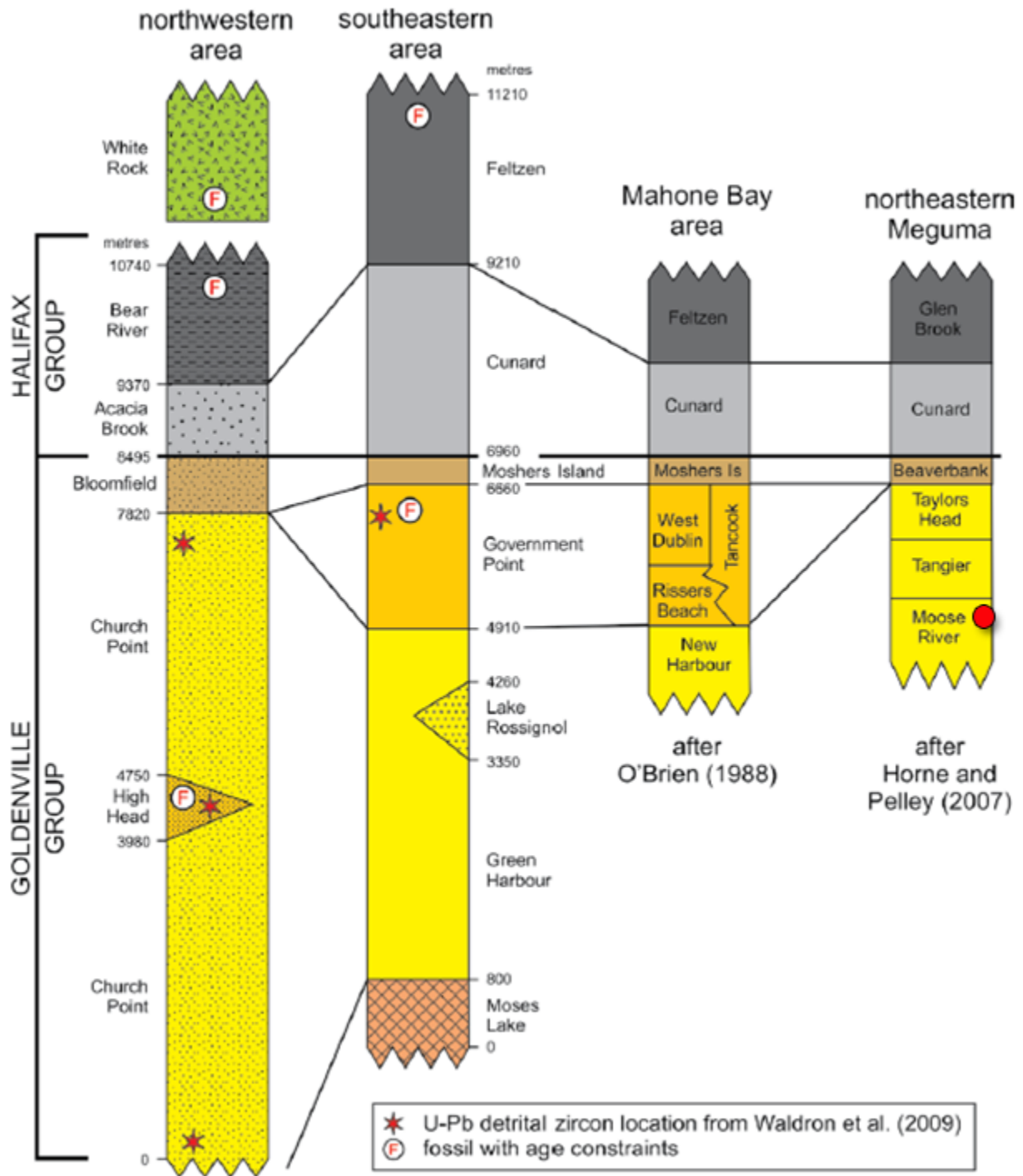
Figure 2.1: Stratigraphy of the Meguma, compiled by White (2010). The red circle is the stratigraphic location of the Touquoy deposit.

In the southeastern part, the basal unit is the Moses Lake Formation, which consists of predominantly grey, thin- to medium-bedded metamorphosed sandstone, with minor layers of green metasiltstone. Structures are common in the formation, with many examples of cross-lamination, ripple marks, and graded bedding (White, 2010). Overlying the Moses Lake Formation in the Green Harbour Formation; it is dominated by thick-bedded, grey, medium-grained metamorphosed sandstone (White, 2010). Above, in the Government Point Formation, this comprises a combination of thin-and thick-bedded grey metasandstone, green and grey-green metasiltstone, and black slate (White, 2010). In certain areas where the metamorphic grade is high, sediments contain andalusite, garnet and sillimanite (White, 2010).

Finally, the uppermost formation in the southeastern part is the Moshers Island Formation. The Moshers Island Formation consists of green, greenish-grey, and grey-purple metasiltstone and slate with minor beds of metasandstone; a characteristic feature of this formation is the presence of steel-blue manganese-rich nodules (White, 2010).

Within the Goldenville of the northeastern Meguma, which contains the study area, the basal unit is the Moose River Formation, which comprises thick layers of green and dark grey slate and metasiltstone, with some disseminated sulfides including pyrrhotite (Horne and Pelly, 2007). The Moose River Formation is overlain by the Tangier Formation, which is composed of sequences of metasandstone-dominated cycles (Horne and Pelly, 2007), but due to the lack of outcrop exposure, further study is needed to determine the differences between it and the overlying Taylor Hear Formation. The Taylor Head Formation is dominated by metasandstone and metasiltstone cycles, which include local fin-grained conglomerate, sand volcanoes, and planar lamination (Horne and Pelly, 2007). The uppermost unit of the Goldenville in the

northeastern part of the Meguma is the Beaverbank Formation. The formation consists of grey to green, thinly bedded metasiltstone and slate (Horne and Pelly, 2007).

2.2.1 Touquoy Zone

The Touquoy deposit is found in the Moose River gold district and is centered on the regional Moose River – Fifteen Mile stream anticline (Fig. 2.2), which is dominated by the fine-grained metamorphosed siltstone and mudstone of the Moose River Formation (Horne and Pelly, 2007), in addition to minor amounts of metagreywacke and sandy metasiltstone (Bierlein and Smith, 2003). The Touquoy ore-body is located in the Touquoy argillite (Horne and Pelly, 2007) of the Moose River Formation. The area has been subjected to low-grade metamorphism in the greenschist facies (Bierlein and Smith, 2003). Regional structures and stratigraphic units are also visible in aeromagnetic maps prepared by King (2000) as in Fig. 2.3.
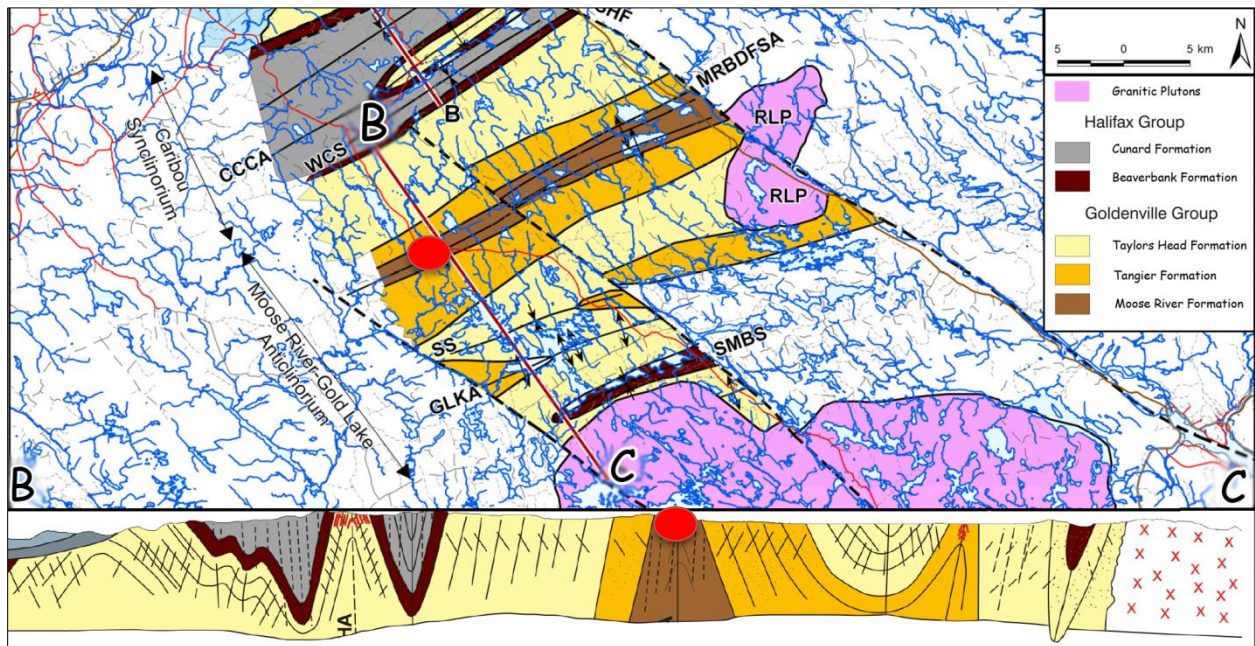
Figure 2.2: Plan view and cross-section of the structure of southeast Nova Scotia. Touquoy deposit represented as a red circle. SHF = Sheet Harbor Fault, CCCA = Caribou-Cameron Dam-Cochrane Hill Anticline, WCS = Wyses Corner Syncline, MRBDFSA = Moose River-Beaver

Dam–Fifteen Mile Stream Anticline, RLP = River Lake Pluton, SS = South Syncline, GLKA =
Gold Lake–Killag Anticline, and SMBS = St. Mary's Bay Syncline. Modified from Horne and
Pelly (2006).
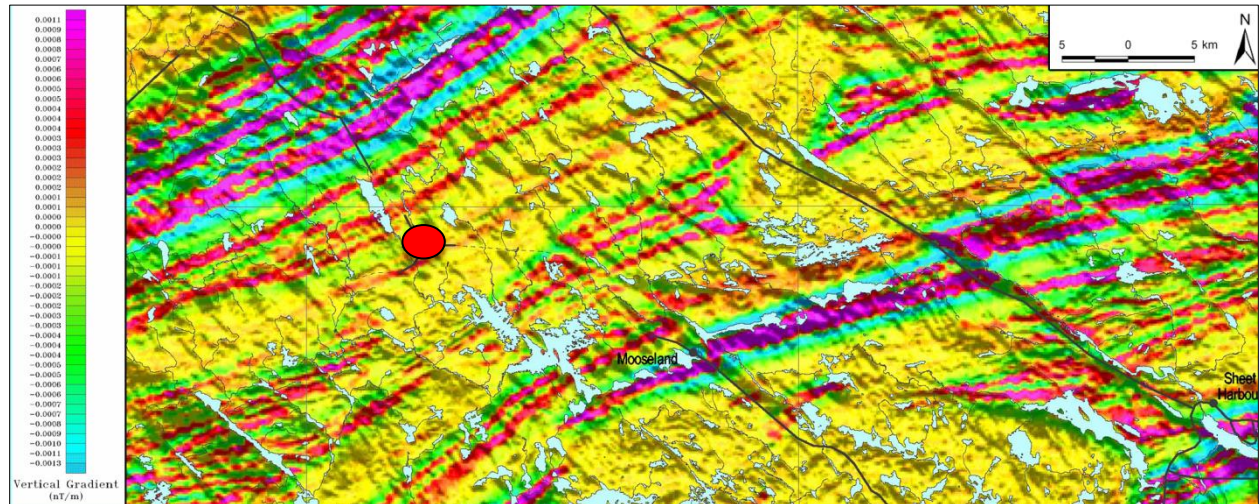
Figure 2.3: Regional aeromagnetic map of the Moose River region. From King, 2000. The red
circle indicates the location of the Touquoy deposit.

The deposit itself is situated on a secondary upright anticline on the south limb of the
regional anticline (Bierlein and Smith, 2003). Traditionally, gold mining from this district has
been concentrated on the bedding-concordant quartz veins; in 1987, Seabright Exploration
discovered disseminated gold, as shown in Fig. 2.4, in the argillite adjacent to the quartz veins
(Ryan and Smith, 1998).
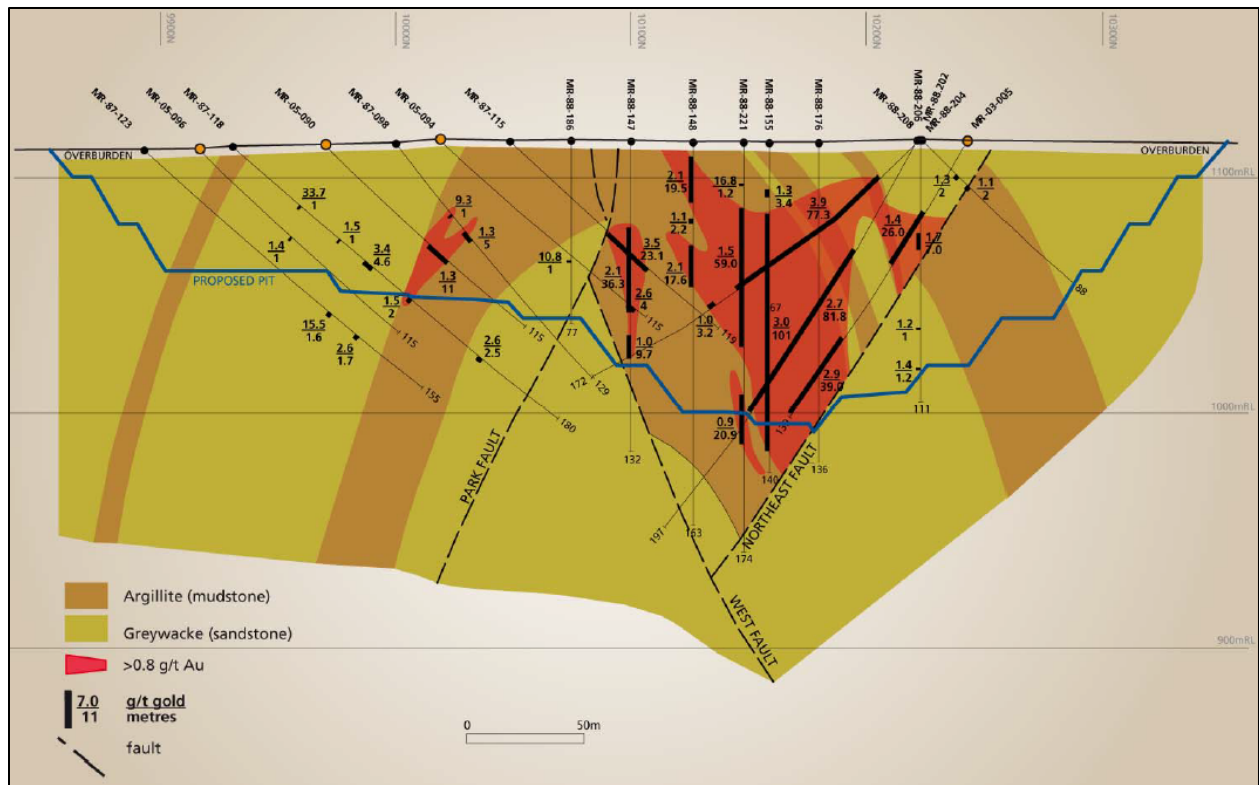
Figure 2.4: Cross section of the Touquoy deposit showing the shape of the disseminated ore body. From Bucknell (2014).

2.3 Halifax Group

The Halifax Group comprises a variety of different formations throughout the terrane and though they may fit into similar positions stratigraphically, they have been labelled with different names due to differences in composition (White, 2010). Many formations however, contain Bouma sequences, leading to an interpretation that the Halifax Group was formed in a deep marine environment (Stow et al., 1984). The basal unit throughout the eastern portion of the Meguma is the Cunard Formation. The Cunard consists of black or rusted slate with minor black metasiltstone and metasandstone beds. Locally, the formation contains ample sulfides such as arsenopyrite, and pyrrhotite (White, 2010). In the northwestern part of the Meguma, the basal unit of the Halifax Group is the Acacia Brook Formation. The formation is predominantly grey

and dark grey slate, with only minor metasiltstone and metasandstone (White, 2010). Similar to the Cunard Formation, the Acacia Brook Formation is abundant in sulfides locally, including pyrrhotite, pyrite and arsenopyrite (White, 2010). Both the Cunard and Acacia Brook formations have been interpreted by White (2010) as being formed by turbidites.

In the northeastern part of the Meguma, the Glen Brook Formation overlies the Cunard Formation, but the contact is not visible (Horne and Pelly, 2007). The Glen Brook consists of green to grey metamorphosed silt- and sandstone, which is laminated and cross-laminated. The formation generally lacks sulfides and has a weak aeromagnetic response when compared to the underlying Cunard Formation (Horne and Pelly, 2007). The Feltzen Formation overlies the Cunard Formation in the southeast part of the Meguma. It is composed of light- blue-grey slate, with interbedded metasandstone (White, 2010). The Feltzen Formation is also noted for the abundance of trace fossils (O'Brien, 1988). Finally, the Bear River Formation overlies the Acacia Brook Formation in the northwestern portion of the Meguma. The Bear River Formation consists of light- and dark-grey, laminated metasiltstones (White, 2010).

2.4 Post-Halifax Group

Formations overlying the Halifax Group until the Emsian have been summarized below. Most information has been taken from the review by Keppie (2000) unless otherwise noted. The White Rock Formation of western Nova Scotia, as shown in Fig. 2.5, predominantly contains intra-plate alkali mafic volcanics, some intermediate and felsic volcanics, interbedded with silicic and tuffaceous sediments, all which have been metamorphosed to amphibolite facies (MacDonald et al., 2002). The formation is in faulted contact with the Halifax Group; however the White Rock is dated to the Silurian, while the youngest part of the Halifax Group is Early Ordovician (MacDonald et al., 2002).

Overlying the White Rock Formation is the Kentville Formation, which is interpreted to be a shallow marine depositional environment. The succession includes shallow marine slate, silty slate, siltstone and limestone.

The New Canaan Formation overlies the Kentville Formation. It has been interpreted as a shallow marine depositional environment, and includes shallow marine breccia, siltstone, slate, limestone and volcanics.

Finally, the Torbrook Formation overlies the New Canaan Formation, and contains shallow marine mudstone, shale, siltstone, iron formation and minor limestone.

2.5 Acadian Orogeny

The Acadian Orogeny was the large mountain-building event which occurred during the Devonian. The effects of the orogeny have been noted along eastern North America from Pennsylvania to Newfoundland (Murphy and Keppie, 2010) and notably through the study area of this thesis. Deformation in the Meguma began at approximately 415 Ma and continued into the Late Devonian, leading to greenschist- and local amphibolite-facies metamorphism (Murphy and Keppie, 2010). The resultant regional structures are northeast-trending, shallowly plunging, periclinal folds (Murphy and Keppie, 2010). Magmatism followed deformation between approximately 380-370 Ma as the granitoid South Mountain Batholith intruded. However, some authors have suggested that Acadian deformation didn't cease immediately, as structural evidence suggests the South Mountain batholith was deformed (e.g. Benn et al., 1999). Murphy and Keppie (2010) have also suggested that due to the similar Paleozoic history between the Avalon and Meguma terranes, the terranes were accreted before the Acadian orogeny, suggesting an Andean- or Cordilleran-type setting. However, the theory is contested by others (e.g. Waldron

et al., 2009) who state that the Meguma and Avalon terranes were separate prior to the Acadian orogeny.

2.5.1 South Mountain Batholith

The South Mountain Batholith is a large granitic intrusion which is emplaced throughout the central part of the Meguma Terrane. The intrusion has been dated to 380Ma, and several authors have suggested, based on structural evidence, that it was emplaced during the Acadian Orogeny (e.g. Clarke et al., 2009). The South Mountain Batholith is predominantly granodiorite, monzogranite, leucomonzogranite and leucogranite; during emplacement studies have shown that a large amount of contamination from wall-rock assimilation has occurred, leading to zones rich in garnet, cordierite or biotite (e.g. Erdmann et al., 2009). The South Mountain Batholith is important to this study, as previous authors (e.g. Emmons, 1937; Kontak et al., 1990) have suggested that its emplacement is directly linked to gold mineralization.

2.5.2 Liscomb Complex

The Liscomb Complex is an area in central Nova Scotia, as shown in Fig. 2.5, which many authors have proposed was composed of gneiss and schist derived from the basement rocks of the Meguma (e.g. Clarke et al., 1993; Dostal et al., 2006). The model that was proposed was that the Liscomb Complex is a core complex. The complex was thought to have formed when extension began in the Middle to Late Devonian, leading to pull-apart tectonics along the Cobequid-Chedabucto fault zone, allowing for the rapid ascent of the so-called Liscomb gneiss diapir (Dostal et al., 2006). However, recent studies by White et al. (2009) do not support the hypothesis that the complex is Meguma basement, but rather suggest
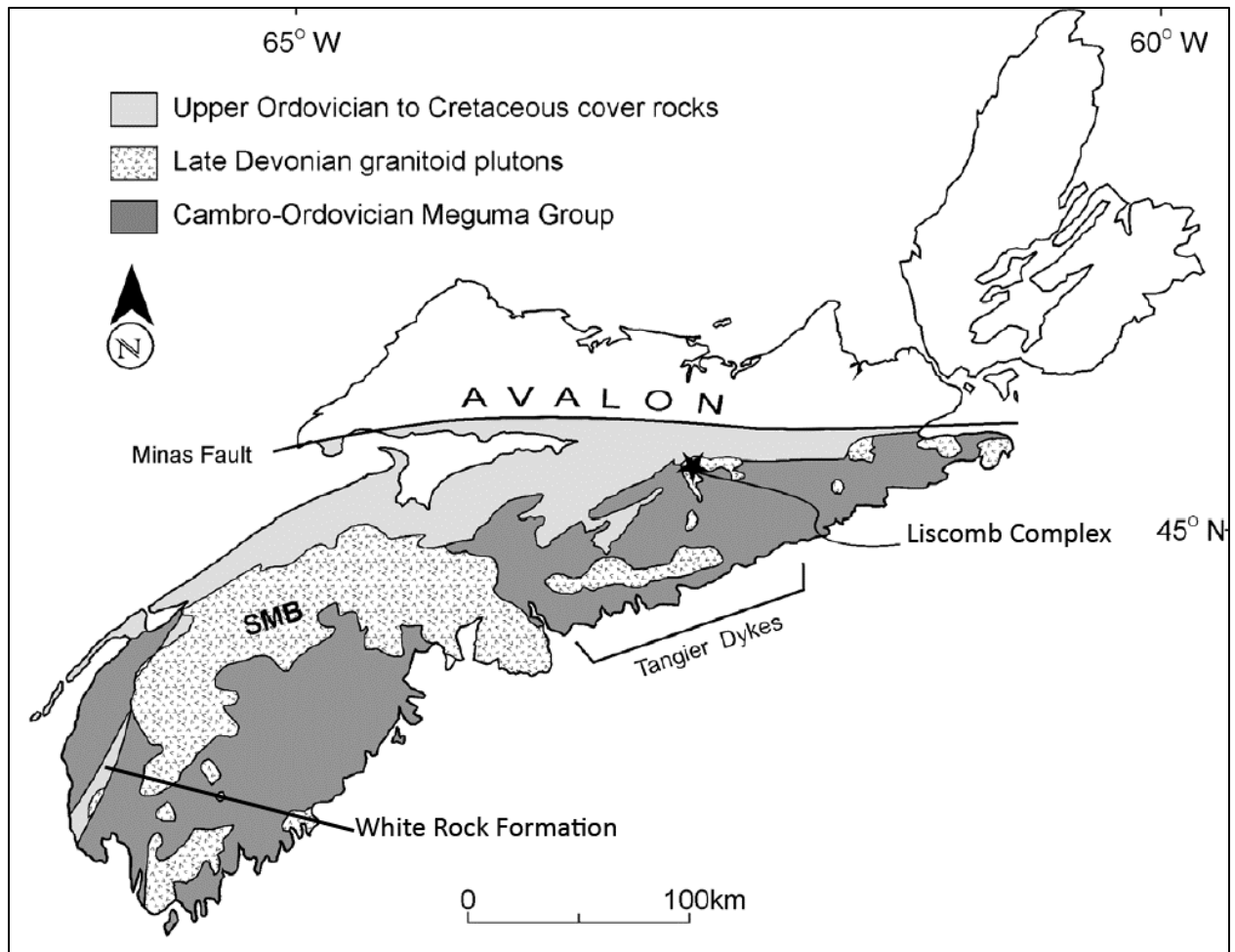
Figure 2.5: Geologic map showing the location of the Liscomb Complex and the White Rock Formation. Modified from Dostal et al., 2006.

that previously identified metamorphic textures are actually superimposed protomylonitic fabric or possibly textures from magma mixing. The latest work suggests that the Liscomb metamorphic suite could in fact represent sub-Meguma basement (Owen et al., 2010).

CHAPTER 3: DEPOSIT FORMATION

3.1 Touquoy Deposit

The Touquoy deposit has been described by Bierlein and Smith (2003) and their study has been heavily drawn from in the following summary. The main deposit is located in a secondary-order, northeast trending, and upright anticline within the regional Moose River Anticline. The deposit has been disrupted by late faulting, which occurred post-folding. The faults, generally trending northeast, northwest or east-west, are steeply dipping with evidence for both normal and reverse fault movements. The faults closest to the mineralized zone have been suggested to have played an important role in controlling the location of mineralization (Bierlein and Smith, 2003); nevertheless, recent drilling indicates the faults themselves are not mineralized and may well be post-ore. Mineralization in the deposit is not associated with any substantial bedding-parallel quartz veins in excess of 10 cm, unlike other deposits in the Meguma. Within the deposit Bierlein and Smith (2003) found that arsenopyrite and pyrite are the most common sulfides in the deposit, but noted that pyrrhotite, possibly diagenetic, also constitutes up to 2-3% by volume. Gold mineralization appears to be spatially tied to arsenopyrite, as attached grains, or as inclusions or filling in fractures, but gold is also found as discrete grains in metasiltstones or attached to other sulfides (Bierlein and Smith, 2003). Morelli et al. (2005) attempted to date 19 Nova Scotia gold deposits, including Touquoy, by rhenium-osmium geochronology using arsenopyrite, however the data for the Touquoy deposit did not allow for a calculation of a precise age (457 ±110 Ma; Cambrian to Carboniferous).

Rocks within the deposit have undergone various amounts of alteration including sericitisation, carbonitisation, chloritisation and silicification (Ryan and Smith, 1998; Bierlein and Smith, 2003); additionally Bierlein and Smith (2003) noted a strong correlation between the

carbonate alteration in the form of ankerite, and gold mineralization. Finally, through isotopic analysis, Sangster (1992) found that the isotopic composition of both the carbon and sulfur within Meguma veins were most likely organic in origin and is further supported by recent work by Kontak (2014).

3.2 Vein Formation

Multiple theories with varying degrees of support exist in regards to vein and deposit formation within the Meguma. In their review of Meguma gold deposits, Sangster and Smith (2007) summarized the three following theories. In the syngenetic model, vein formation is attributed to processes happening at the same time as sedimentation, such as a hot spring or hydrothermal type system.

Syntectonic theories state that vein and deposit formation occurred either pre- or syn-folding of the Acadian Orogeny and prior to granite emplacement. The vein source materials (and presumably metals) from the surrounding host rocks would be mobilized by prograde metamorphic fluids. During greenschist metamorphism, the change in temperature will cause dehydration of hydrous minerals such as chlorite. The increase in pore pressure due to this additional fluid (lithostatic and higher) can cause fractures to form parallel to the maximum principal stress (e.g. Graves and Zentilli, 1982). When the fracture forms and pressure suddenly decreases, carbonate precipitates first followed by quartz in the newly created space. The newly created veins would then be folded further by the continuing stress. Bedding-parallel veins are predominantly located within shaly beds rather than along contacts because of their inherent lack of permeability, as suggested by Graves and Zentilli (1982), and Windh (1995). The lack of permeability within fine-grained beds will cause pore pressure to be greater during dewatering and metamorphism; fractures would then preferentially form and propagate along these beds.

Other authors suggest that the gold-bearing quartz veins formed late in the Acadian deformation, or in various deformational events, an interpretation that is compatible with recent rhenium-osmium geochronology.

Finally, a later syntectonic model involves direct hydrothermal influences synchronous with the emplacement of the South Mountain Batholith and associated plutons (e.g. Emmons, 1937; Kontak et al., 2001). Metamorphic fluids and materials are suggested to have been mobilized from magmatic, lower-crustal and sedimentary sources, or a combination. Graves and Zentilli (1982) describe xenoliths of quartz arsenopyrite veins within undeformed granite, in the Mount Uniake gold district, suggesting that the batholith must be younger than the deformation and the formation of the gold veins.

3.3 Transport and Deposition

Gold is able to be dissolved into solution by a wide variety of complexes in a lab; however, only two major complexes are thought to readily occur in hydrothermal deposits. Gold may be transported as either a chloride or bisulfide complex depending on the temperature of the fluid and on the composition of the fluid and surrounding rock. Factors such as temperature, oxygen fugacity, pH and mode of precipitation will affect which complex is involved in the deposition of gold. Within hydrothermal deposits which are formed between 200° to 300° C, the main complex thought to be involved is the bisulfide complex. However, at higher temperatures typical of magmatic systems, gold is transported as a chloride complex. Furthermore, gold in a chloride complex is typically soluble in more oxidizing fluids, while bisulfides are stable in more reducing fluids as shown in Fig. 3.1. A third and more enigmatic complex is a thioarsenide complex, which may also transport gold, and the often close spatial relationship between gold

20

and arsenic in the form of arsenopyrite is reason to suspect that gold may be transported by it
(Romberger 1988).
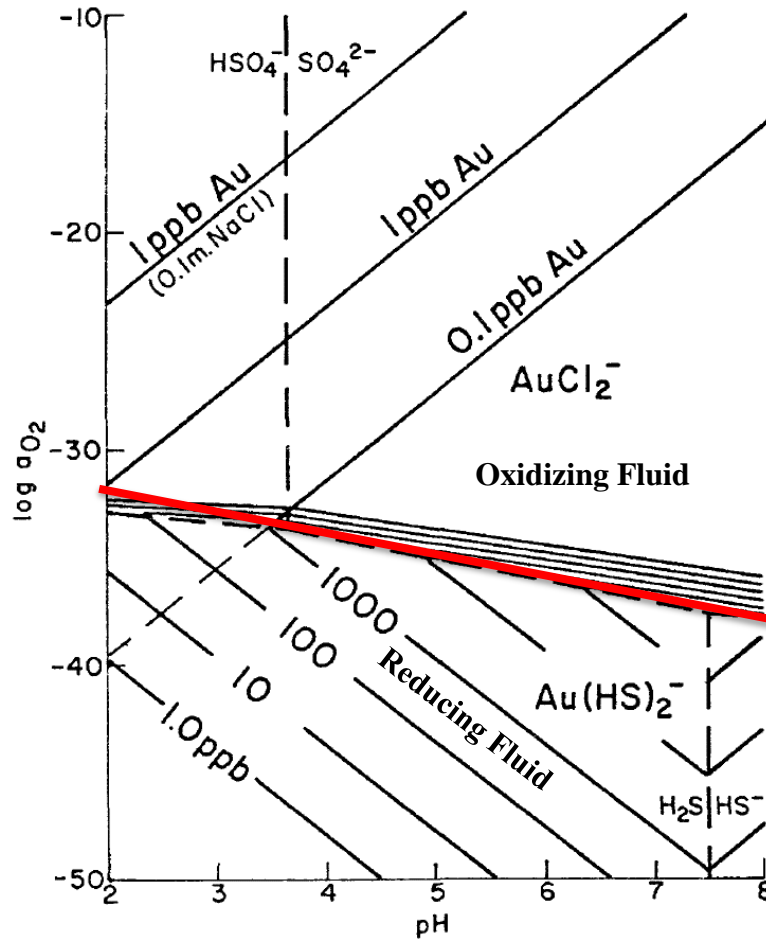
Figure 3.1: Calculated oxygen activity-pH diagram for the Au-NaCl-H_2O system at 250°C
showing the relative solubility's of gold chloride and bisulfide complexes: 1M NaCl and 0.01M
S in aqueous solution. From Romberger (1988).

Gold deposition within the Touquoy deposit is thought by Bierlein and Smith (2003) to
be a low salinity, CO_2-rich fluid at between 250° - 350°C. At these temperatures, gold in
hydrothermal deposits are mainly thought to be dissolved and deposited according to the
following two bisulfide equations from Williams-Jones et al. (2009):

21

1. $Au_s + HS^- + H^+ + 1/4O_2 \leftrightarrow Au(HS)^0 + \frac{1}{2} H_2O$

2. $Au_s + 2HS^- + H^+ + 1/4O_2 \leftrightarrow Au(HS)_2^- + 1/2H_2O$
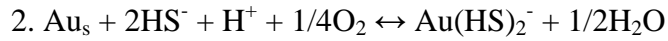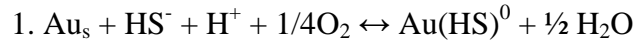
The two preceding bisulfide complexes have temperature stabilities up to 250° and 350°C respectively (Williams-Jones et al., 2009). Once in solution the gold is able to be transported along pressure gradients until the solution meets a barrier which causes the gold complex to break up and the gold to be precipitated.

Gold is deposited from the bisulfide complex through one of many reactions. Of importance to sedimentary hosted orogenic gold deposits are sulfidation (e.g. Bierlein and Smith, 2003) and oxidation (e.g. Large et al., 2011). During sulfidation iron-bearing minerals within the host strata are sulfidized to form minerals such as pyrite.
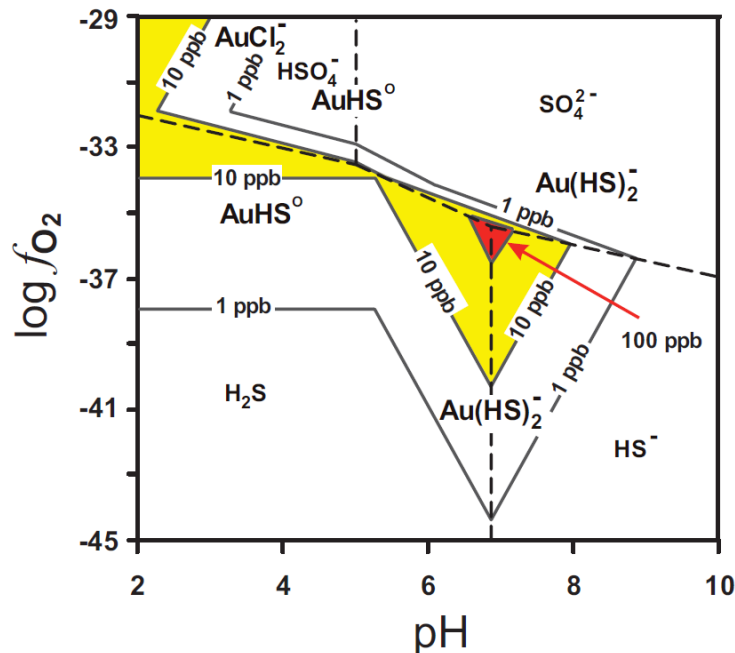
Figure 3.2: Solubility of gold complexes as they relate to oxygen fugacity and pH. From Williams-Jones et al. (2009).

Oxidation occurs when the oxygen fugacity of the solution increases, leading to a significant drop in the solubility of gold as in Fig. 3.2. Breaking of the complex and precipitation of gold can occur when the hydrothermal solution interacts with an oxidizing substance, such as oxygenated meteoric waters, or hematite-bearing source rock (Williams-Jones et al., 2009).

Reduction is the other process which will allow dissolved gold to be precipitated. Gold in an oxidizing fluid will travel as a chloride complex, such as $AuCl_2^-$. In the case of a chloride complex, the solution would need to mix with a reducing fluid in order for the complex to be broken and the gold to precipitate. This process has been suggested as a depositional mechanism in the Hill End deposit of Australia by Windh (1995) who states that deposition may have occurred when deeply derived, oxidised, and gold-bearing fluids containing H_2O-CO_2-CH_4, mixed with fluids which had reached equilibrium with the wall rocks and became reducing. Metamorphism also preferentially releases more oxidising fluids and oxidising fluids are very efficient at the extraction of gold; indeed, some of the largest gold regions such as Kirkland Lake, Ontario have been formed from gold travelling in oxidized fluids (Cameron, 1993). In order for the gold to come out of solution however, the chloride complex it travels in must be broken, buy reducing the gold within it. Petroleum or bitumen could provide the necessary reduction (e.g. Zentilli et al., 1997; Hitzman et al., 2010).

3.4 Petroleum Interactions

Liquid petroleum is known to contain heightened levels of metals, and recently it has been recognized that many gold deposits, from the Witwatersrand basin in South Africa to the Carlin-type deposits in Nevada, contain either bitumen or liquid hydrocarbon inclusions (Williams-Jones and Migdisov, 2006). In experiments conducted by Williams-Jones and

Migdisov (2006), they determined that it was possible to dissolve between 9 to 14 ppm gold into

crude oil at temperatures between 150° to 200°C. Even though this temperature range is below

that of the formation of the Touquoy deposit, and above the ideal oil formation window,

Williams-Jones et al. (2009) state that the presence of liquid hydrocarbon inclusions in black

chimneys and through pyrolysis experiments, petroleum could stand to be heated to around

300°C for a considerable amount of time. Not only could petroleum act as a transport

mechanism, but also as a reductant of oxidizing fluids. In a study of some of the largest copper

deposits in the world, Hitzman et al. (2010) state that the copper was most likely precipitated due

to interactions with in-situ organic matter or hydrocarbons which supports earlier work by

Zentilli et al. (1997) in their study of central Chilean manto-type copper deposits.

CHAPTER 4: METHODS

4.1 Introduction

This study aims to determine if there was an active relationship between gold and organic carbon in the Touquoy deposit, of Moose River, Nova Scotia. Through the use of geochemical analysis, transmitted and reflected light microscopy, and by using the electron microprobe, various theories about the relationship will be tested. Geochemical analysis allows graphing of constituent elements to be graphed to look for correlations, and the data from this study is compared with similar data sets from other authors. Reflected- and transmitted-light microscopy is used to complete petrographic descriptions of each thin section, and allow a visual inspection for any spatial correlations between minerals. Finally, analysis of polished thin sections with Dalhousie University's electron microprobe allow point analysis for specific elements, and for the visual inspection of textures, such as the ejection of gold from a sulfide's structure, which may be too small to see with light microscopy.

4.2 Sampling

Representative samples of drill-core were taken from two separate drill holes, both of which intersected the Touquoy ore zone as shown in Fig. 4.1. Six core samples were taken from drill hole MR-05-081 and five core samples were taken from drill hole MR-05-079, and were selected with the aid of Atlantic Gold NL personnel. Samples were preferentially selected from areas with higher grades of gold mineralization, or the presence of visible sulfides. Samples from drill hole MR-05-081 were taken from a depth between 15.9 m and 56.72 m. Samples from drill hole MR-05-079 were taken from depths between 10.77 m and 40.1 m.

Each sample was on average 0.15 m long; an example is shown in Fig. 4.2. The depths and gold assay values for each sample are listed in Appendix 1 and detailed sample descriptions are listed in Appendix 2.
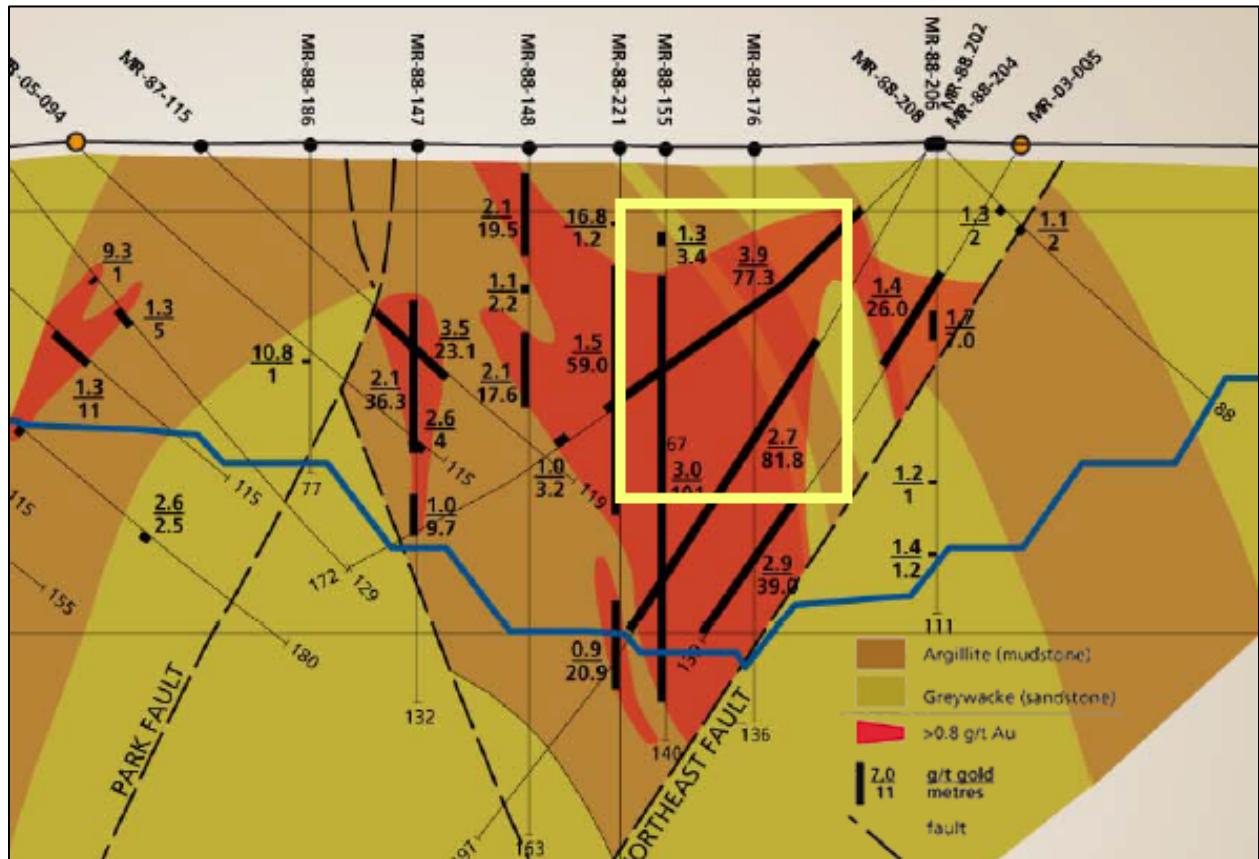
Figure 4.1: The yellow box highlights the area which was sampled in the Touquoy ore zone. Modified from Bucknell (2014).

Atlantic Gold NL has a library of pulp samples from the Touquoy deposit. Pulp samples, or pulps, were meter intervals of drill core which were ground to -200 mesh (74 μm) before portions are sent for assay. 100 g of each pulp specimen, which contained the previously sampled drill core, were taken; in addition to one high-grade pulp sample (MR-12).

Figure 4.3: Core sample MR-04. The photo was taken while the core was dry. Note the large arsenopyrite crystals in the middle of the top edge; gold is visible within those crystals under the electron microprobe. The serpentine veinlet of carbonate indicates buckling representing ~45% shortening perpendicular to incipient foliation.

In total, 12 pulp samples weighing approximately 30 g each were sent to Activation Laboratories at 1348 Sandhill Drive, Ancaster, Ontario, L9G 4V5, Canada for a full geochemical analysis (Raw data in Appendix 3).

The 11 core samples were cut with a diamond-blade rock saw into small blocks, and made into thin sections in the Thin Section lab at Dalhousie University in Halifax, Nova Scotia, resulting in one thin section and one polished section per core sample. Areas with veining or visible sulfides were preferentially selected to be made into slides. Samples with visible sulfides were selected because some genetic hypotheses for orogenic gold suggest that metals, such as gold, could have been scavenged from turbidites and black shales by sulfide minerals, such as pyrite, during their formation (e.g. Gregory et al., 2011). Furthermore, the gold could have been mobilized during prograde metamorphism (e.g. Graves and Zentilli, 1982; Henderson et al., 1991) by oxidized complexes. By looking at the sulfide minerals with reflected light microscopy, and with Dalhousie University's microprobe, textures which indicate exsolution of gold from sulfide mineral structure may be visible.

4.3 Geochemical Analysis

The 12 pulp samples were completely characterized according to Actlabs 4E code, with additional infrared analysis using research grade procedures. The complete analytical results are contained in Appendix 3. The 4E code includes a combination of processes including Instrumentation Neutron Activation Analysis (INAA), Total Digestion - Inductively Coupled Plasma (TD-ICP) and Fusion – Inductively Couples Plasma (FUS-ICP) to analyze for the following elements and compounds: SiO_2, Al_2O_3, Fe_2O_3, MnO, MgO, CaO, Na_2O, K_2O, TiO_2, P_2O_5, Au, As, Ba, Be, Bi, Br, Cd, Co, Cr, Cs, Cu, Hf, Hg, Ir, Mo, Ni, Pb, Rb, Sb, S, Sc, Se, Sr, Ta, Th, U, V, W, Y, Zn, Zr, La, Ce, Nd, Sm, Eu, Tb, Yb, and Lu. Additionally, infrared (IR) analysis was used to determine the amount of carbon and sulfur within the samples. The geochemical characterization of the samples allows different elements and compounds to be compared to determine any correlation, and for comparison with data sets from similar deposits

28

in the region (e.g. Bierlein and Smith, 2003). Due to financial constraints, duplicates were unable to be analyzed to check for reproducibility. In this study, where geochemical results fell below the detection limit, the amount has been rounded down to half of the detection limit for the sake of standardization. Detection limits are listed with results in Appendix 3. All graphs were made using the Actlab's geochemical results, rather than previously obtained assay values.

4.3.1 Instrumentation Neutron Activation Analysis (INAA)

In INAA, the sample is encapsulated before being irradiated at Actlabs nuclear reactor, and the emissions are measured instrumentally. INAA was used to look for Au, Ag, As, Br, Co, Cr, Cs, Hf, Hg, Ir, Rb, Sb, Sc, Se, Ta, Th, U, W, La, Ce, Nd, Sm, Eu, Tb, Yb and Lu.

3.3.2 Total Digestion – Inductively Coupled Plasma (TD-ICP)

In TD-ICP the sample is digested by four acids: hydrochloric, nitric, perchloric and hydrofluoric. The solution is then analyzed using Inductively Coupled Plasma – Optical Emission Spectrometry (ICP-OES). ICP-OES works by analysing the emissions of a sample which is introduced to plasma. By comparing the emission and its intensity, the concentration of trace elements is calculated. TD-ICP was used to look for Ag, Bi, Cd, Cu, Mo, Ni, Pb, S and Zn.

4.3.3 Fusion – Inductively Coupled Plasma (FUS-ICP)

In FUS-ICP the sample is dissolved with a flux, in this case lithium borate, in a platinum crucible at very high temperatures (Delijska et al., 1988). The fused bead is then dissolved in a weak nitric acid solution before being analyzed with ICP-OES. FUS-ICP was used to look for SiO_2, Al_2O_3, Fe_2O_3, MnO, MgO, CaO, Na_2O, K_2O, TiO_2, P_2O_5, Ba, Be, Sr, V, Y and Zr.

4.3.4 Infrared Analysis (IR)

In IR analysis for carbon, a sample is combusted in a pure oxygen environment. During combustion any carbon is liberated, and quickly binds with oxygen forming with CO or CO_2. As the gasses flow through the detector, CO and CO_2 absorb specific IR wavelengths which are measured. Thus, IR analysis for carbon includes carbon contained as carbonate

Similar to analyzing for carbon, when looking for sulfur the sample is combusted in a pure oxygen environment where it becomes reduced and binds to oxygen forming SO_2. As SO_2 passes through the detector it absorbs specific IR wavelengths, which are measured.

4.4 Reflected Light Microscopy

Reflected light microscopy was used to look at polished thin sections from the deposit in order to determine if any specific structures or patterns of mineralization are identifiable. The main texture to look for is gold inclusions within pyrite or arsenopyrite, possibly indicative of gold being allowed into the sulfide's crystal structure. Gold can be allowed into the crystal either as nanoparticles of Au^0 or covalently bonded with an oxidation state between Au^{1-} and Au^{3+} (Pokrovski et al., 2002). When the sulfide crystal undergoes hydrothermal alteration, some of the invisible gold from the rim of the crystal is removed and may form large enough accumulations to be visible (Morey et al., 2008). Framboidal pyrite may also incorporate trace metals, such as gold, in its structure during formation. In the gold deposition model proposed by Large et al. (2007) and supported by Gregory et al. (2011), sediments are deposited in an anoxic environment, which prevents organic breakdown. The organic sediments act as ligands which bind to metals in solution. As the sediments settle, the anoxic environment promotes the formation of pyrite, which leads to the incorporation of many of the metal ions which were

bound to organic sediments. Upon recrystallization due to metamorphism, the trace elements are ejected to be carried away by hydrothermal fluids, or trapped as inclusions. By looking at pyrite crystals, through microscopy and microprobe analysis, ejected gold or other trace metals may be visible.

4.5 Electron Microprobe

The electron microprobe at Dalhousie University, Halifax, Canada is used to take point-analyses from individual sulfide crystals, to look for evidence of increased trace metals near the core of the crystal versus the rim. Microprobe analysis was also used to construct element maps, listed in Appendix 5, of sulfide crystals, to look at the concentration of gold and arsenic within the entire crystal. Additionally, the high magnification of the microprobe was useful for looking for textures or inclusions which were too small to be seen through reflected light microscopy. 88 point analyses were conducted on sulfides including pyrite, chalcopyrite, pyrrhotite and arsenopyrite. Standards were also analyzed at regular intervals and at the beginning and end to check for consistency.

CHAPTER 5: RESULTS

5.1 Geochemistry

The complete geochemical analysis of the Touquoy pulp samples is contained in Appendix 3. Major elements were plotted, along with trace elements, before this data set was compared with the Touquoy dataset from Bierlein and Smith (2003) and the Meguma Supergroup dataset by Graves and Zentilli (1987).

5.1.1 Major Elements

Within the ore zone, there is a strong correlation (Fig. 5.1) between K_2O and Al_2O_3, which is in line with the findings of Bierlein and Smith (2003), who state that the relationship is indicative of alteration to sericite, which is common in sediment-hosted orogenic gold deposits.
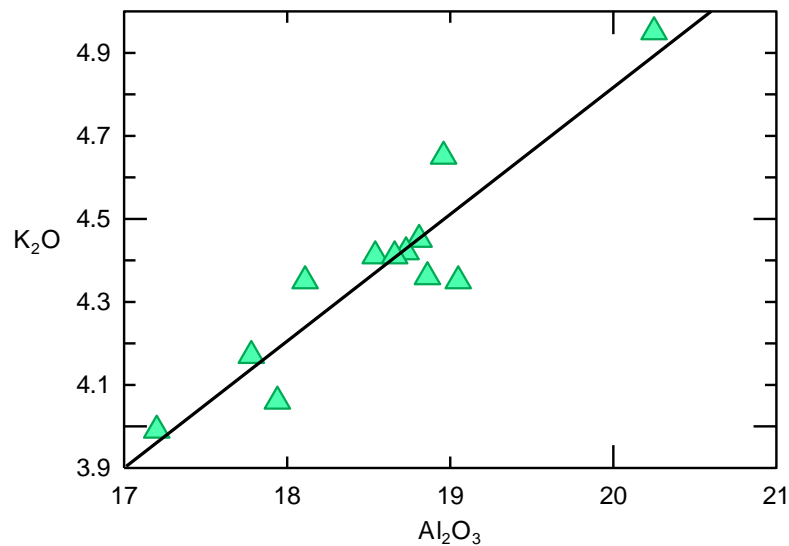
Figure 5.1: The relationship ($R^2 = 0.86$) between K_2O and Al_2O_3 (both in Wt. %) suggests sericite alteration (e.g. Bierlein and Smith, 2003).

There appears to be a negative correlation between arsenic and gold (Fig. 5.2), however, the limited sample size prevents this result from being conclusive.
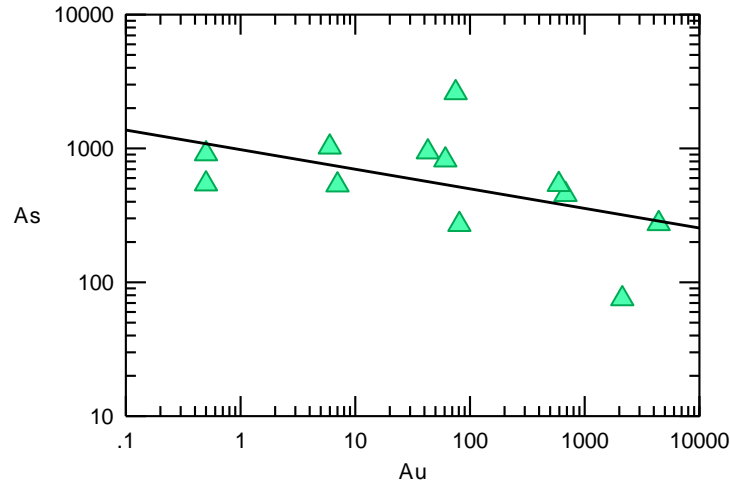
Figure 5.2: An apparent negative correlation ($R^2 = 0.25$) between As (ppm) and Au (ppb).

There is a weak ($R^2 = 0.13$) positive correlation between Au and K_2O/Na_2O (Fig. 5.3). There could be a positive correlation between sericite alteration and gold; however more samples are needed to enhance the reliability of this correlation.
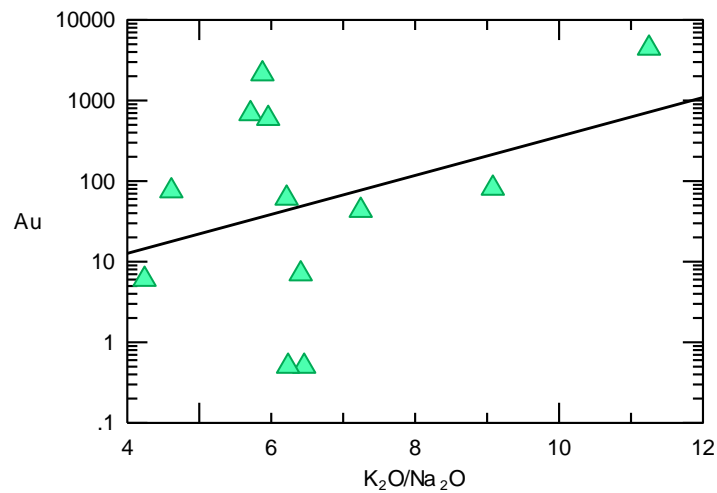
Figure 5.3: Relationship ($R^2 = 0.13$) between K_2O/Na_2O (Wt. %) and Au (ppb).

There is a negative correlation (Fig. 5.4) between total carbon and gold within the Touquoy ore zone. This is in contrast to the deposit scale positive correlation.
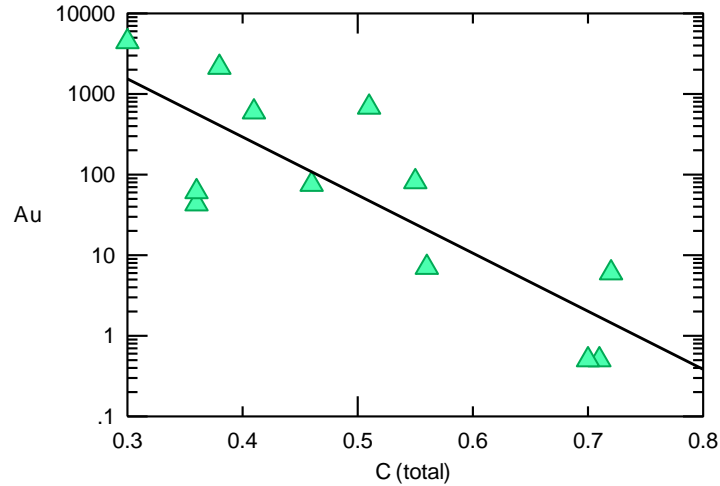
Figure 5.4: Relationship ($R^2 = 0.68$) between Au (ppb) and total carbon (%)

There does not appear ($R^2 = 0.05$) to be a correlation (Fig. 5.5) between total sulfur and gold within the Touquoy ore zone.
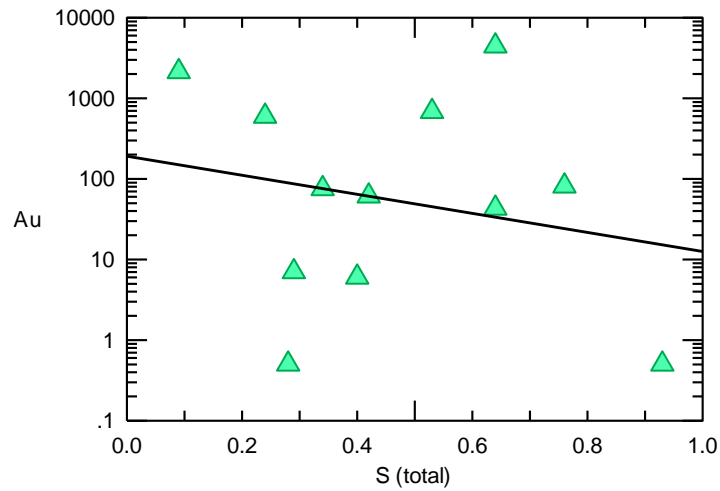
Figure 5.5: Relationship ($R^2 = 0.05$) between total sulfur (%) and gold (ppb).

Fig. 5.6 shows the strong ($R^2 = 0.72$) negative correlation between CaO and gold. This may be explained by the amount of hydrothermal alteration which exists throughout the ore zone of the Touquoy deposit.
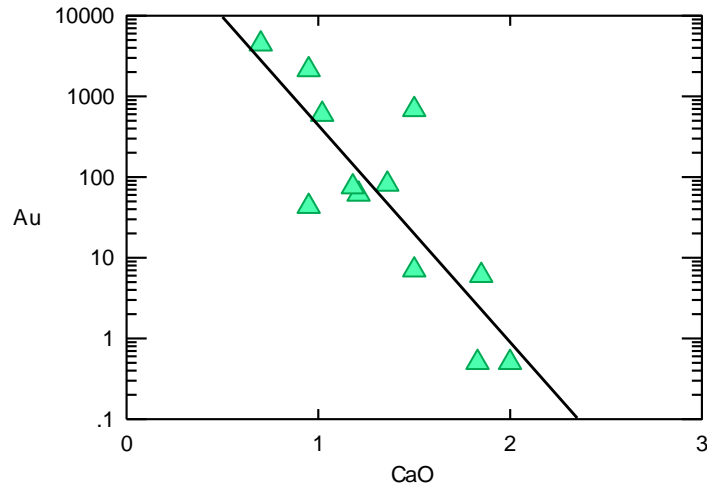
Figure 5.6: The apparent negative correlation ($R^2 = 0.72$) between gold (ppb) and CaO (Wt. %).

When the data are entered into the sandstone characterization diagrams of Bhatia (1983), based on major elements, on two of the diagrams (Figs. 5.7 and 5.8) the data plot within field A, which suggests an ocean island arc origin for sediments within the ore zone. However, for the second two diagrams, they points fell well outside any of the fields. This could be due to hydrothermal alteration which has affected the ore zone (Bierlein and Smith, 2003).
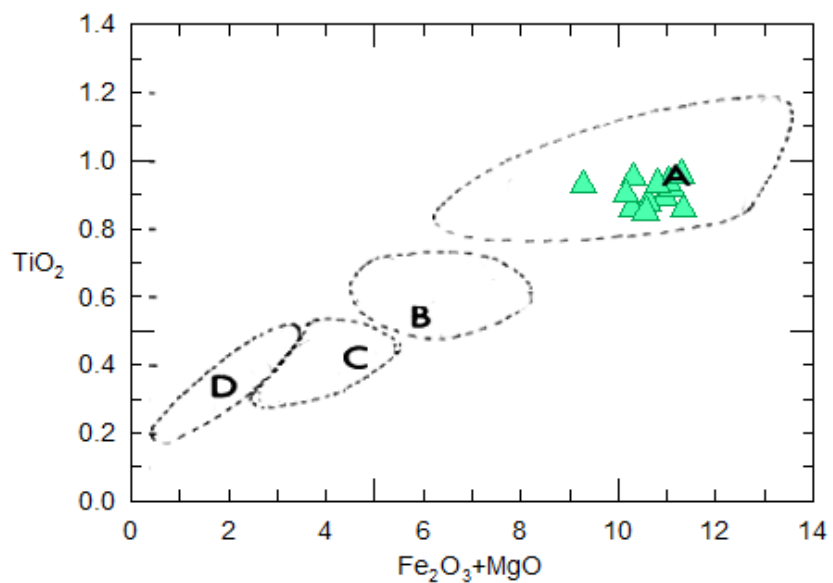
Figure 5.7: Major element plots show this study's data plot well within field A. A – Oceanic island arc. B- Continental island arc, C- Active continental margin, D- Passive margin. After Bhatia (1983).
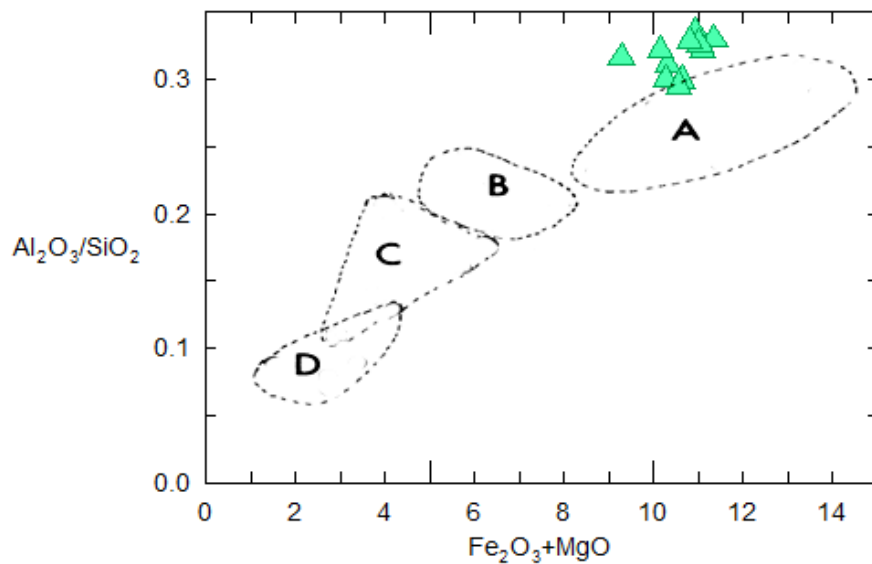
Figure 5.8: Data plot just above A – Continental island arc. After Bhatia (1983).

5.1.2 Trace Elements

When certain trace elements from the Touquoy samples were compared, few interesting apparent correlations became obvious. However, there appears to be a negative correlation between Au and W, within the ore zone as in Fig. 5.9.
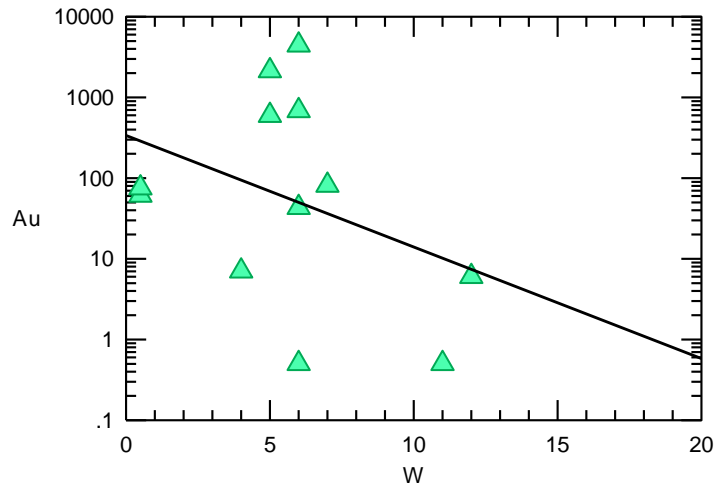
Figure 5.9: The relationship ($R^2 = 0.13$) between gold concentration (ppb) and tungsten (ppm)

5.2 Comparative Geochemistry

The dataset from this thesis along with the Touquoy dataset from Bierlein and Smith (2003), and the Meguma Supergroup dataset from Graves and Zentilli (1987) were combined, and compared to enhance the size of the dataset, and to compare the geochemistry of the Touquoy deposit with the rest of the Meguma. It should be noted that Bierlein and Smith's (2003) data set includes samples from both the wall-rock and ore zone, while this thesis only includes ore zone geochemistry. The legend for the following diagrams is given in Fig. 5.10.
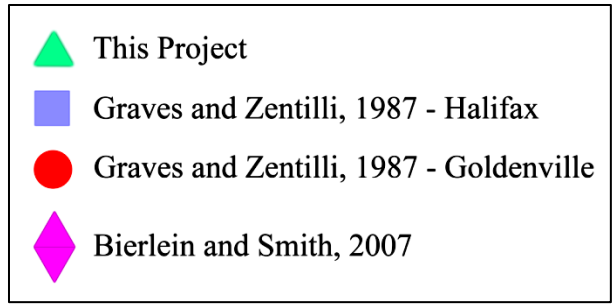
Figure 5.10: The legend for the following geochemical graphs.

5.2.1 Bierlein and Smith (2003)

The study by Bierlein and Smith (2003) was a detailed look at the Touquoy deposit, and features extensive geochemical analysis which are easily combined with the results of this study. Through combining the two datasets of the same deposit, the number of samples if effectively increased. Fig. 5.11 shows the ratio between Al_2O_3 and K_2O indicative of sericite alteration.
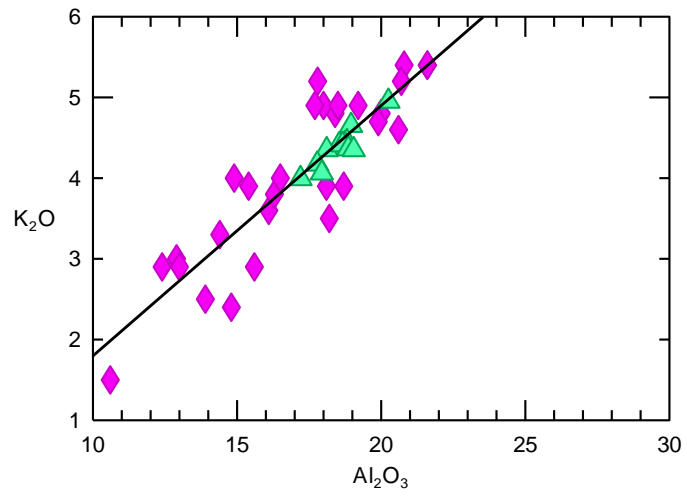
Figure 5.11: The correlation ($R^2 = 0.79$) between Al_2O_3 and K_2O is further supported by the addition of Bierlein and Smith's (2003) data.

Fig. 5.12 shows additional evidence of the negative correlation at the sample scale between total carbon and gold. Fig. 5.13 shows the weak ($R^2 = 0.13$) positive correlation between total carbon and arsenic.
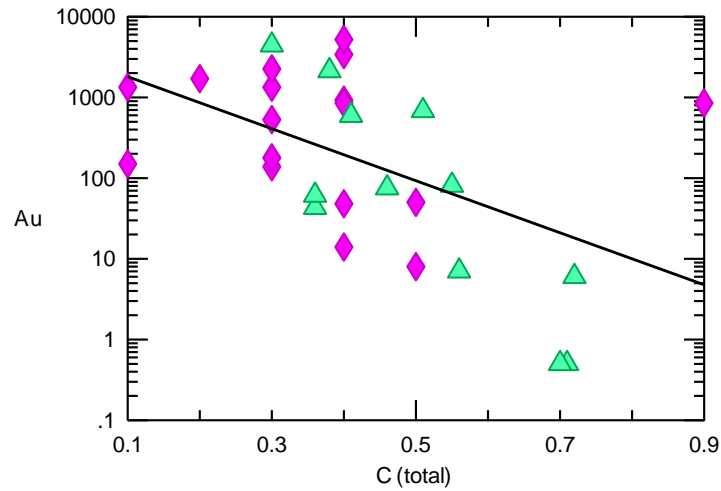
Figure 5.12: The apparent negative correlation ($R^2 = 0.27$) between gold (ppb) and total carbon (%) is further constrained by the combination of the two data sets.
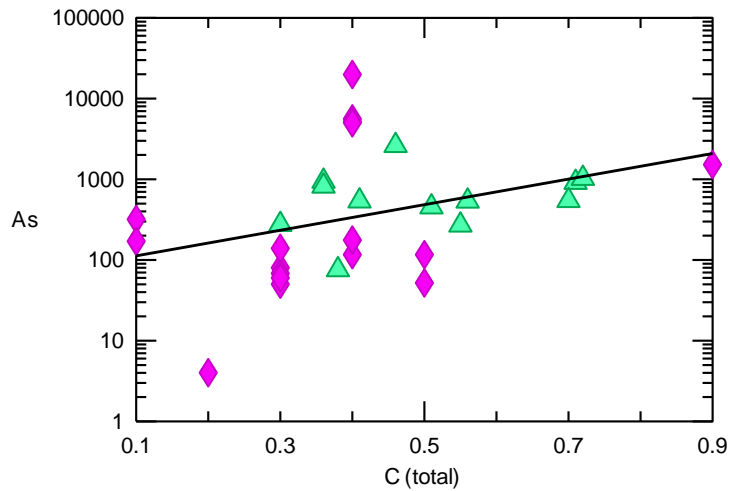
Figure 5.13: The correlation ($R^2 = 0.13$) between carbon (Wt%) and arsenic (ppm) is slightly improved by the combination of the two datasets

5.2.2 Graves and Zentilli (1987)

The study by Graves and Zentilli (1987) was conducted to geochemically characterize the

transition zone between the Goldenville and Halifax groups, called the Goldenville-Halifax

Transition (GHT). The study involved collecting over 400 samples from formations of both the

Halifax and Goldenville groups. When the data are plotted together, including the data from

Bierlein and Smith (2003), the amount of total carbon in the Touquoy deposit is between one and

two orders of magnitude higher than in the sampled formations from the Halifax Group (Fig.

5.14). However, there is still a negative correlation between increasing gold and carbon within

the datasets.
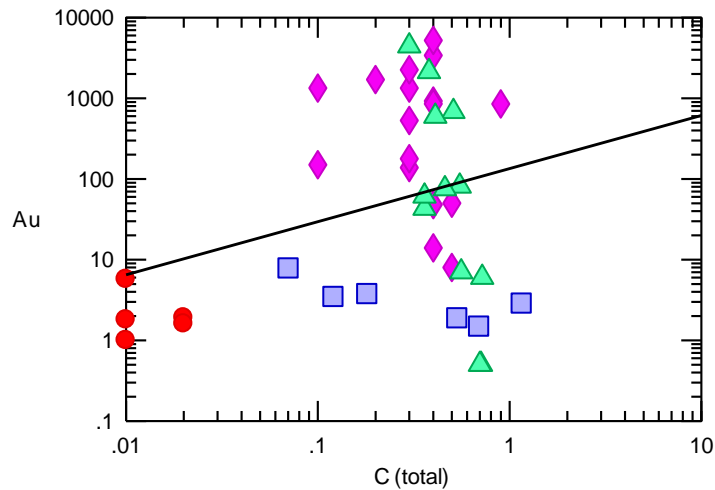
Figure 5.14: The amount of total carbon ($R^2 = 0.08$) in the Touquoy deposit is significantly

greater than found in the Goldenville Group.

When the data are again plotted according to Bhatia and Crooke's (1986) sedimentary

tectonic-provenance diagrams using immobile elements (Fig. 5.15 and Fig. 5.16), the data from

the Meguma again plot within the oceanic island and continental island arc fields.

40
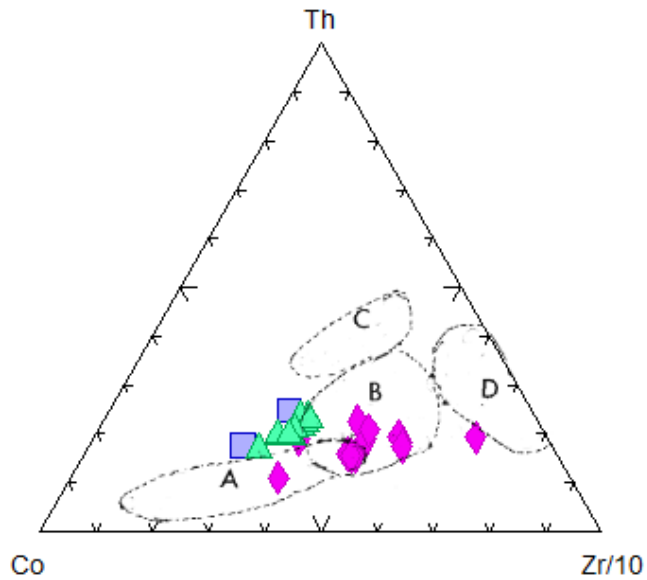
Figure 5.15: The three data sets plot approximately in the A or B fields. A – Oceanic island arc. B- Continental island arc, C- Active continental margin, D- Passive margin. After Bhatia and Crooke (1986).
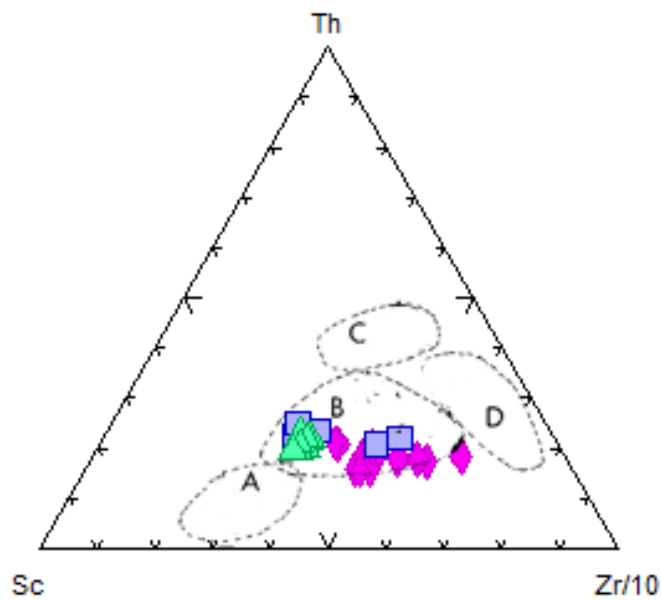
Figure 5.16: The data plots well within field B. A – Oceanic island arc. B- Continental island arc, C- Active continental margin, D- Passive margin. After Bhatia and Crooke (1986).

5.3 Petrology

Complete qualitative petrographic descriptions are listed in Appendix 2. The samples are predominantly dark grey, very fine- to fine-grained argillites, with some lenses of metagreywacke, such as in MR-03. Oxidation is visible on most fractures of the hand samples and often visible in thin section as well. Chlorite alteration is visible in all samples, though the amount varies by sample. Calcite/ankerite is found in every sample, often in veins and as subhedral crystals within the groundmass. Sulfides, including pyrrhotite, pyrite, chalcopyrite and arsenopyrite are disseminated throughout, with some samples such as MR-04 having larger concentrations. In the case of MR-04, there are well formed euhedral arsenopyrite crystals, as shown in Fig. 5.17.
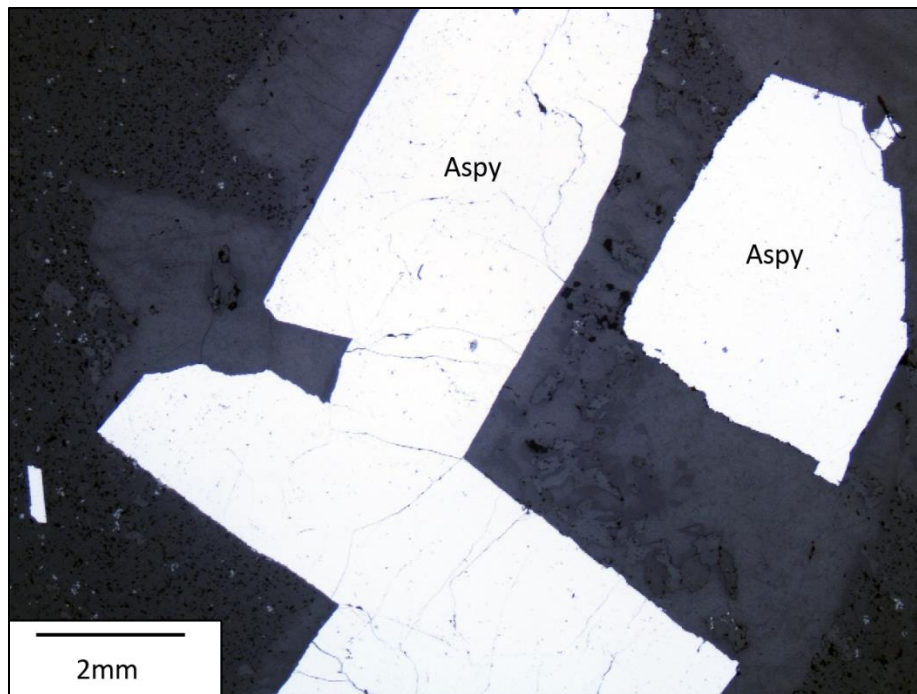
Figure 5.17: Arsenopyrite crystal from MR-04

The arsenopyrite crystals in MR-04 are the host of small inclusions of gold, in addition to a small bleb within a crack of the crystal, as shown in Fig. 5.18.
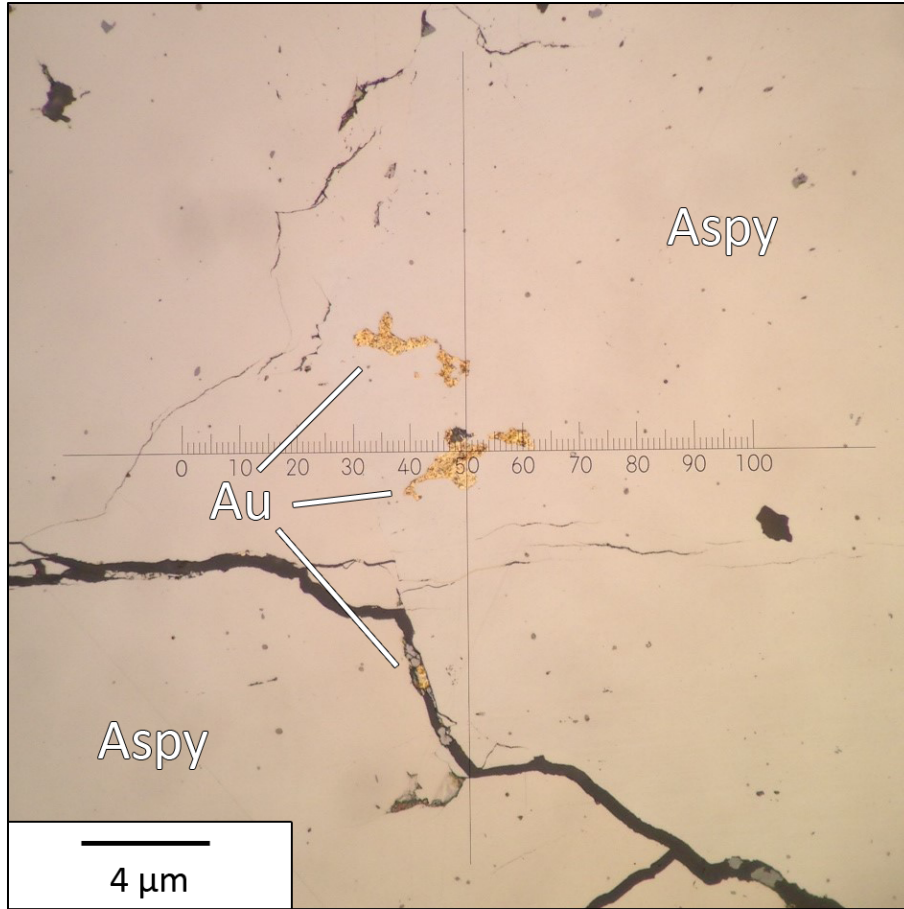
Figure 5.18: Gold inclusion in arsenopyrite in MR-04.
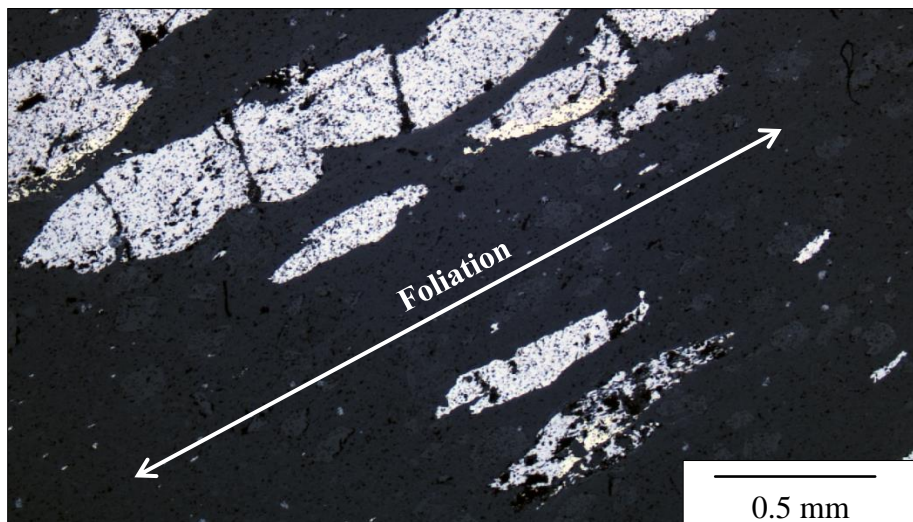
Figure 4.19: Pyrrhotite crystals under reflected light microscopy in sample MR01. Note the

pyrrhotite crystals are aligned in the direction of foliation.

In Fig. 5.20, pressure shadows surrounding ankerite crystals are visible in line with foliation, suggesting they formed prior to ductile deformation.
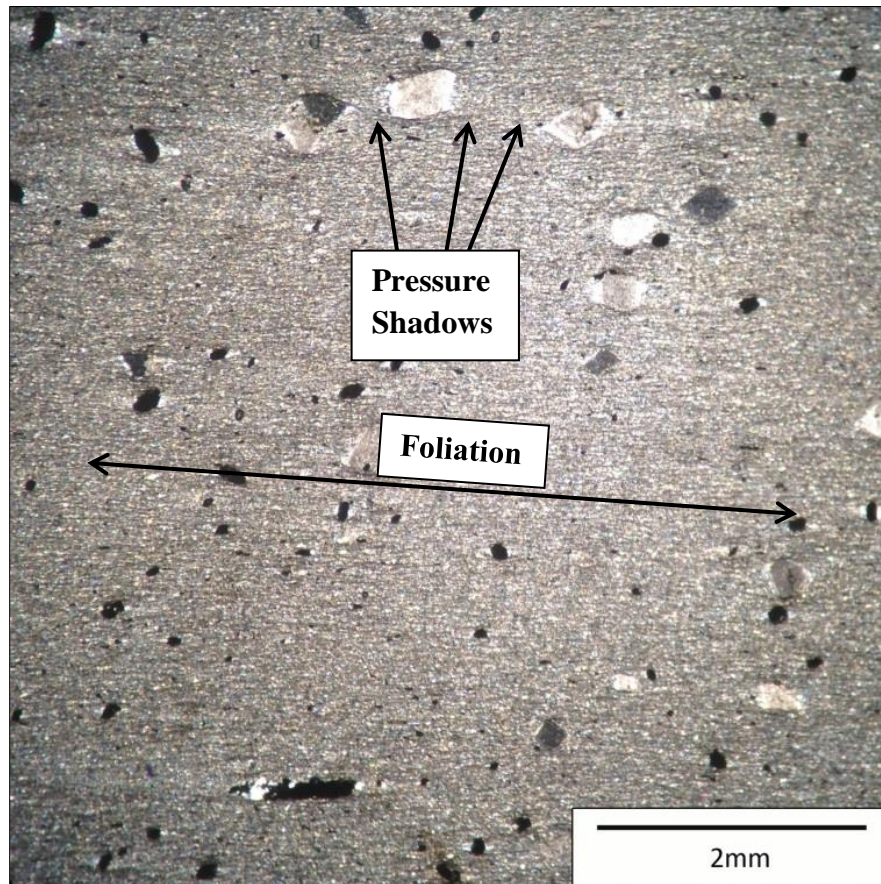
Figure 5.20: Ankerite crystals in sample MR01 under transmitted light microscopy. Note the pressure shadows in the direction of foliation.

5.4 Electron Microprobe

The complete electron microprobe data values are listed in Appendix 4. By plotting the atomic percentages of iron and sulfur against one another for pyrrhotite analysis, the resulting graph indicates that the sampled pyrrhotite within the Touquoy deposit is almost entirely mono-clinic pyrrhotite, the magnetic stoichiometric end member as shown in Fig. 5.19.
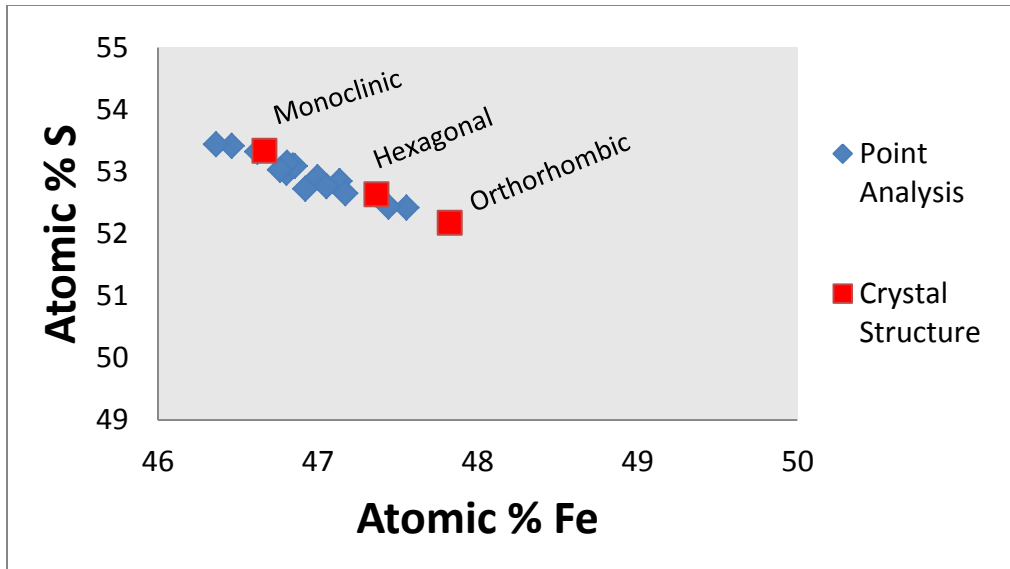
Figure 5.21: Many of the pyrrhotite crystals contain between 46 and 47% Fe, which means they are monoclinic pyrrhotite, and therefore magnetic (e.g. Fox et al., 1997).
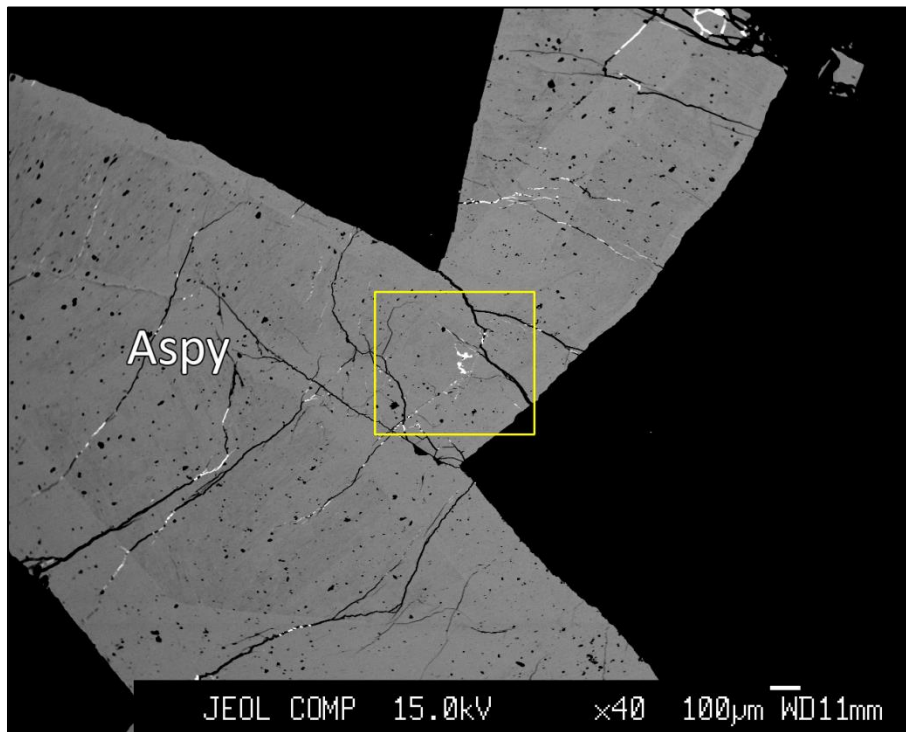
Figure 5.22: Microprobe image of an arsenopyrite crystal in sample MR-04, the yellow box indicates the field of view of Fig. 5.21.
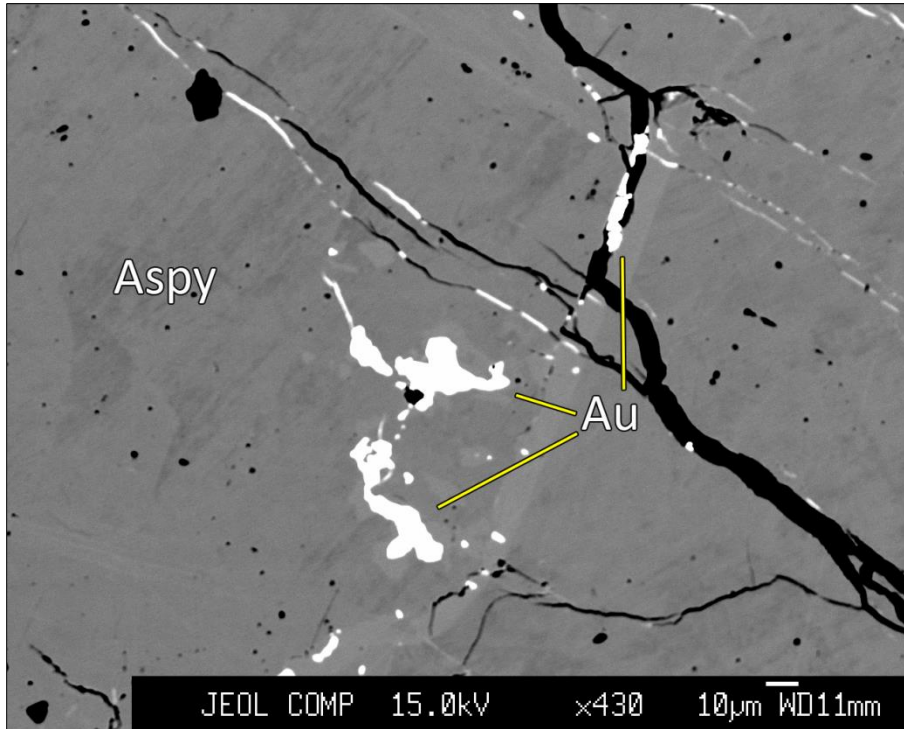
Figure 5.23: A closer look at the arsenopyrite crystal from in MR-04 in Fig. 20. Gold forms inclusions within the crystal, in addition to filling a crack in the crystal.

Gold blebs appeared as small inclusions within the arsenopyrite crystal, and within cracks in the local area, as in Fig. 5.21.

CHAPTER 6: DISCUSSION & CONCLUSIONS

6.1 Discussion

The geochemical analysis, electron microprobe analysis and petrological results require discussion with reference to the related literature. Since there are a variety of findings to discuss, they have been broken down into headings which will discuss the following: the presence monoclinic pyrrhotite in the deposit, gold in sulfides, the both positive and negative relationship between gold and carbon and finally the provenance of the Meguma Supergroup. This chapter will end with a section regarding limitations of this study and recommendations for future research.

6.1.1 Monoclinic Pyrrhotite

The qualitative point-analysis of pyrrhotite crystals with Dalhousie University's electron microprobe suggests that the majority of the pyrrhotite within the sampled area of the Touquoy deposit is monoclinic pyrrhotite. Sangster and Smith (2007) found in their review of gold in Nova Scotia, that pyrrhotite, not strictly monoclinic, is abundant in the majority of gold deposits. Pyrrhotite is known to accept gold in its structure (e.g. Cameron, 1993), and its transformation to pyrite could release that gold into the ore system. Monoclinic pyrrhotite is the magnetic stoichiometric end member of pyrrhotite. This is interesting for two very different reasons. According to the official NI43-101 report by Hellman & Schofield (2011), the hinge and limbs of the Moose River Anticline are often magnetic, and have been used to help define the trend of the structure. Though the monoclinic pyrrhotite is not confined just to the ore zone, its magnetic signature could help delineate where an ore zone might be. In terms of geochemistry, it means that reducing conditions have been preserved in its immediate environment, and this reducing environment is probably preserved by the presence of carbon in the form of bitumen or graphite.

Unfortunately, other minerals which have a magnetic signature such as magnetite also have a large presence with the Meguma Supergroup, as detailed in an aeromagnetic study by King (1997).

The second factor which is of importance it that pyrrhotite has been directly linked to Acid Rock Drainage (ARD). A study by Fox et al. (1997) on the association between pyrrhotite and ARD within the Halifax Group showed that in multiple areas, the breakdown of pyrrhotite from exposed Halifax Group slates caused serious and ongoing environmental damage. Pyrrhotite is more reactive than pyrite, and Fox et al. (1997) found that it within regions which had undergone greenschist facies metamorphism, the pyrrhotite grains were coarser and aligned with the cleavage planes. Activities such as construction can lead to fracturing of the rock, which preferentially fractures along cleavage, exposing the maximum amount of pyrrhotite for oxidation, leading to ARD. As the Touquoy deposit will be an open pit mine, mitigation or prevention of pyrrhotite oxidation will be of the utmost importance to prevent ARD. Indeed ARD is a worldwide environmental and health concern in regions with similar geology, and ongoing research is needed (e.g. Belzile, 2004) to offset the effects.

6.1.2 Gold in Arsenopyrite

In this study, and as noted by others (e.g. Graves and Zentilli, 1982; Bierlein and Smith, 2003; Sangster and Smith, 2007) there is a close spatial relationship between arsenopyrite and gold. One possible reason for this close spatial relationship is possible transport of the gold in a thioarsenide complex (e.g. Romberger, 1988) however, due to the lack of literature on the subject of thioarsenides, future work is needed. Another theory is that arsenopyrite, and other sulfides, could allow gold into their crystal structure while they are expanded due to thermal conditions. Upon cooling the gold would then be ejected, and presumably crystalize in the vicinity of the

ejecting crystal. In their review of gold in Nova Scotia, Graves and Zentilli (1982) suggested that this could be the case based on their observations. These observations are supported by work by Hinchey et al. (2003) who found that gold was distributed homogenously with no nugget effect within arsenopyrite crystals from the Lodestar Prospect in Newfoundland. Cook et al. (2013) looked at gold within arsenopyrite grains in an orogenic gold deposit in the Tanami district of Australia. Though the geologic environment is slightly different than the Meguma, their work suggested that upon brittle fracture of arsenopyrite, gold in the grain is remobilized and fills fractures and concentrates on the edges of grains. Further work mapping the concentration of gold with Touquoy sulfides is needed to see if the work by Cook et al. (2013) applies here. Indeed recent laboratory research on the solubility of gold within arsenopyrite suggests that up to ~2 Wt. % of gold may be incorporated into the structure of arsenopyrite, either as Au^0 nanoparticles or with Au^+ in solid solution (Reich et al., 2005). However, the complicated relationship between gold and arsenic doesn't end there. Work by Pokrovski et al. (2002) states that in conditions coming to many hydrothermal deposits, arsenopyrite in local dissolution creates reducing conditions, which could provide the reduction needed to bring gold out of a chloride complex, and maintain the close spatial relationship between gold and arsenopyrite.

6.1.3 Gold and Carbon

The intention of this study was to investigate the possible relationship between the deposition of gold in the Touquoy deposit and organic carbon by geochemical and other analytical means. At the deposit scale, there is a positive correlation between the amount of carbon and the amount of gold, however there appears to be a negative correlation at the metre scale. Additionally, there is a slight positive correlation between arsenic and carbon at the metre scale within the ore zone. Though the results of this study are not conclusive, they provide

49

interesting data from which may assist future studies. For instance, the contrast between the amount of carbon between the mineralized zone (very high) in Touquoy and barren formations from Goldenville Group (very low) deserves a closer look. Within the ore zone itself though, as indicated in the above chapters, there is a negative correlation between non-carbonate carbon and gold. One possible interpretation for this negative correlation would be that carbon is consumed (by oxidation to CO_2) as gold precipitated when gold-carrying complexes are destroyed by reduction. This interesting possibility should be investigated theoretically and experimentally. Another possible theory is related to the disseminated style of the Touquoy deposit. As the ore zone is disseminated rather than confined to veins, upon precipitation of gold and the break-down of the carrying complex, carbon in the form of CO_2 would then be able to dissipate away from the site of precipitation, leading to a negative sample-scale correlation. A review of the recent literature shows an increasing amount of data in support of relationships between organic carbon, in either the form of hydrocarbons or organic matter (e.g. Coveney and Pasava, 2004; Craw et al., 2010; Greenwood et al., 2013). Within the Touquoy deposit the isotopic signature of sulfur suggests a biogenic origin, and the carbon in carbonate was most likely oxidized organic carbon (Kontak and Kerrich, 1997; Sangster and Smith, 2007). Further research into isotopes from Meguma gold deposits suggest that, along with carbon and sulfur, gold itself may have originated from within the Meguma strata (Kontak, 2014), which is in direct conflict with previously held theories that Meguma gold must have come from a magmatic source (e.g. Kontak and Archibald, 2002).

6.1.4 Provenance of the Meguma

Some hypotheses about the source of the gold in the Meguma deposits propose that the gold was extracted from the sedimentary rocks themselves, and carried within a metamorphic

fluid to the sites of deposition, where the fluid lost its carrying capacity and dropped it to form ore deposits. If the Meguma Supergroup was a passive margin and its sediments were reworked sands from a distant source, their gold could be negligible. On the other hand, if sediments represented epiclastic volcanic debris of an actively eroding igneous arc, the rocks could be rick in metals such as gold.

Speculations regarding the origins of the Meguma are largely broken into two camps. One theory, which is based on detrital zircon data and Sm-Nd isotopic comparisons, states that the Meguma Supergroup sediments would have been deposited in a rift basin between Avalonia and West Africa (e.g. Waldron et al., 2009). Furthermore, the two terranes would have been separate during the late Neoproterozoic, before they were accreted during the Acadian Orogeny.

The other model suggests that, also based on detrital zircon data and similar basement Nd isotopic data, the Meguma Supergroup was juxtaposed to the Avalon Terrane during the early Paleozoic and resided on the same side of the Rheic Ocean (e.g. Murphy et al. 2004). The authors suggest that the Meguma was formed in an Andean-type setting, rather than a passive margin.

The data from this study, in addition to the data from Bierlein and Smith (2003) and Graves and Zentilli (1987) were combined to improve the size of the data set in Chapter 4. When the data are plotted according to the sedimentary provenance diagrams of Bhatia and Crooke (1986), they do not plot in a field which would suggest a passive or rifting margin. Rather, they plot on fields which strongly suggest an oceanic island arc.

Based on the assumptions, by Bhatia and Crooke (1986), about element immobility during sedimentation and by using Nb/Y vs Zr/TiO_2 graph of Winchester and Floyd (1977) the

data from Bierlein and Smith (2003) and Graves and Zentilli (1987) were plotted to obtain a

potential source rock for Meguma sediments as in Fig. 6.1. The data from this study could not be

plotted as Nb was not analyzed for.
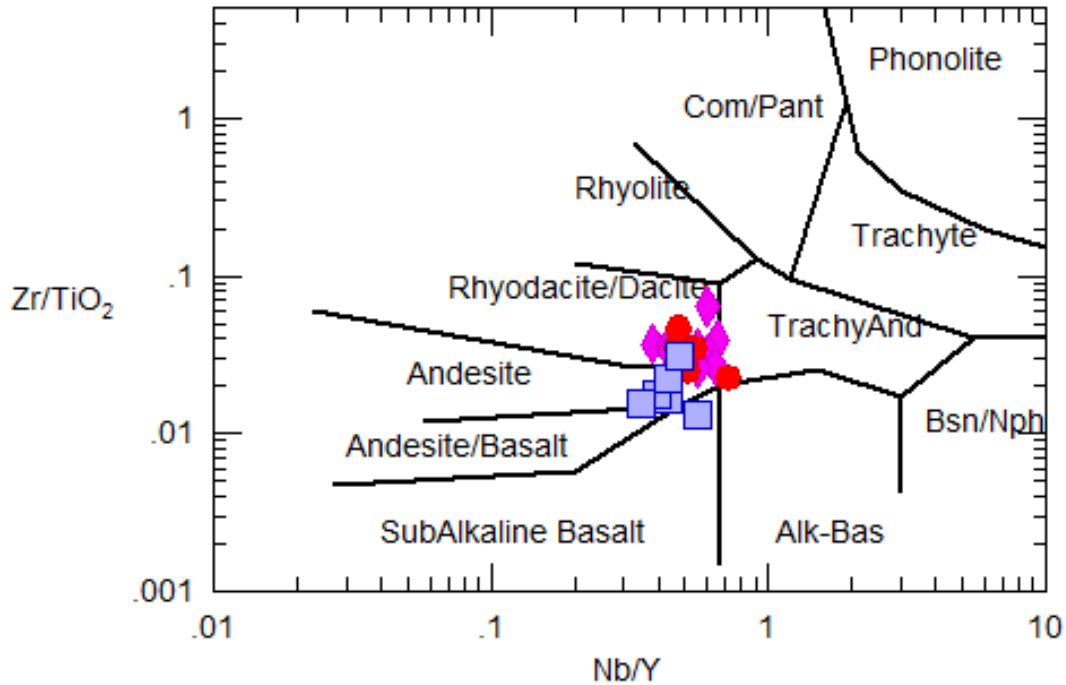
Figure 6.1: The composition of Meguma metasedimentary rocks plotted in a graph designed for

volcanic rocks, by Winchester and Floyd (1977). As equivalent intrusive rocks, they would be

diorites to granodiorites.

The graph clearly shows that the source rocks for Meguma sediments could between

andesite to dacite in composition. This adds to the argument that the Meguma could have been

formed off an active Andean-type margin rather than a passive one. Furthermore, the Andes are

known to be rich in metals including gold, copper, silver and elements such as arsenic.

Sediments rich in these metals could then be a potential source of metals to be scavenged from.

6.1.5 The Ore Deposit Model

The data from this study allows the proposal of the following genetic model:

1. Source: The data are compatible with a model whereby the source of the ore components in the Touquoy deposit (and by extension to most gold deposits in the Meguma) was dispersed in immature sedimentary rocks originating from erosion of an active tectonic arc, essentially epiclastic volcanic rock debris of andesite-dacite (or diorite-granodiorite) composition. There is no need to look for an extraneous source.

2. Transportation: The gold would have been mobilized from dispersed clastic components or diagenetic iron sulfides and transported into a prograde metamorphic fluid. Dehydration of clays and chlorites to form dryer phases, driven by heat alone, would have generated large volumes of fluids which would have sought escape along a hydraulic gradient, utilizing any permeable conduits. Any hydrocarbons generated during this time would have migrated ahead of the water, accumulating in domains with a permeability contrast, such as under shales or argillites.

3. Precipitation: The gold-laden metamorphic fluids may have been oxidising, and the gold transported as a chloride complex, or reducing and transported as a bisulfide complex. In the first case, complexes would destabilize by sudden decompression, whereby CO_2 would be released, precipitating carbonate, quartz and gold, or by reaction with a reduced, more stagnant fluid (presumably hydrocarbon rich) whereby the carbon would be oxidized and consumed, and accompanying reduction would precipitate sulfides and gold.

Metamorphic fluids at ca. 10km depth would have been at >300°C (data from fluid inclusions and arsenopyrite geothermometry) from lithostatic pressure and the rocks ductile like toothpaste. Sudden tectonic stresses would have let the pore fluid pressure to exceed the

tensional strength of the rocks; hydro fracturing of the rocks, in areas where volume increases was possible, would occur. In some areas crack-seal veins were formed within tensional domains of folds or thrusts. Early formed veins were compressed as the rocks developed slaty cleavage (Fig. A2-9). In the Touquoy deposit, few veins were formed, and the mineralizing fluid permeated the rocks and lost its gold load without fracturing the host-rocks; instead it developed halos of carbonatisation. Gold may have been contained in solid solution in arsenopyrite, and was exsolved during cooling, or co-precipitated with arsenopyrite.

4. Carbon or no carbon: There are very similar gold deposits in turbidites such as Australia and Taiwan (e.g. Craw et al., 2010). Carbon is generally present in turbidites, but it would seem that its presence is not a prerequisite for gold deposition, or at least authors tend to disregard its role. Considering the volumes of fluid involved, probably the mechanical processes of sudden creation of permeability are more important than the chemical processes, but the geochemical data suggest carbon was constructively involved in gold precipitation.

6.2 Limitations

Though the data acquired in this study touches on many subjects there were limitations in data collection. The pulp samples collected from the Touquoy deposit were homogenized metre-intervals, and therefore there was no distinction made between lithologies. The limited sample size and spatial distribution prevented some of the leading questions we had hoped to answer. Limited time constraints prevented a second visit to the electron microprobe in order to construct element concentration maps of gold within sulfide minerals. However, the data we were able to acquire provide a strong starting point for future studies in the area.

6.3 Conclusions and Recommendations

In conclusion, geochemical analysis, electron microprobe analysis, and petrological descriptions were completed in order to ascertain if there was a relationship between organic carbon and gold in the Touquoy deposit on Nova Scotia. Though limitations in sample size prevented a conclusive answer coming to light, the data was never the less useful. The large difference in carbon between the formations within the Halifax Group and carbon present within mineralized Touquoy strata showed that a closer look at the relationship is warranted. The close spatial relationship with gold and arsenopyrite provides additional evidence with regards to the close tie between the two elements during deposit formation. The presence of monoclinic pyrrhotite within the deposit, and potentially others, could be a useful tool in exploration. The oxidation of pyrrhotite is a cause of ARD and therefore needs careful attention during the disruption of units rich in pyrrhotite. Finally, the geochemical properties of Meguma strata suggest that it was formed off a margin which was volcanically active, potentially providing sediments which would be rich in metals, to be scavenged to form deposits.

Future areas of study include looking at the original source of the oxidized carbon from the deposit. Similar to the metals, carbon might have been brought into the deposit by migrating fluids. Additionally, further study into the spatial relationship between pyrrhotite and gold is warranted as it could be an excellent exploration tool.

References

Amend, J.P. and Teske, A., 2005, Expanding frontiers in deep subsurface microbiology: Paleogeography, Paleoclimatology, Paleoecology, v. 219, p. 131-155.

Alexander, M.L., Smith, M.R., Hartman, J.S., Mendoza, A., and Koppenaal, D.W., 1998, Laser ablation inductively coupled mass spectrometry: Applied surface science, v. 127-129, p. 255-261.

Belzile, N., Chen, Y., Cai, M., Li, Y., 2004, A review on pyrrhotite oxidation; Journal of Geochemical Exploration, v. 84, p. 65-76.

Benn, K., Horne, R.J., Kontak, D.J., Pignotta, G.S., and Evans, N.G., 1997, Syn-Acadian emplacement model for the South Mountain Batholith, Meguma Terrane, Nova Scotia: Magnetic fabric and structural analyses: GSA Bulletin, v. 109, n. 10, p. 1279-1293.

Benn, K., Roest, W.R., Rochette, P., Evans, N.G. and Pignotta, G.S., 1999, Geophysical and structural signatures of syntectonic batholith construction: The South Mountain Batholith, Meguma Terrane, Nova Scotia: Geophysics Journal International, v. 136, p. 144-158.

Bhatia, M.R., 1983, Plate tectonics and geochemical composition of sandstones: The Journal of Geology, v. 91, n. 6, p. 611-627.

Bhatia, M.R. and Crook, K.A.W., 1986, Trace element characteristics of graywackes and tectonic setting discrimination of sedimentary basins: Contrib Mineral Petrol, v. 92, p. 181-193.

Bierlein, F.P., Christie, A.B. and Smith, P.K.,2004, A comparison of orogenic gold mineralisation in central Victoria (AUS), western South Island (NZ) and Nova Scotia (CAN): Implications for variations in the endowment of Paleozoic metamorphic terrains: Ore Geology Reviews, v. 25, p. 125-168.

Bierlein, F.P. and Smith, P.K., 2003, The Touquoy Zone deposit: An example of "unusual"

    orogenic gold mineralization in the Meguma Terrane, Nova Scotia, Canada: Canadian

    Journal of Earth Sciences, v. 40, p. 447-466.

Bucknell, W.R., 2014, Pipeline of Gold Production in Nova Scotia [PowerPoint slides].

    Retrieved from http://www.atlanticgold.com.au/html/announcements.htm

Cameron, E.M., 1993, Precambrian gold: Perspectives from the top and bottom of shear zones:

    The Canadian Mineralogist, v. 31, p. 917-944.

Carrillo-Rosua, J., Boyce, A.J., Morales-Ruano, S., Morata, D., Roberts, S., Munizaga, F., and

    Moreno-Rodriguez, V., 2014, Extremely negative and inhomogeneous sulfur isotope

    signatures in Cretaceous Chilean manto-type Cu-(Ag) deposits, coastal range of central

    Chile: Ore Geology Reviews, v. 56, p. 13-24.

Clarke, L.A., 1960, The Fe-As-S system: Phase relations and applications: Economic Geology,

    v. 55, p. 1631-1652.

Clarke, D.B., Chatterjee, A.K. and Giles, P.S., 1993, Petrochemistry, tectonic history, and Sr-Nd

    systematics of the Liscomb Complex, Meguma lithotectonic zone, Nova Scotia: Canadian

    Journal of Earth Sciences, v. 30, n. 3, p. 449-464.

Cook, N.J., Ciobanu, C.L., Meria, D., Silcock, D. and Wade, B., 2013, Arsenopyrite-Pyrite

    Association in an Orogenic Gold Ore: Tracing Mineralization History from Textures and

    Trace Elements: Economic Geology, v. 108, p. 1273-1283.

Coveney, R.M. and Pasava, J., 2004, Diverse connections between ores and organic matter: Ore

    Geology Reviews, v. 24, p. 1-5.

Craw, D., Upton, P., Yu, B., Horton, T. and Chen, Y., 2010, Young orogenic gold mineralization

    in active collisional mountains, Taiwan: Miner Deposita, v. 45, p. 631-646.

Delijska, A., Blazheva, T., Petkova, L. and Dimov, L., 1988, Fusion with lithium borate as sample preparation for ICP and AAS analysis: Fresenius Z Anal Chem, v. 332, p. 362-365.

Dostal, J., Keppie, D.J., Jutras, P., Miller, B.V. and Murphy, B.J., 2006, Evidence for the granulite-granite connection: Penecontemporaneous high-grade metamorphism, granitic magmatism and core complex development in the Liscomb Complex, Nova Scotia, Canada: Lithos, v. 86, p. 77-90.

Douglas, G.V., 1948, Structure of the gold veins of Nova Scotia: Structural Geology of Canadian Ore Deposits: Canadian Institute of Mining and Metallurgy, Jubilee Volume, p. 919-926.

Emmons, E.R., 1937, Gold deposits of the world, with a section on prospecting. New York: McGraw-Hill Book Company.

Erdmann, S., Jamieson, R.A. and MacDonald, M.A., 2009, Evaluating the origin of garnet, cordierite and biotite in granitic rocks: A case study from the South Mountain Batholith, Nova Scotia: Journal of Petrology, v. 50, n. 8, p. 1477-1503.

Fallara, F., Savard, M.M., and Paradis, S., 1998, A structural, petrographic, and geochemical study of the Jubilee An-Pb deposit, Nova Scotia, Canada, and a new metallogenic model: Economic Geology, v. 93, p. 757-778.

Faribault, E.R. 1899, The gold measures of Nova Scotia and deep mining: Journal of the Canadian Mining Institute, v. 2, p. 119-129.

Fox, D., Robinson, C. and Zentilli, M., 1997, Pyrrhotite and associated sulphides and their relationship to acid rock drainage in the Halifax Formation, Meguma Group, Nova Scotia: Atlantic Geology, v. 33, p. 87-103.

Graves, M.C. and Zentilli, M., 1982, A review of the geology of gold in Nova Scotia: Special

      Volume – Canadian Institute of Metallurgy, v. 24, p. 233-242.

Graves M.C. and Zentilli, M. (1987) Geochemical characterization of the Goldenville - Halifax

      Transition of the Meguma Group of Nova Scotia: Progress Report III. Mineral

      Development Agreement, NSDME Report 87-5, pp. 217-219.

Graves, M.C. and Zentilli, M. (1988) Geochemical characterization of the Goldenville Formation

      Halifax Formation Transition Zone of the Meguma Group of Nova Scotia. Geological

      Survey of Canada Open File Report #1829, 45 p.

Gregory, D., Meffre, S., Large, R., and Bull, S., 2011, Gold accumulation in diagenetic

      framboidal pyrite from the Derwent Estuary, Tasmania: 11th SGA Biennial Meeting.

Greenwood, P.F., Brocks, J.J., Grice, K., Schwark, L., Jaraula, C.M.B, Dick, J.M. and Evans,

      K.A., 2013, Organic geochemistry and mineralogy. I. Characterisation of organic matter

      associated with metal deposits: Ore Geology Reviews, v. 50, p. 1 – 27.

Hellman & Schofield Pty. Ltd, 2011, Mineral Resource Estimate for The Touquoy Gold Project,

      Nova Scotia. Sydney, AUS: Neil Schofield.

Henderson, J.R., Wright, T.O., and Henderson, M.N., 1986, A history of cleavage and folding:

      an example from the Goldenville Formation, Nova Scotia: Geological Society of America

      Bulletin, v. 97, p. 1354-1366.

Hinchey, J.G., Wilton, D.H.C and Tubrett, M.N., 2003, A LAM-ICP-MS study of the

      distribution of gold in arsenopyrite from the Lodestar Prospect, Newfoundland, Canada:

      The Canadian Mineralogist, v. 41, p. 353-364.

Hitzman, M.W., Selley, D. and Bull, S., 2010, Formation of sedimentary rock-hosted stratiform

      copper deposits through earth history: Economic Geology, v.105, p. 627-639.

Horne, R.J. and Pelly, D., 2006, Geological transect of the meguma terrane from centre

    Musquodoboit to Tangier: Nova Scotia Department of Natural Resources Report of

    Activities, p. 71-89.

Keppie, J.D. (compiler), 2002, Geologic map of the province of Nova Scotia: Nova Scotia

    Department of Natural Resources, Minerals and Energy Branch, Map ME 2000-1, scale

    1:500000

King, M.S., 1997, Magnetic susceptibility mapping: Applications for the Meguma Group,

    Central Nova Scotia: Atlantic Geology, v. 33, p. 121-131.

King, M.S., 2000, Enhanced aeromagnetic and digital elevation map of eastern Nova Scotia

    (11C/13, 11D/10, 11D/11, 11D/12, 11D/13, 11D/14, 11D/15, 11D/16, 11E/01, 11E/02,

    11E/03, 11D/04, 11F/04, 11F/05, 11F/06); Nova Scotia Department of Natural

    Resources, Mineral Resource Branch, Map 2000-2, scale 1:250 000.

Kontak, D.J., 1995, A study of fluid inclusions in sulfide and nonsulfide mineral phases from a

    carbonate-hosted Zn-Pb deposit, Gay's River, Nova Scotia, Canada: Economic Geology,

    v. 93, p. 793-817.

Kontak, D.J., 2014, Reconciliation and implications of SEM-EDS microscopy and fluid

    inclusion chemistry for the origin of the Meguma gold deposits, Nova Scotia [Abstract]:

    Atlantic Geoscience Colloquium, p. 25.

Kontak, D. J. and Archibald, D. A., 2002, 40Ar/39Ar dating of hydrothermal biotite from high-

    grade gold ore, Tangier gold deposit, Nova Scotia: Further evidence for 370 Ma gold

    metallogeny in the Meguma Terrane: Economic Geology, v. 97, n. 3, p. 619-628.

Kontak, D.J. and Kerrich, R., 1995, Geological and geochemical studies of a metaturbidite-hosted lode gold deposit: The Beaver Dam deposit, Nova Scotia: II. Isotopic studies: Economic Geology, v. 90, p. 885-901.

Kontak, D.J. and Kerrich, R., 1997, An isotopic (C, O, Sr) study of vein gold deposits in the Meguma Terrane, Nova Scotia: Implication for source reservoirs: Economic Geology, v. 92, P. 161-180.

Kontak, D.J. and Smith, P.K.,1989, Sulfur isotopic composition of sulfides from the Beaver Dam and other Meguma-Group-hosted deposits, Nova Scotia: Implications for genetic models: Canadian Journal of Earth Sciences, v. 26, p. 1617-1629.

Kontak, D.J., Smith, P.K., Kerrich, R. and Williams, P.F., 1990, Integrated model of Meguma Group lode gold deposits, Nova Scotia, Canada: Geology, v. 18, p. 238-242.

Large, R.R., Bull, S.W., and Maslennikov, V.V., 2011, A carbonaceous sedimentary source-rock model for Carlin-type and orogenic gold deposits: Economic Geology, v. 106, p. 331-358.

Large, R.R., Maslennikov, V.V., Robert, F., Danyushevsky, L.V. and Chang, Z., 2007, Multistage sedimentary and metamorphic origin of pyrite and gold in the Giant Log Deposit, Lena Gold Province, Russia: Economic Geology, v. 102, p. 1233-1267.

MacDonald, L.A., Barr, S.M., White ,C.E. and Ketchum, J.W.F., 2002, Petrology, age, and tectonic setting of the White Rock Formation, Meguma Terrane, Nova Scotia: Evidence for Silurian continental rifting: Canadian Journal of Earth Science, v. 39, p. 259-277.

Morelli, R.N., Creaser, R.A., Selby, D., Kontak, D.J., and Horne, R.J., 2005, Rhenium-Osmium Geochronology of arsenopyrite in Meguma Group gold deposits, Meguma Terrane, Nova

Scotia, Canada: Evidence for multiple gold-mineralizing events: Economic Geology, v. 100, p. 1229-1242.

Morey, A.A., Tomkins, A.G., Bierlein, F.P., Weinberg, R.F. and Davidson, G.J., 2008, Bimodal distribution of gold in pyrite and arsenopyrite: Examples from the Archean Boorara and Bardoc Shear Systems, Yilgarn Craton, Western Australia: Economic Geology, v. 103, p. 599-614.

Murphy, J.B., Fernandez-Suarez, J., Keppie, D.J. and Jeffries, T.E., 2004, Contiguous rather than discrete Paleozoic histories for the Avalon and Meguma terranes based on detrital zircon data: Geology, v. 32, n. 7, p. 585-588.

Murphy, B.J. and Keppie, J.D., 2005, The Acadian orogeny in the northern Appalachians: International Geology Review, v. 47, p. 668-687.

O'Brien B.H., 1988, A Study of the Meguma Terrane in Lunenburg County, Nova Scotia: Geologic Survey of Canada Open File 1823, p.1-80.

Owen, J.V., Corney, R., Dostal, J. and Vaughan, A., 2010, Significance of "gneissic" rocks in the Liscomb Complex, Nova Scotia: Canadian Journal of Earth Sciences, v. 47, p. 927-940.

Pokrovski, G.S., Kara, S. and Roux, J., 2002, Stability and Solubility of Arsenopyrite, FeAsS, in crustal fluids: Geochimica et Cosmochimica Acta, v. 66, n. 13, p. 2361-2378.

Reich, M., Kesler, S.E., Utsunomiya, S., Palenik, C.S., Chryssoulis, S.L., and Ewing, R.C., 2005, Solubility of gold in arsenian pyrite: Geochimica et Cosmochimica Acta, v. 69, n. 11, p. 2781-2796.

Reynolds, P.H., Clarke, D.B., and Bogutyn, P.A., 2004, $^{40}Ar/^{39}Ar$ Laser dating of zoned white micas from the Lake Lewis leucogranite, South Mountain Batholith, Nova Scotia, Canada: The Canadian Mineralogist, v. 42, n. 4, p. 1129-1137.

Richardson, J.M., Bell, K., Blenkinsop, J., and Watkinson, D.H., 1989, Rb-Sr age and geochemical distinctions between the Carboniferous tin-bearing Davis Lake complex and the Devonian South Mountain batholith, Meguma Terrane, Nova Scotia: Canadian Journal of Earth Sciences, v. 26, p. 2044-2061.

Romberger, S.B., 1988, Geochemistry of Gold in Hydrothermal Deposits: U.S. Geological Survey Bulletin, v. 1857-A, p. A9 - A25.

Ryan, R.J. and Smith, P.K., 1998, A review of the mesothermal gold deposits of the Meguma Group, Nova Scotia, Canada: Ore Geology Reviews, v. 13, p. 153-183.

Sangster, A.L., 1992, Light stable isotope evidence for a metamorphic origin for bedding-parallel gold-bearing veins in Cambrian flysch, Meguma Group, Nova Scotia: Exploration and Mining Geology, v. 1, n. 1, p. 69-79.

Sangster, A.L. and Smith, P.K., 2007, Metallogenic summary of the Meguma gold deposits, Nova Scotia. Mineral Deposits of Canada: A synthesis of major deposit-types, district metallogeny, the evolution of geologic provinces, and exploration methods: Geologic Association of Canada, Mineral Deposits Division, Special Publication, v. 5, p. 723-732.

Schenk, P.E., 1997, Sequence stratigraphy and provenance on Gondwana's margin: The Meguma zone (Cambrian to Devonian) of Nova Scotia, Canada: GSA Bulletin, v. 109, p. 395-409.

Smith, P. K., Kontak, D. J., 1996, Gold deposits in the Meguma Group of Nova Scotia. Department of Natural Resources, Minerals and Energy Branch, Information Circular 51.

Southam, G. and Saunders, J.A., 2005, The geomicrobiology of ore deposits: Economic Geology, v. 100, p. 1067-1084.

Stow, D.A.V, Alam, M. and Piper, D.J.W., 1984, Sedimentology of the Halifax Formation, Nova Scotia: Lower Paleozoic fine-grained turbidites: Geological Society, London, Special Publications, v. 15, p.127-144.

Tilling, R.I., Gottfried, D. and Rowe, J.J., 1973, Gold abundance in igneous rocks: Bearing on gold mineralization: Economic Geology, v. 68, p. 168-186.

Tomkins, A.G., 2013, A biogeochemical influence on the secular distribution of orogenic gold: Economic Geology, v. 108, n. 2, p. 193-197.

Waldron, J.W.F., White, C.E., Barr, S.M., Simonetti, A., and Heaman, L.M., 2009, Provenance of the Meguma terrane, Nova Scotia: rifted margin of early Paleozoic Gondwana: Canadian Journal of Earth Sciences, v. 46, p.1-8.

White, C.E., 2009, Pre-Carboniferous bedrock geology of the Annapolis Valley Area (NTS 21A/14, 15 and 16; 21H/01 and 02), Southern Nova Scotia: Nova Scotia Department of Natural Resources Report of Activities, p. 137-155.

White, C.E., 2010, Stratigraphy of the Lower Paleozoic Goldenville and Halifax groups in southwestern Nova Scotia: Atlantic Geology, v. 46, p. 136-154.

White, C.E., Scallion, K-L, Barr, S.M. and Jamieson, R.A., 2009, The Liscomb Complex, Meguma Terrane, Nova Scotia: Basement or Urban Legend?: Atlantic Geoscience Society 35th Colloquium and Annual General Meeting, Program and Abstracts, p.34.

Wilkin, R.T. and Barnes, H.L., 1997, Formation processes of framboidal pyrite: Geochimica et Cosmochimica Acta, v. 61, n. 2, p. 323-339.

Williams-Jones, A.E., Bowell, R.J., and Migdisov, A.A., 2009, Gold in Solution: Elements, v. 5, n. 5, p. 281-287.

Williams-Jones, A.E. and Migdisov, A.A., 2006, An experimental study of the solubility of gold in crude oil: Implications for ore genesis [Abstract]: Goldschmidt Conference Abstracts, p. A703

Winchester, J. A. and Floyd, P. A., 1977, Geochemical discrimination of different magma series and their differentiation products using immobile elements: Chemical geology, v. 20 p. 325-343.

Windh, J., 1995, Saddle reef and related gold mineralization, Hill End Gold Field, Australia. Economic Geology, v. 90, p. 1764-1775.

Zentilli, M. and Graves, M.C., 1990, Carbon compounds and ore deposit models. Abstract, 8th IAGOD Symposium, Ottawa, Canada, 12-18 August., A110-A111

Zentilli, M. and Graves, M.C., 1992, The role of carbon in metallogenetic processes: a framework for assessment. Abstract, invited talk, Logan Club, Geological Survey of Canada, Ottawa. Alice Wilson Hall, April 23/92

Zentilli, M., Graves, M.C., Mulja, T., and MacInnis, I., 1986, Geochemical characterization of the Goldenville – Halifax transition of the Meguma Group of Nova Scotia: preliminary report. Geological Survey of Canada, Paper 86-1A, pp. 423–428.

Zentilli, M., Munizaga, F., Graves, M.C., Boric, R., Wilson, N.S.F., Mukhopadhay, P.K., and Snowdon, L.R., 1997, Hydrocarbon involvement in the genesis of ore deposits: An example in Cretaceous stratabound (Manto-type) copper deposits of central Chile: International Geology Review, v. 39, p. 1-21.

Appendix 1

Sample Locations and Assay Values

Table 1: Depths of each sample from drill hole MR-05-081, in addition to gold values from assay. Note MR-12 is the high grade pulp sample with no associated core sample.

Sample ID	Depth from (m)	Depth to (m)	Au from Assay (ppm)
MR-01	15.9	16.03	-0.01
MR-12	29	30	23.90
MR-02	31.72	31.9	0.54
MR-03	34.5	34.65	0.61
MR-04	39	39.13	0.07
MR-05	51.7	51.9	1.28
MR-06	56.5	56.72	0.05

Table 2: Depths of each sample from drill hole MR-05-079, in addition to gold values from assay.

Sample ID	Depth from (m)	Depth to (m)	Au from Assay (ppm)
MR-07	10.77	10.85	0.09
MR-08	32	32.15	0.16
MR-09	34.2	34.35	1.99
MR-10	35	35.15	0.36
MR-11	39.95	40.1	1.15

Petrographic Descriptions

MR01
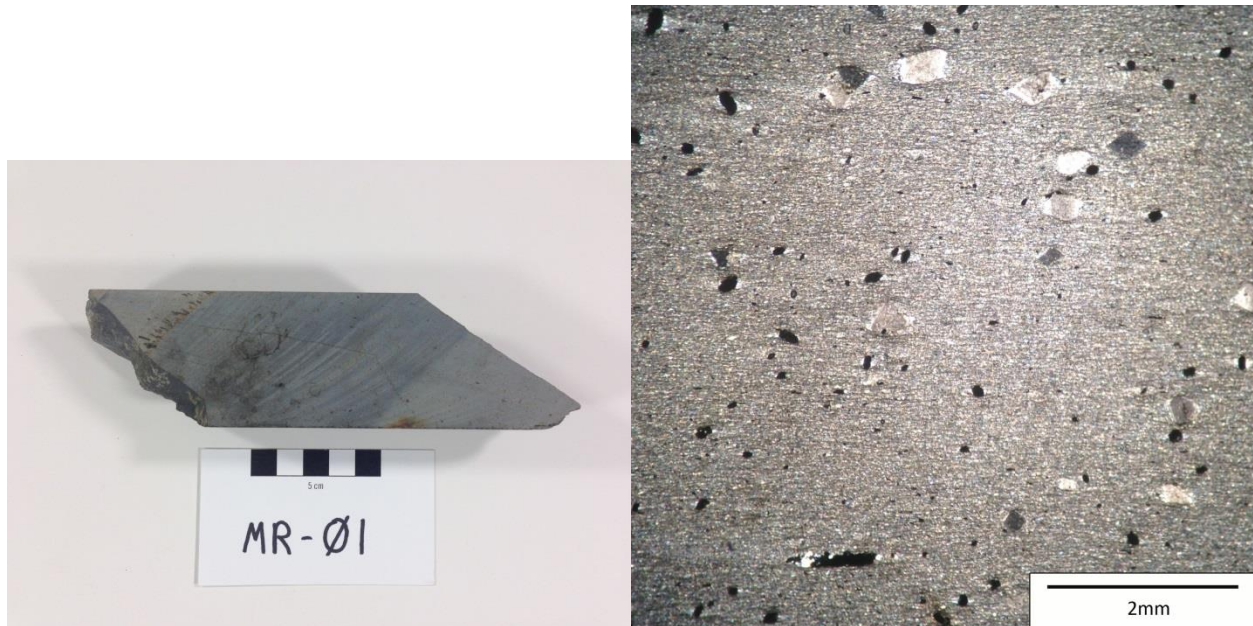
Figure A2-1: MR-01, Dry, note colour change and sulfides at top left of hand sample.

Hand Sample: MR-01 is fine grained, dark grey argillite. Minor sulfides are visible in the, mostly pyrrhotite. Additionally, small yellow-white carbonate minerals are visible. In the hand specimen, no bedding or foliation is visible, however colour and grain size boundaries are visible in hand sample (Fig. 1).

Transmitted Light: Under higher magnification, foliation is visible, but weak. Chlorite alteration is visible but sparse throughout. Minor asymmetric strain shadows are visible surrounding carbonate minerals and sulfides alike.

MR-02
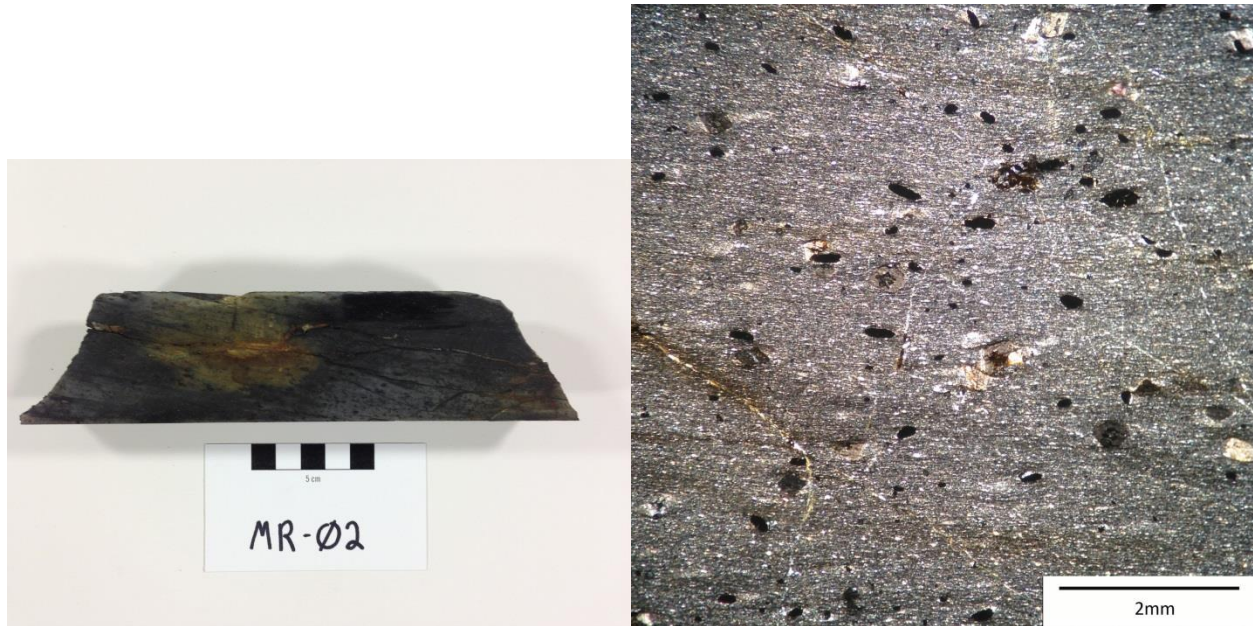
Figure A2-2: MR02 - Note heavy oxidation in hand sample, and in thin section.

Hand Sample: The hand sample is dark grey, fine-grained argillite, and bedding is not visible. The hand sample has been heavily oxidized along fractures. Minor carbonate and sulfide minerals are visible throughout the sample. No veining is visible.

Transmitted Light: Under higher magnification chlorite alteration is visible throughout. Minor anhedral sulfides and subhedral carbonate minerals are throughout, with small strain shadows around some crystals. There are small hairline fractures throughout the sample.

MR-03
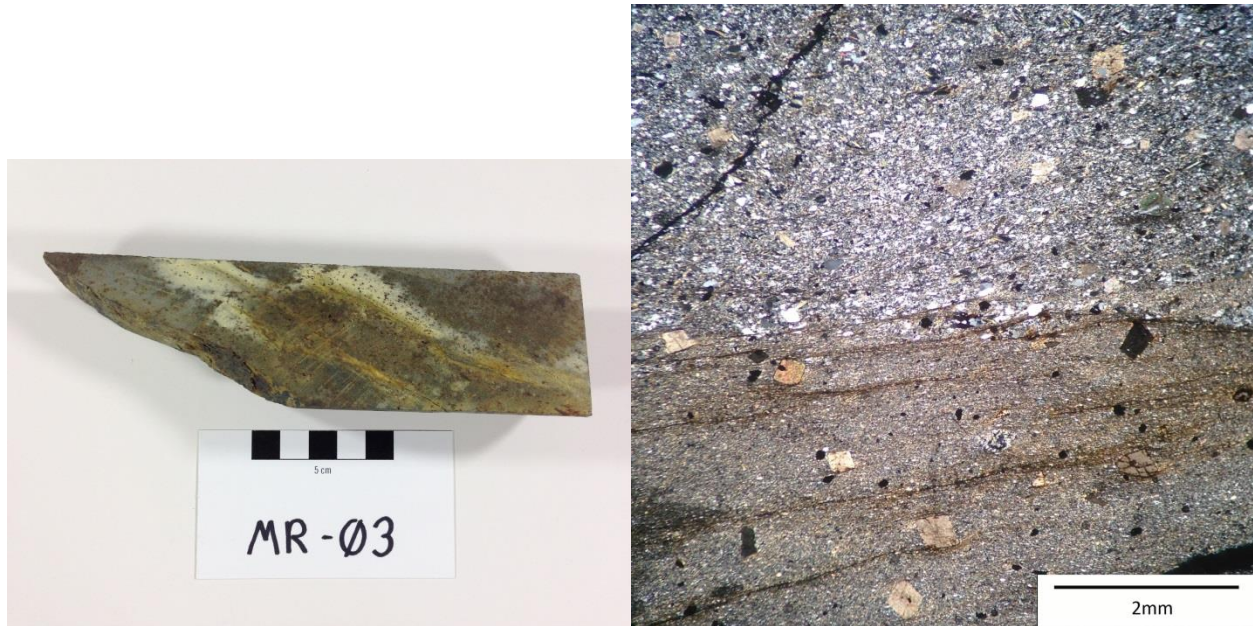
Figure A2-3: MR03 - Note heavy oxidation of the hand sample and thin section. Also note the grain-size boundary in the thin section.

Hand Sample: In hand sample there appears to be argillite with lenses of coarser grained greywacke. The fractures in hand sample are highly oxidized and obscure many textures. Within localized areas, minor blebs of pyrrhotite and chalcopyrite are visible.

Transmitted Light: Under higher magnification, the greywacke exhibits minor foliation, while argillite is more pervasive. There is chlorite alteration visible throughout the sample. Minor fractures within the sample have been filled with quartz and sulfides. Carbonate minerals within the argillite have a dark brown alteration rim, while carbonates in the greywacke do not.

MR-04
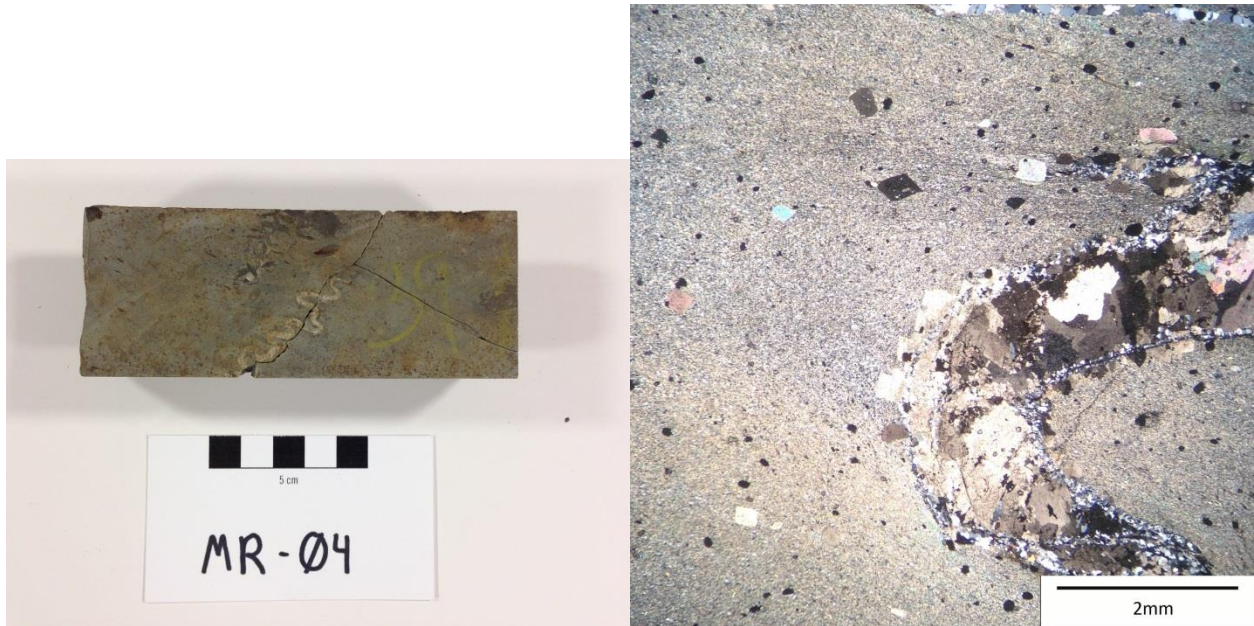
Figure A2-4: Note carbonate vein and cluster of arsenopyrite along the top edge of hand sample.

Hand Sample: Very fine grained, dark grey argillite. Within the sample, minor blebs of carbonate minerals and sulfides are visible. One small vein crosscuts the sample, and has been folded. Along one edge of the sample, large euhedral arsenopyrite crystals are visible.
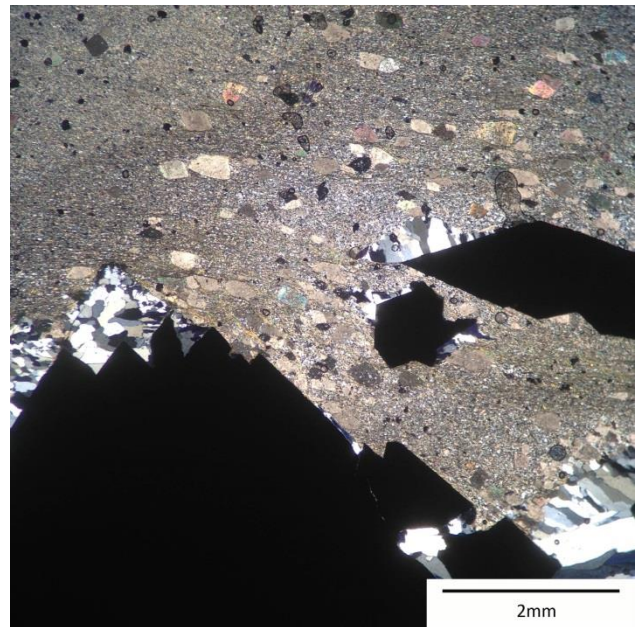
Transmitted Light: The vein walls are small quartz crystals, while the core is larger carbonates. The vein contains subhedral sulfides including pyrrhotite, chalcopyrite and pyrite. The sample exhibits some chloritization. There are minor fractures in the sample which have been filled with quartz. Finally, the large arsenopyrite crystals are surrounded by fine to medium grained quartz.

MR-05
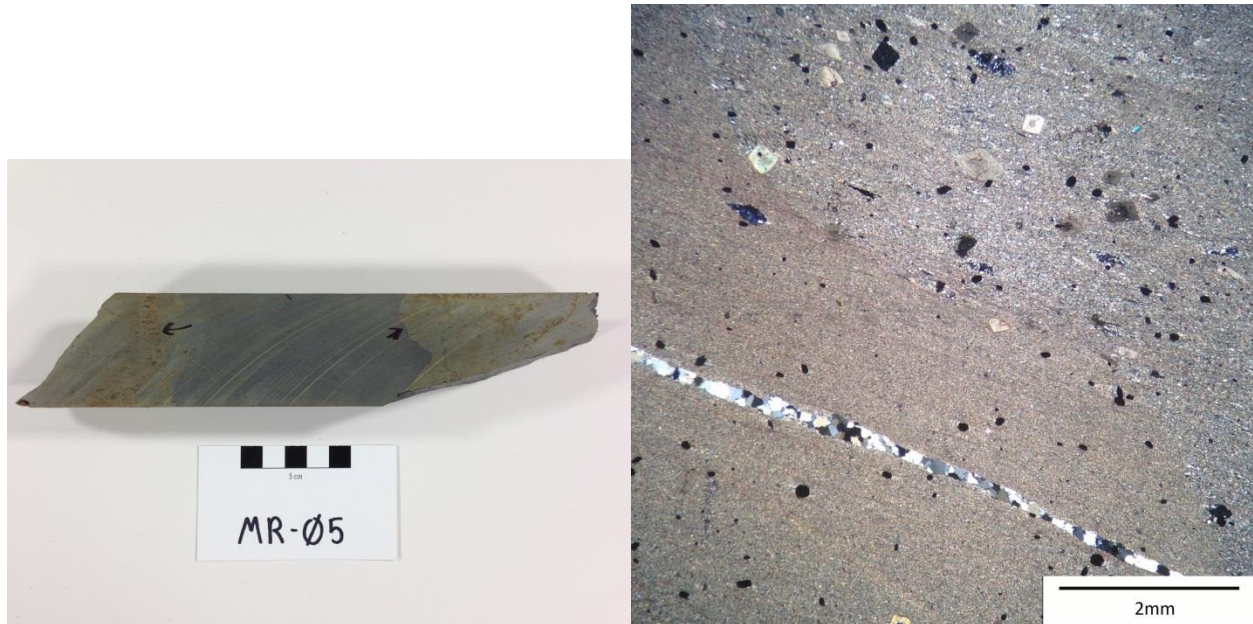
Figure A2-5: MR05 - Note distinct boundaries marked by arrows on the hand sample. Within the thin section note the grain size boundary.

Hand Sample: The sample is fine grained, dark grey argillite. Minor amounts of pyrrhotite are visible in the sample along with small carbonate crystals. The fractures in the sample have been oxidizes. Bedding appears to be barely visible.

Transmitted Light: Under higher magnification, grain size varies from very fine to fine. Chlorite alteration is visible throughout the sample. No strain shadows are visible around any larger grains. Carbonate crystals appear subhedral, while sulfides are anhedral with irregular edges.

MR - 06
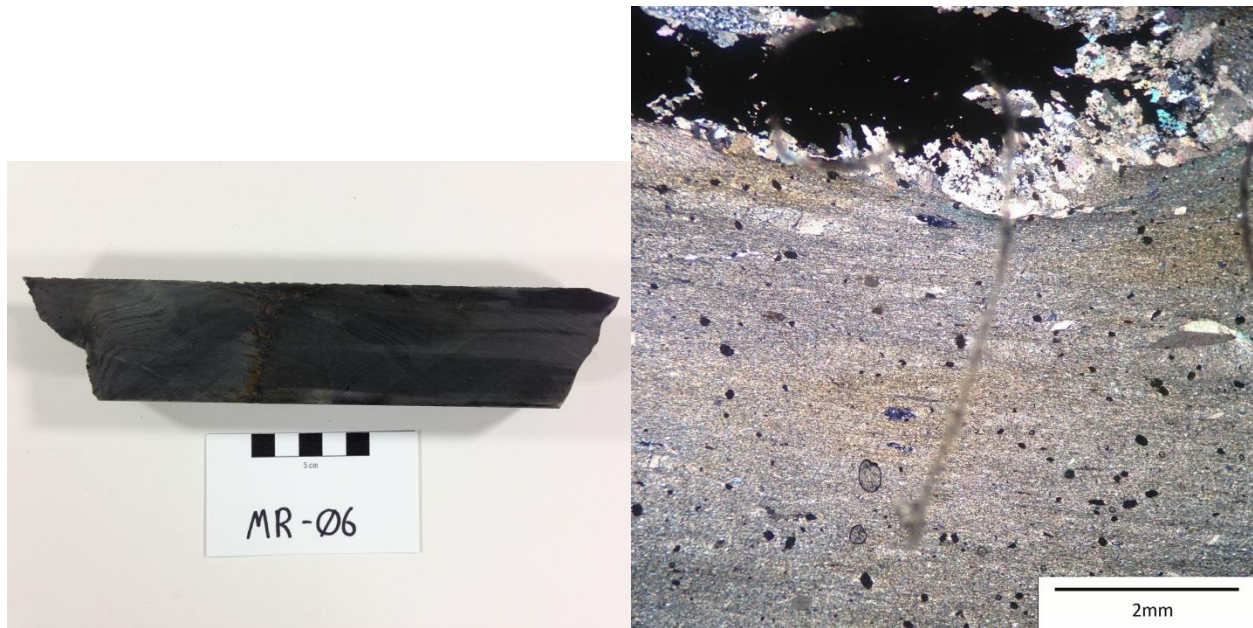
Figure A2-6: MR06 - Note folded bedding on the left and vertical cluster of sulfides in the centre. The line through the centre of the thin section is the etched slide number. Note the carbonate rim surrounding the irregular sulfide growth.

Hand Sample: The sample is fine grained, dark grey argillite. Minor bedding appears to be visible in hand sample. Sulfides including pyrrhotite, pyrite and chalcopyrite are visible in hand sample. Minor carbonate crystals are visible throughout the sample.

Transmitted Light: Under higher magnification, the sample is fine grained and moderately chloritized. Carbonate crystals are subhedral and throughout the sample. Larger carbonates have small strain shadows. The sulfides shown in Fig. 6 are surrounded by a rim of carbonate minerals, and the sulfides themselves have many inclusions of carbonates.

MR-07
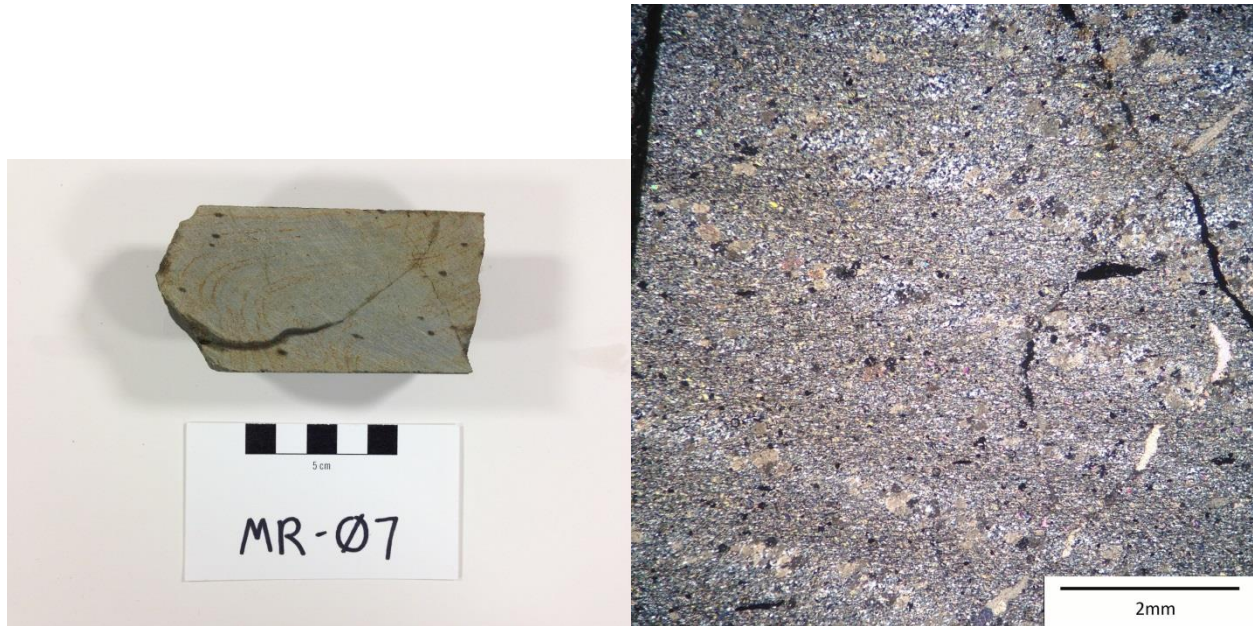
Figure A2-7: MR07 - Note folded, oxidized bedding in hand sample. Note regular grain size changes in the thin section.

Hand Sample: The sample is fine grained, dark grey argillite. Weak bedding is visible, and is highlighted by oxidation, as in Fig. 7. Minor fractures in the sample are also oxidized. Additionally, small blebs of arsenopyrite are also visible.

Transmitted Light: The lighter bands are richer in carbonate minerals and are coarser grained than the darker bands. Chlorite alteration is visible throughout the sample. Dark brown alteration rims are visible on the majority of the carbonate crystals. Finally, minor fractures have been filled with carbonate.

MR-08
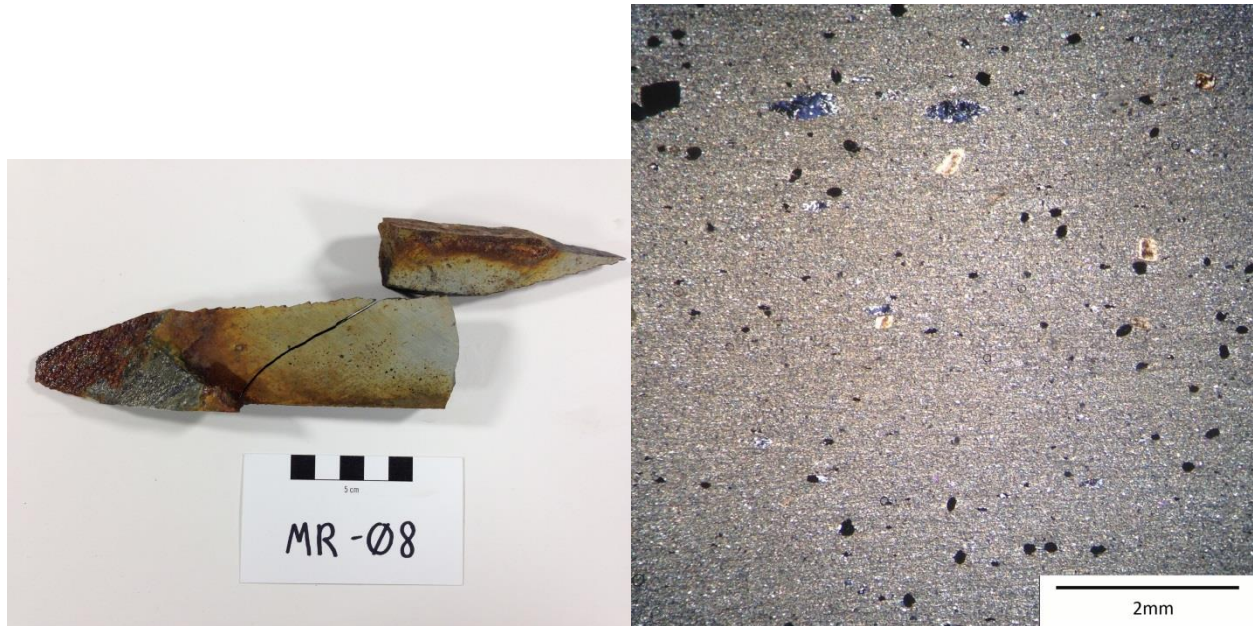
Figure A2-8: MR08 - Note heavy oxidation along fractures in the hand sample.

Hand Sample: The sample is lighter grey, very fine grained argillite. Throughout the sample, minor pyrrhotite crystals are visible, along with minor carbonates. Bedding and foliation are not visible at hand sample scale, and oxidation along fractures obscures and structures.

Transmitted Light: Foliation is weak but visible in this sample. Chloritization is present throughout. The pyrrhotite and other opaque sulfides are all anhedral.

MR-09
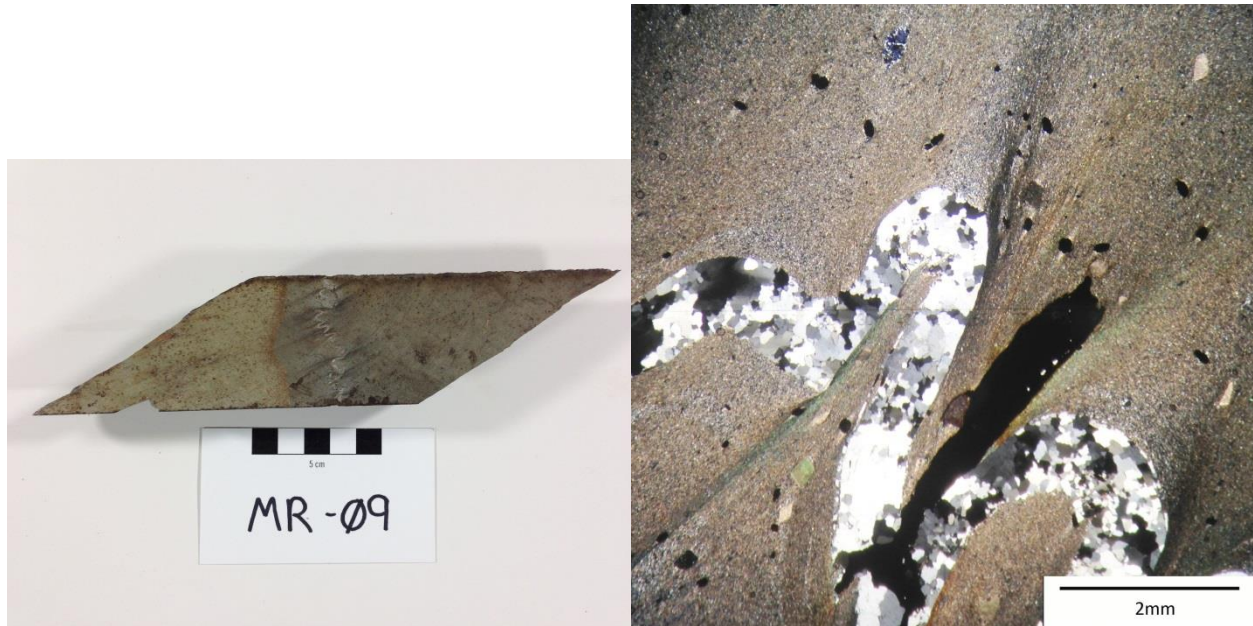
Figure A2-9: MR09 - Note deformed quartz vein in the centre, and the grain size boundary to the left on the hand sample. The vein has been highlighted in the picture to the right.

Hand Sample: The sample is very fine grained, dark grey argillite. However there is a portion of the sample which appears to be a lens of greywacke. A folded vein crosscuts the sample, and strain shadows are visible near the hinges. Along the vein, fingers of pyrite extend from the vein, as visible in the thin section in Fig. 9.

Transmitted Light: Throughout the sample chlorite alteration is visible. Small carbonate minerals are subhedral and do not have any alteration rims. Within the vein, there are no visible carbonate minerals, only quartz and sulfides. At the hinges of the vein, pressure shadows are clearly visible as in Fig. 9.

MR-10
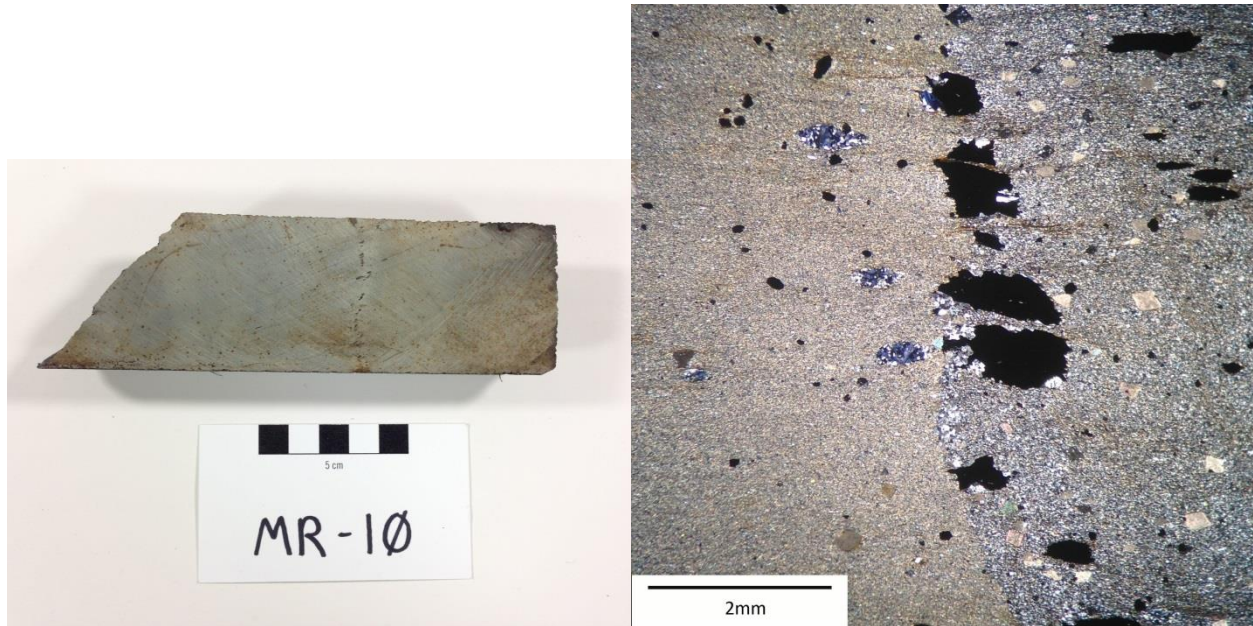
Figure A2-10: MR10 - Note vertical line of sulfides in the centre of the hand sample, which is highlighted in the thin section.

Hand Sample: The sample is fine grained, dark grey argillite, with a slight grain size boundary highlighted in Fig. 10. The sulfides visible in hand sample include pyrrhotite, chalcopyrite and pyrite, which almost all occur at the grain size boundary. Minor carbonate crystals are throughout. No foliation or bedding is visible.

Transmitted Light: Under higher magnification, chlorite is visible throughout, as shown to the left of the thin section grain boundary in Fig. 10. Carbonate crystals are subhedral, with no alteration rims or strain shadows. Sulfide minerals are visible throughout, but the largest are located at the grain size boundary.

MR-11
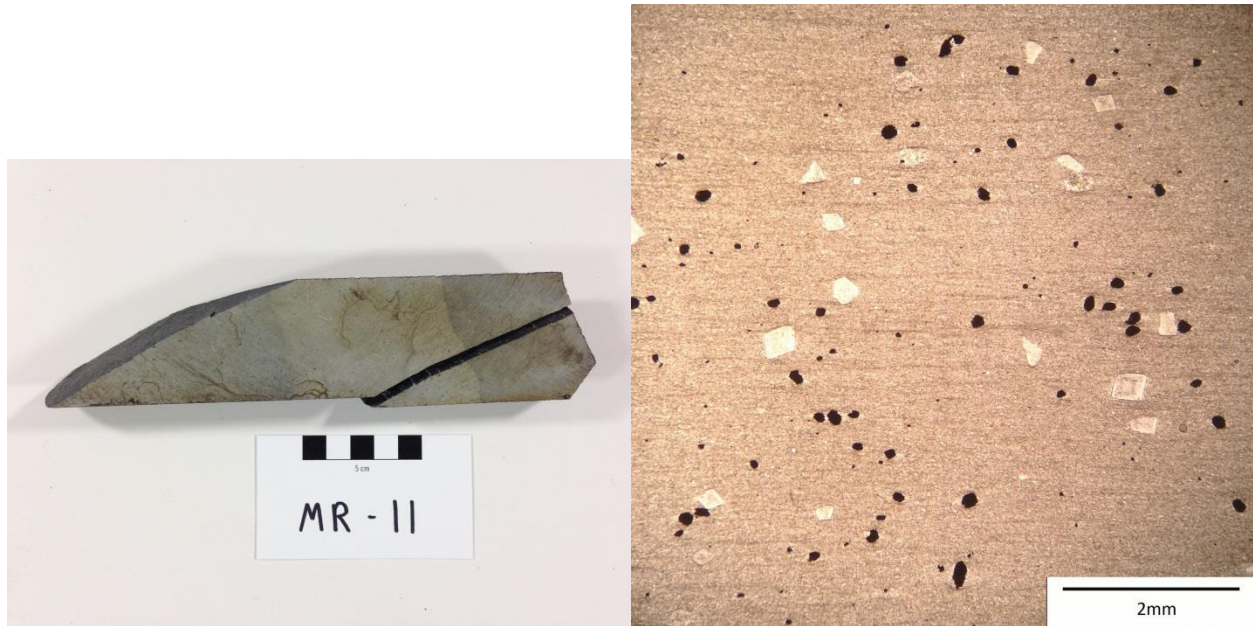
Figure A2-11: MR11 - Note grain size and colour change on right side of the hand sample.

Hand Sample: The sample is fine grained, dark to light grey argillite. Disseminated sulfides and carbonates are located throughout. Some oxidation is visible, especially along fractures. Minor bedding is visible in hand sample.

Transmitted Light: Minor chlorite alteration is visible throughout the sample. The carbonate minerals are subhedral, and do not exhibit any alteration rims or strain shadows. Sulfides throughout are anhedral, and do not exhibit strain shadows.

Appendix 3

Geochemical Results Including Detection Limits

Analyte Symbol	Unit Symbol	Detection Limit	Analysis Method	MR 01	MR 02	MR 03	MR 04	MR 05	MR 06	MR 07	MR 08	MR 09	MR 10	MR 11	MR 12
SiO2	%	0.01	FUS-ICP	56.67	57.02	58.7	58.12	58.37	59.42	59.92	58.29	58.02	57.77	58.05	56.19
Al2O3	%	0.01	FUS-ICP	18.96	18.81	18.54	18.73	18.11	17.78	17.94	17.2	18.66	18.86	19.05	20.25
Fe2O3(T)	%	0.01	FUS-ICP	8.49	8.74	7.06	8.46	7.98	8.06	7.81	8	7.8	8.44	8.2	8.62
MnO	%	0.001	FUS-ICP	0.119	0.101	0.11	0.096	0.096	0.122	0.095	0.15	0.088	0.119	0.092	0.084
MgO	%	0.01	FUS-ICP	2.45	2.61	2.22	2.63	2.34	2.56	2.45	2.56	2.35	2.58	2.6	2.67
CaO	%	0.01	FUS-ICP	1.83	1.36	1.85	0.95	1.21	1.5	1.18	2	1.02	1.5	0.95	0.7
Na2O	%	0.01	FUS-ICP	0.72	0.49	1.04	0.61	0.7	0.73	0.88	0.64	0.74	0.68	0.74	0.44
K2O	%	0.01	FUS-ICP	4.65	4.45	4.41	4.42	4.35	4.17	4.06	3.99	4.41	4.36	4.35	4.95
TiO2	%	0.001	FUS-ICP	0.889	0.857	0.927	0.916	0.95	0.876	0.86	0.84	0.909	0.901	0.935	0.931	0.957
P2O5	%	0.01	FUS-ICP	0.11	0.13	0.12	0.11	0.12	0.11	0.11	0.11	0.1	0.1	0.11	0.11
LOI	%		FUS-ICP	5.39	4.93	4.87	4.54	4.27	4.7	4.91	5.08	4.44	4.94	4.46	4.43
Total	%	0.01	FUS-ICP	100.3	99.5	99.85	99.58	98.52	100	100.2	98.87	98.52	100.3	99.53	99.41
Au	ppb	1	INAA	< 1	81	6	43	61	681	75	< 1	595	7	2130	4420
Ag	ppm	0.5	MULT INAA / TD-ICP	< 0.5	< 0.5	< 0.5	< 0.5	< 0.5	< 0.5	< 0.5	< 0.5	< 0.5	< 0.5	< 0.5	< 0.5
As	ppm	1	INAA	909	269	1020	937	816	451	2600	541	535	532	75	273
Ba	ppm	1	FUS-ICP	668	633	632	630	618	592	592	571	636	625	626	701
Be	ppm	1	FUS-ICP	3	3	3	3	3	3	3	3	3	3	3	3
Bi	ppm	2	TD-ICP	< 2	2	2	2	2	2	2	< 2	< 2	< 2	< 2	< 2
Br	ppm	0.5	INAA	< 0.5	< 0.5	< 0.5	< 0.5	< 0.5	< 0.5	< 0.5	< 0.5	< 0.5	< 0.5	< 0.5	< 0.5
Cd	ppm	0.5	TD-ICP	< 0.5	< 0.5	< 0.5	< 0.5	< 0.5	< 0.5	< 0.5	0.9	< 0.5	< 0.5	< 0.5	< 0.5
Co	ppm	0.1	INAA	24.1	18.8	21.4	24.9	21.2	20.9	25.8	18.8	20	18.4	21	21.8
Cr	ppm	0.5	INAA	103	105	98.5	91.9	84.1	101	63.1	76.1	85.1	78.3	83.4	86.2
Cs	ppm	0.2	INAA	3.7	5.4	6	5.9	5.3	4.7	3.8	4.6	6.2	4.8	4.2	4.2
Cu	ppm	1	TD-ICP	52	62	61	75	36	39	21	25	34	52	25	70

78

Analyte Symbol	Unit Symbol	Detection Limit	Analysis Method	MR 01	MR 02	MR 03	MR 04	MR 05	MR 06	MR 07	MR 08	MR 09	MR 10	MR 11	MR 12
Hf	ppm	0.2	INAA	4.2	5	5.6	4.1	4.7	3.5	2.2	4.2	5	4.6	4	3.5
Hg	ppm	1	INAA	< 1	< 1	< 1	< 1	< 1	< 1	< 1	< 1	< 1	< 1	< 1	< 1
Ir	ppb	1	INAA	< 1	< 1	< 1	< 1	< 1	< 1	< 1	< 1	< 1	< 1	< 1	< 1
Mo	ppm	2	TD-ICP	< 2	< 2	< 2	< 2	< 2	< 2	< 2	< 2	< 2	< 2	< 2	< 2
Ni	ppm	1	TD-ICP	43	41	41	46	46	48	55	41	45	49	49	45
Pb	ppm	5	TD-ICP	17	9	22	17	5	22	57	29	7	< 5	6	10
Rb	ppm	10	INAA	160	130	110	150	130	120	150	130	140	140	120	160
Sb	ppm	0.1	INAA	0.8	0.8	1.5	1.1	1.5	0.5	3.7	0.6	1.1	0.6	0.2	0.2
Analyte Symbol	Unit Symbol	Detection Limit	Analysis Method	MR 01	MR 02	MR 03	MR 04	MR 05	MR 06	MR 07	MR 08	MR 09	MR 10	MR 11	MR 12
S	%	0.001	TD-ICP	0.731	0.722	0.416	0.637	0.447	0.507	0.344	0.265	0.223	0.282	0.091	0.621
Sc	ppm	0.01	INAA	21.4	21.9	20.8	21	21.4	19.9	19.4	19.1	21.1	20.3	21.3	22.5
Se	ppm	0.5	INAA	< 0.5	< 0.5	< 0.5	< 0.5	< 0.5	< 0.5	< 0.5	< 0.5	< 0.5	< 0.5	< 0.5	< 0.5
Sr	ppm	2	FUS-ICP	95	77	95	76	81	82	91	88	80	89	78	73
Ta	ppm	0.3	INAA	< 0.3	< 0.3	< 0.3	< 0.3	< 0.3	< 0.3	< 0.3	< 0.3	< 0.3	< 0.3	< 0.3	< 0.3
Th	ppm	0.1	INAA	9.8	10.9	10	10.2	10.6	9	8.2	10	11.1	10.3	9.8	9.4
U	ppm	0.1	INAA	1.4	1.7	2.3	1.8	2.9	1.9	1.4	1.3	2	2.1	2.4	2.4
V	ppm	5	FUS-ICP	129	127	125	121	127	122	120	113	124	122	127	138
W	ppm	1	INAA	11	7	12	6	< 1	6	< 1	6	5	4	5	6
Y	ppm	1	FUS-ICP	28	29	28	27	31	29	30	25	27	27	29	31
Zn	ppm	1	MULT INAA / TD-ICP	88	107	96	102	113	108	125	425	102	106	115	113
Zr	ppm	2	FUS-ICP	164	168	168	169	178	164	151	163	165	167	165	165
La	ppm	0.05	INAA	30.6	33.1	35.5	35.2	35.1	34.7	31.4	35.1	31.5	33.1	32.5	28
Ce	ppm	1	INAA	59	67	68	74	69	68	62	72	66	66	67	61
Nd	ppm	1	INAA	27	31	34	27	32	28	29	31	34	34	33	27
Sm	ppm	0.01	INAA	6.06	6.53	6.61	6.49	6.78	6.77	6.08	6.79	6	6.35	6.46	5.71
Eu	ppm	0.05	INAA	1.27	1.67	1.49	1.52	1.73	1.46	1.32	1.45	1.59	1.63	1.62	1.65
Tb	ppm	0.1	INAA	1	0.9	1.1	0.9	1.2	0.8	1	0.9	0.7	0.6	0.6	0.7
Yb	ppm	0.05	INAA	3.08	3.38	2.98	2.89	3.6	2.95	2.74	2.84	2.76	3.12	2.87	3.66
Lu	ppm	0.01	INAA	0.55	0.55	0.46	0.43	0.55	0.42	0.48	0.5	0.58	0.55	0.52	0.55
Mass	g		INAA	1.066	1.027	1.065	1.045	1.069	1.058	1.041	1.064	1.05	1.041	1.043	1.036

C-Total	%	0.01	IR	0.71	0.55	0.72	0.36	0.36	0.51	0.46	0.7	0.41	0.56	0.38	0.3
Total S	%	0.01	IR	0.93	0.76	0.4	0.64	0.42	0.53	0.34	0.28	0.24	0.29	0.09	0.64
CO_2	%	0.01	IR	1.84	1.31	1.79	0.97	1.01	1.46	1.32	2.25	1.15	1.75	1.07	0.64

Appendix 4

Electron Microprobe Point Analyses – Mass Percent

Mass percent   Page   1

No.	Au	S	As	Mn	Pb	Ag	Fe	Sb	Co	Ti	Ni	Cu	Zn	Total	Comment
1	0	36.325	0	0.009	0.068	0	63.421	0	0.059	0	0	0	0.006	99.888	Pyrr239 ctrl 1
2	0.029	35.952	0	0	0.068	0	63.377	0.013	0.035	0	0.029	0	0.022	99.525	Pyrr239 ctrl 2
3	0	34.583	0	0.015	0.012	0	30.712	0.02	0.016	0	0.028	34.661	0.156	100.203	Cpy ctrl 1
4	0	34.569	0	0.015	0.071	0	30.618	0.063	0.029	0	0.029	34.778	0.144	100.316	Cpy ctrl 2
5	0	21.732	45.009	0.075	0	0.035	35.898	0.113	0.145	0.037	0.173	0.127	0.249	103.593	Aspy 200 ctrl 1
6	0.029	21.538	44.709	0.063	0	0.026	35.961	0.083	0.177	0.031	0.165	0.142	0.255	103.179	Aspy 200 ctrl 2
7	0	32.724	0	0.013	0.004	0	30.131	0.002	0.12	0	35.752	0.074	0.038	98.858	Pentlandite ctrl 1
8	0	32.823	0	0.033	0	0.006	0.013	0.051	0.015	0.011	0.079	0.115	65.498	98.644	Sphalerite ctrl
9	0	36.011	0	0	0.02	0	63.467	0	0.061	0	0.016	0.011	0.027	99.613	Pyrr239 ctrl
10	0.014	34.328	0	0.02	0.046	0	30.799	0.041	0.036	0	0.064	34.822	0.124	100.294	Cpy ctrl
11	0.074	21.534	44.755	0.06	0	0.021	35.263	0.056	0.139	0.03	0.203	0.127	0.18	102.442	Aspy ctrl
12	0	51.768	0	0	0.039	0	45.57	0	0.046	0	0.258	0	0	97.681	MR01_PY_CORE_1
13	0	52.434	0	0.008	0.024	0	45.794	0	0	0	0.117	0	0	98.377	MR01_PY_CORE_2
14	0.03	52.087	0	0	0.063	0	44.917	0	0.037	0	0.403	0	0	97.537	MR01_PY_RIM_1
15	0.045	51.967	0	0.005	0.047	0	45.519	0	0.016	0	0.159	0	0	97.758	MR01_PY_RIM_2
16	0.105	19.762	46.594	0.073	0	0.006	33.645	0.056	0.623	0.047	0.239	0.122	0.198	101.47	MR01_ASPY_RIM_1
17	0.002	19.873	47.363	0.085	0	0.005	32.417	0.092	2.266	0.07	0.342	0.116	0.222	102.853	MR01_ASPY_RIM_2
18	0.037	19.498	47.082	0.053	0	0.061	31.575	0.061	2.632	0.045	0.254	0.142	0.228	101.668	MR01_ASPY_CORE_1
19	0.03	19.715	47.529	0.044	0	0.024	31.805	0.052	2.654	0.041	0.233	0.127	0.217	102.471	MR01_ASPY_CORE_2
20	0.008	51.243	0	0	0	0	45.067	0	0.025	0	0.197	0	0	96.54	MR01_PO_CORE_1
21	0	51.985	0	0	0.059	0	45.745	0	0.019	0	0.09	0	0	97.898	MR01_PO_CORE_2
22	0.05	52.005	0	0	0	0	46.122	0	0	0.004	0.048	0	0	98.229	MR01_PO_RIM_1
23	0	51.541	0	0.002	0	0	45.425	0	0	0	0.022	0	0	96.99	MR01_PO_RIM_2
24	0	33.88	0	0.022	0	0	29.891	0	0.023	0	0.051	33.77	0.094	97.731	MR01_CPY_CORE_1
25	0	34.034	0	0.025	0	0	30.04	0.014	0.031	0.019	0.057	33.59	0.118	97.928	MR01_CPY_CORE_2
26	0.008	33.852	0	0.017	0	0	29.796	0.001	0.026	0.003	0.025	33.341	0.087	97.156	MR01_CPY_RIM_1
27	0	34.106	0	0.023	0	0	29.598	0	0.026	0	0.032	33.278	0.049	97.112	MR01_CPY_RIM_2
28	0	35.945	0	0.004	0	0	63.615	0	0.046	0	0.037	0	0	99.647	Pyrr239 ctrl
29	0	34.803	0.03	0	0.083	0	30.43	0	0.009	0.012	0	34.509	0	99.876	Cpy ctrl

30	0	21.615	44.629	0.035	0	0.032	35.186	0	0.121	0.044	0.159	0.133	0.042	101.996	Aspy ctrl
31	0	20.112	45.652	0.05	0.036	0.023	33.438	0	0.83	0.034	0.718	0.11	0.037	101.04	MR03_ASPY_CORE_1
32	0.005	20.287	45.869	0.026	0	0	30.9	0.073	3.095	0.036	0.718	0.124	0.046	101.179	MR03_ASPY_CORE_2
33	0	19.67	46.073	0.007	0	0.066	33.579	0	0.713	0.084	0.519	0.096	0.058	100.865	MR03_ASPY_RIM_1
34	0.005	19.868	46.368	0.028	0.005	0.049	34.011	0	0.376	0.065	0.353	0.101	0.041	101.27	MR03_ASPY_RIM_2
35	0	37.538	0	0	0.088	0	59.417	0	0.027	0	0.077	0	0	97.147	MR03_PY_CORE_1
36	0	38.01	0.024	0	0.096	0	58.961	0	0.015	0	0.042	0	0	97.148	MR03_PY_CORE_2
37	0	37.964	0.028	0	0.084	0	58.46	0	0.018	0	0.229	0	0	96.783	MR03_PY_RIM_1
38	0	38.449	0.024	0	0.152	0	58.809	0	0.022	0.011	0.222	0	0	97.689	MR03_PY_RIM_2
39	0	19.996	45.5	0.053	0	0.038	30.31	0	3.776	0.028	0.758	0.09	0.008	100.557	MR03_ASPY_CORE_3
40	0	19.883	45.585	0.049	0	0.011	29.042	0.026	4.884	0.042	0.899	0.127	0.064	100.612	MR03_ASPY_CORE_4
41	0.018	20.371	45.406	0.031	0.085	0.027	33.915	0.034	0.203	0.059	0.464	0.108	0.052	100.773	MR03_ASPY_RIM_3
42	0	19.826	46.539	0.039	0	0.04	33.797	0	0.478	0.051	0.451	0.124	0.022	101.367	MR03_ASPY_RIM_4
43	0	21.511	44.035	0.019	0	0.011	35.39	0.002	0.076	0.057	0.063	0.103	0.035	101.302	MR04_ASPY_CORE_1
44	0	21.413	44.031	0.027	0	0.044	35.299	0	0.091	0.051	0.068	0.109	0.01	101.143	MR04_ASPY_CORE_2
45	0	20.452	45.347	0.033	0	0.046	34.8	0.033	0.077	0.022	0.089	0.1	0.011	101.01	MR04_ASPY_RIM_1
46	0	20.068	45.997	0.026	0	0.032	34.655	0.061	0.1	0.048	0.088	0.1	0.045	101.22	MR04_ASPY_RIM_2
47	0	20.789	44.884	0.039	0	0.074	34.766	0.002	0.09	0.053	0.067	0.084	0.03	100.878	MR04_ASPY_CORE_3
48	0.001	20.629	45.165	0.019	0	0.012	35.008	0.036	0.073	0.046	0.049	0.114	0.043	101.195	MR04_ASPY_CORE_4
49	0	20.619	45.288	0.002	0.103	0.001	34.902	0.045	0.03	0.037	0.025	0	0	101.052	MR04_ASPY_RIM_3
50	0	20.298	45.427	0	0	0	34.413	0.029	0.066	0.007	0.03	0	0	100.27	MR04_ASPY_RIM_4
51	0.306	13.18	0.179	0.232	92.137	0.171	1.617	0.284	0.378	0.268	0.581	0.745	1.132	111.21	MR04_ASPY_FRACINFIL_1
52	0.211	15.991	18.288	0.18	64.223	0.146	14.439	0.278	0.282	0.176	0.416	0.517	0.76	115.907	MR04_ASPY_FRACINFIL_2
53	0.051	20.207	40.874	0.024	8.677	0.014	31.41	0.024	0.084	0.024	0.077	0.027	0.133	101.626	MR04_ASPY_FRACINFIL_3
54	0	38.585	0	0	0.12	0	59.636	0	0	0	0.081	0	0	98.422	MR05_PY_CORE_1
55	0.028	38.568	0	0	0.184	0	59.503	0	0	0	0.13	0	0	98.413	MR05_PY_CORE_2
56	0	38.496	0	0	0.088	0	59.707	0	0	0	0.22	0	0	98.511	MR05_PY_RIM_1
57	0	38.329	0	0	0.148	0	59.403	0	0.001	0	0.175	0	0	98.056	MR05_PY_RIM_2
58	0.046	20.397	45.661	0	0.103	0	30.999	0.033	2.776	0.015	1.265	0	0	101.295	MR05_ASPY_CORE_1
59	0	20.389	45.969	0	0.09	0	31.435	0.031	2.669	0	1.282	0	0	101.865	MR05_ASPY_CORE_2
60	0	20.504	45.474	0	0	0.032	30.825	0.007	3.656	0.027	0.386	0	0	100.911	MR05_ASPY_RIM_1
61	0	20.319	45.813	0	0	0.018	31.129	0	3.563	0.026	0.451	0	0	101.319	MR05_ASPY_RIM_2
62	0	34.293	0	0	0.095	0	30.554	0	0	0	0	33.726	0	98.668	MR05_CPY_CORE_1
63	0	33.923	0	0	0.079	0	30.047	0	0	0	0	33.801	0	97.85	MR05_CPY_RIM_1
64	0	38.29	0	0	0.072	0	59.492	0	0	0	0	0	0	97.854	MR05_PO_CORE_1

65	0	37.82	0	0	0.116	0	59.769	0	0	0	0	0	0	97.705	MR05_PO_CORE_2
66	0	39.185	0	0	0.168	0	59.378	0	0.004	0	0.116	0	0	98.851	MR05_PO_RIM_1
67	0	38.936	0	0	0.192	0	58.842	0	0	0	0.204	0	0	98.174	MR05_PO_RIM_2
68	0	20.168	46.318	0	0.018	0.01	27.776	0.117	3.397	0.009	3.638	0	0	101.451	MR05_ASPY_CORE_3
69	0.034	19.729	46.185	0.037	0.198	0.017	31.724	0.099	2.261	0	0.744	0.053	0	101.081	MR05_ASPY_CORE_4
70	0.061	19.999	45.857	0.022	0.108	0.018	30.694	0.046	3.831	0	0.263	0	0	100.899	MR05_ASPY_RIM_3
71	0.01	20.335	45.846	0.008	0	0.015	31.84	0.071	2.907	0	0.266	0	0	101.298	MR05_ASPY_RIM_4
72	0	38.055	0	0	0.204	0	59.977	0	0.002	0	0.101	0	0	98.339	MR05_PO_CORE_3
73	0.067	38.653	0	0	0.124	0	58.871	0	0	0	0.019	0	0	97.734	MR05_PO_CORE_4
74	0.029	38.317	0	0	0.108	0	59.292	0	0	0	0.086	0	0	97.832	MR05_PO_RIM_3
75	0.061	38.264	0	0	0.216	0	58.885	0	0	0	0.201	0	0	97.627	MR05_PO_RIM_4
76	0	0	0	0	0	0	0	0	0	0	0	0	0	0	MR05_PO_RIM_5
77	0.058	35.836	0	0	0.297	0	63.241	0	0.003	0	0	0	0	99.435	Pyrr239 ctrl
78	0.015	34.979	0	0	0.182	0	30.722	0	0	0	0	34.441	0	100.339	Cpy ctrl
79	0.105	21.436	44.334	0.019	0	0	35.786	0	0.135	0	0.151	0	0	101.966	Aspy ctrl
80	0.099	38.666	0	0	0.28	0	59.345	0	0.002	0	0	0	0	98.392	MR06_PO_CORE_1
81	0.003	38.636	0	0	0.28	0	59.382	0	0.002	0	0	0	0	98.303	MR06_PO_CORE_2
82	0.058	38.15	0	0	0.196	0	58.657	0	0	0	0	0	0	97.061	MR06_PO_RIM_1
83	0.006	38.732	0	0	0.204	0	59.433	0	0.008	0	0	0	0	98.383	MR06_PO_RIM_2
84	0.015	34.468	0	0	0.232	0	30.182	0	0	0	0	33.995	0	98.892	MR06_CPY_CORE_1
85	0.045	34.27	0	0	0.178	0	30.157	0	0	0	0	33.914	0	98.564	MR06_CPY_CORE_2
86	0	34.114	0	0.006	0.137	0	29.754	0	0	0	0	33.739	0	97.75	MR06_CPY_RIM_1
87	0.064	34.334	0	0.024	0.211	0	29.45	0	0	0	0	33.462	0	97.545	MR06_CPY_RIM_2
88	0.026	38.51	0	0	0.204	0	59.268	0	0	0	0	0	0	98.008	MR06_PY_CORE_1
89	0	38.883	0.019	0.006	0.116	0	59.555	0	0.091	0	0.121	0	0	98.791	MR06_PY_CORE_2
90	0.063	38.54	0.018	0.026	0.096	0.023	59.275	0.005	0.082	0	0.11	0	0	98.238	MR06_PY_RIM_1
91	0	38.418	0	0.02	0.264	0.032	59.104	0.013	0.074	0	0.146	0	0	98.071	MR06_PY_RIM_2
92	0.014	38.312	0	0.003	0.112	0	59.148	0	0.109	0	0.049	0	0	97.747	MR06_PY_CORE_3
93	0	38.501	0	0.015	0.228	0.036	59.003	0	0.064	0.105	0.057	0	0	98.009	MR06_PY_CORE_4
94	0	38.596	0	0.013	0.128	0.033	59.123	0	0.076	0	0.124	0	0	98.093	MR06_PY_RIM_3
95	0.026	38.449	0.01	0.033	0.192	0	58.456	0	0.058	0	0.112	0	0	97.336	MR06_PY_RIM_4
96	0.033	21.376	44.584	0.067	0.215	0.093	35.421	0.081	0.129	0.039	0.173	0.144	0.195	102.55	MR04_ASPY_CORE_5
97	0.074	21.265	44.458	0.07	0.013	0.057	35.303	0.075	0.123	0.046	0.127	0.121	0.16	101.892	MR04_ASPY_CORE_6
98	0.03	20.304	46.021	0.092	0	0.056	34.725	0.136	0.182	0.045	0.278	0.161	0.158	102.188	MR04_ASPY_RIM_5
99	0.091	20.276	46.009	0.079	0	0.064	34.683	0.091	0.195	0.046	0.18	0.123	0.169	102.006	MR04_ASPY_RIM_6

100	89.15	0.124	0.395	0.332	0.374	11.294	1.235	0.454	0.479	0.348	0.724	1.026	1.377	107.312	MR04_AU1
101	84.982	0.167	0.395	0.327	0.56	10.54	1.192	0.461	0.494	0.322	0.7	0.925	1.266	102.331	MR04_AU2
102	0.088	19.528	46.384	0.063	0	0.046	33.63	0.026	0.838	0.044	0.563	0.129	0.135	101.474	MR03_ASPY_CORE_3
103	0	19.754	46.532	0.072	0.09	0.05	34.061	0.03	0.746	0.053	0.445	0.115	0.194	102.142	MR03_ASPY_CORE_4
104	0.033	19.755	46.345	0.074	0.054	0.059	33.871	0.034	0.441	0.044	0.335	0.157	0.165	101.367	MR03_ASPY_RIM_3
105	0.061	20.083	45.701	0.091	0	0.036	34.569	0.07	0.466	0.062	0.395	0.149	0.139	101.822	MR03_ASPY_RIM_4
106	0	37.938	0	0.023	0.2	0	59.211	0	0.034	0	0.116	0	0	97.522	MR03_PO_CORE_1
107	0.017	37.972	0	0.018	0.096	0.005	58.985	0	0.027	0.006	0.129	0.019	0	97.274	MR03_PO_CORE_2
108	0.023	38.031	0.003	0.016	0.168	0.036	58.958	0	0.046	0	0.327	0	0	97.608	MR03_PO_RIM_1
109	0.001	38.481	0	0	0.028	0.008	59.119	0	0.068	0	0.198	0	0	97.903	MR03_PO_RIM_2
110	0.006	36.027	0.001	0	0	0.039	63.504	0.013	0.072	0	0	0.051	0	99.713	Pyrr239 ctrl
111	0.092	34.642	0	0.004	0.075	0.003	30.442	0	0.026	0	0.006	34.639	0.122	100.051	Cpy ctrl
112	0.028	21.416	44.913	0.032	0	0.069	35.447	0.114	0.208	0.03	0.257	0.167	0.197	102.878	Aspy ctrl
Min	0	0	0	0	0	0	0	0	0	0	0	0	0	0	
Max	89.15	52.434	47.529	0.332	92.137	11.294	63.615	0.461	4.884	0.348	35.752	34.822	65.498	115.907	
Average	1.578	30.195	17.656	0.028	1.555	0.212	41.128	0.033	0.496	0.026	0.551	4.927	0.667	99.052	
Sigma	11.583	11.123	22.186	0.054	10.578	1.451	15.662	0.075	1.06	0.055	3.381	11.937	6.185	9.824	

Atomic Ratio

Atomic ratio Page 1

No.	Au	S	As	Mn	Pb	Ag	Fe	Sb	Co	Ti	Ni	Cu	Zn	Total	Comment
1	0	49.9095	0	0.0072	0.0145	0	50.0211	0	0.0438	0	0	0	0.0038	100	Pyrr239 ctrl 1
2	0.0065	49.6594	0	0.0003	0.0146	0	50.2517	0.0049	0.0263	0	0.0215	0	0.0146	99.9999	Pyrr239 ctrl 2
3	0	49.5348	0	0.0129	0.0028	0	25.2518	0.0074	0.0128	0	0.0222	25.0459	0.1094	100	Cpy ctrl 1
4	0	49.5064	0	0.0122	0.0157	0	25.17	0.0237	0.0225	0	0.0228	25.1257	0.1011	100	Cpy ctrl 2
5	0	35.0138	31.0312	0.0705	0	0.0169	33.2007	0.0479	0.1271	0.0398	0.1519	0.103	0.1971	99.9999	Aspy 200 ctrl 1
6	0.0075	34.8585	30.9638	0.0595	0	0.0124	33.4089	0.0352	0.1554	0.0341	0.1461	0.116	0.2025	100	Aspy 200 ctrl 2
7	0	46.9678	0	0.0109	0.0009	0	24.8246	0.0008	0.0939	0	28.0206	0.0535	0.027	100	Pentlandite ctrl 1
8	0	50.4167	0	0.0295	0	0.0028	0.0112	0.0208	0.0122	0.011	0.0661	0.0887	49.341	100	Sphalerite ctrl
9	0	49.6654	0	0	0.0043	0	50.2463	0	0.0457	0	0.0124	0.008	0.0179	100	Pyrr239 ctrl
10	0.0033	49.2353	0	0.0165	0.0101	0	25.3575	0.0154	0.0281	0	0.0504	25.196	0.0873	100	Cpy ctrl
11	0.0195	35.0969	31.2147	0.0571	0	0.0101	32.9927	0.0241	0.1233	0.033	0.1804	0.1043	0.1439	100	Aspy ctrl

#														Total	Sample
12	0	66.2852	0	0	0.0078	0	33.4946	0	0.0323	0	0.1801	0	0	100	MR01_PY_CORE_1
13	0	66.5462	0	0.0056	0.0046	0	33.3626	0	0	0	0.081	0	0	100	MR01_PY_CORE_2
14	0.0063	66.6706	0	0	0.0124	0	33.0031	0	0.0259	0	0.2816	0	0	100	MR01_PY_RIM_1
15	0.0093	66.4459	0	0.004	0.0094	0	33.4096	0	0.0108	0	0.111	0	0	100	MR01_PY_RIM_2
16	0.0286	33.0742	33.3704	0.0712	0	0.003	32.3236	0.0247	0.5672	0.053	0.2185	0.1029	0.1627	100	MR01_ASPY_RIM_1
17	0.0006	32.87	33.5236	0.0819	0	0.0022	30.7793	0.0402	2.0389	0.0772	0.309	0.0967	0.1803	100	MR01_ASPY_RIM_2
18	0.01	32.7012	33.7895	0.0518	0	0.0302	30.3981	0.0269	2.4017	0.0502	0.2326	0.1202	0.1876	100	MR01_ASPY_CORE_1
19	0.0081	32.7866	33.824	0.0426	0	0.0119	30.3622	0.0228	2.4009	0.0455	0.2117	0.1066	0.1771	100	MR01_ASPY_CORE_2
20	0.0016	66.3458	0	0	0	0	33.4953	0	0.0178	0	0.1396	0	0	100.0001	MR01_PO_CORE_1
21	0	66.3813	0	0	0.0117	0	33.5312	0	0.0134	0	0.0624	0	0	100	MR01_PO_CORE_2
22	0.0104	66.2336	0	0	0	0	33.7195	0	0	0.0033	0.0332	0	0	100	MR01_PO_RIM_1
23	0	66.3934	0	0.0013	0	0	33.5899	0	0	0	0.0154	0	0	100	MR01_PO_RIM_2
24	0	49.6964	0	0.0189	0	0	25.1683	0	0.018	0	0.0412	24.9897	0.0675	100	MR01_CPY_CORE_1
25	0	49.7858	0	0.0215	0	0	25.2251	0.0055	0.0243	0.0191	0.0452	24.7888	0.0846	100	MR01_CPY_CORE_2
26	0.002	49.8853	0	0.0146	0	0	25.2052	0.0003	0.021	0.003	0.0197	24.7862	0.0628	100	MR01_CPY_RIM_1
27	0	50.1897	0	0.02	0	0	25.0026	0	0.0207	0	0.026	24.7057	0.0353	100	MR01_CPY_RIM_2
28	0	49.572	0	0.0036	0	0	50.3616	0	0.0346	0	0.0282	0	0	100	Pyrr239 ctrl
29	0	49.9189	0.0186	0	0.0184	0	25.0547	0	0.0074	0.0115	0	24.9705	0	100	Cpy ctrl
30	0	35.3122	31.2007	0.0332	0	0.0153	32.9982	0	0.1078	0.0479	0.1418	0.1092	0.0336	100	Aspy ctrl
31	0	33.6188	32.6548	0.0493	0.0093	0.0114	32.0853	0	0.7549	0.0383	0.655	0.093	0.0301	100.0002	MR03_ASPY_CORE_1
32	0.0013	33.8834	32.7825	0.0251	0	0.0002	29.6252	0.0321	2.8126	0.0407	0.6553	0.1042	0.0374	100	MR03_ASPY_CORE_2
33	0	33.0647	33.142	0.0064	0	0.0328	32.4022	0	0.6518	0.0941	0.4761	0.0817	0.0481	100	MR03_ASPY_RIM_1
34	0.0013	33.2366	33.1932	0.0272	0.0012	0.0243	32.6606	0	0.3419	0.0727	0.3223	0.0853	0.0335	100	MR03_ASPY_RIM_2
35	0	52.3424	0	0	0.019	0	47.5595	0	0.0207	0	0.0585	0	0	100	MR03_PY_CORE_1
36	0	52.8558	0.0143	0	0.0206	0	47.066	0	0.0114	0	0.0319	0	0	100	MR03_PY_CORE_2
37	0	52.9614	0.0169	0	0.0181	0	46.8157	0	0.0137	0	0.1742	0	0	100	MR03_PY_RIM_1
38	0	53.1203	0.0141	0	0.0325	0	46.6393	0	0.0162	0.01	0.1676	0	0	100	MR03_PY_RIM_2
39	0	33.6386	32.7544	0.0523	0	0.0189	29.27	0	3.4556	0.0311	0.6961	0.0764	0.0067	100	MR03_ASPY_CORE_3
40	0	33.4889	32.856	0.0477	0	0.0056	28.0797	0.0115	4.4756	0.0476	0.8266	0.108	0.0527	99.9999	MR03_ASPY_CORE_4
41	0.005	34.0632	32.49	0.0305	0.0221	0.0134	32.5536	0.0149	0.1845	0.0656	0.4237	0.0912	0.0423	100	MR03_ASPY_RIM_3
42	0	33.1599	33.3081	0.038	0	0.0199	32.448	0	0.4349	0.0566	0.4117	0.105	0.018	100.0001	MR03_ASPY_RIM_4
43	0	35.3405	30.9582	0.0178	0	0.0051	33.3758	0.0008	0.068	0.0626	0.0568	0.0858	0.0286	100	MR04_ASPY_CORE_1
44	0	35.2609	31.0268	0.0261	0	0.0216	33.3671	0	0.0818	0.0567	0.061	0.0903	0.0078	100	MR04_ASPY_CORE_2
45	0	34.0665	32.3224	0.0316	0	0.023	33.2736	0.0145	0.0693	0.0248	0.0811	0.0842	0.0091	100.0001	MR04_ASPY_RIM_1
46	0	33.5063	32.8642	0.0252	0	0.016	33.2148	0.0268	0.0912	0.0541	0.0802	0.0846	0.0366	100	MR04_ASPY_RIM_2

47	0	34.5467	31.9181	0.0375	0	0.0364	33.1643	0.0008	0.0815	0.0588	0.061	0.0705	0.0244	100	MR04_ASPY_CORE_3
48	0.0004	34.2375	32.0773	0.0184	0	0.006	33.3533	0.0157	0.0662	0.051	0.0441	0.0955	0.0348	100.0001	MR04_ASPY_CORE_4
49	0	34.2976	32.2365	0.0015	0.0266	0.0006	33.326	0.0199	0.0273	0.0414	0.0227	0	0	100	MR04_ASPY_RIM_3
50	0	34.0827	32.6401	0	0	0	33.1694	0.013	0.0599	0.0074	0.0276	0	0	100	MR04_ASPY_RIM_4
51	0.164	43.3756	0.2521	0.4452	46.9199	0.1673	3.0553	0.246	0.6768	0.5895	1.045	1.2363	1.827	100	MR04_ASPY_FRACINFIL_1
52	0.0791	36.8191	18.0191	0.2419	22.8814	0.1	19.0842	0.1684	0.3537	0.2711	0.5231	0.6005	0.8582	99.9999	MR04_ASPY_FRACINFIL_2
53	0.0145	35.274	30.5323	0.0243	2.3436	0.0075	31.4738	0.0108	0.0796	0.0278	0.0734	0.0241	0.1143	100	MR04_ASPY_FRACINFIL_3
54	0	52.9422	0	0	0.0254	0	46.9719	0	0	0	0.0604	0	0	100	MR05_PY_CORE_1
55	0.0062	52.9568	0	0	0.0391	0	46.9007	0	0	0	0.0972	0	0	100	MR05_PY_CORE_2
56	0	52.8042	0	0	0.0187	0	47.0127	0	0	0	0.1644	0	0	100	MR05_PY_RIM_1
57	0	52.8328	0	0	0.0316	0	47.0031	0	0.0007	0	0.1318	0	0	100	MR05_PY_RIM_2
58	0.0125	34.0101	32.5797	0	0.0267	0	29.6704	0.0146	2.5181	0.0163	1.1515	0	0	100	MR05_ASPY_CORE_1
59	0	33.8242	32.6336	0	0.0231	0	29.9356	0.0137	2.4086	0	1.1613	0	0	100	MR05_ASPY_CORE_2
60	0	34.2372	32.4934	0	0	0.0161	29.5465	0.0032	3.3215	0.0301	0.3522	0	0	100.0002	MR05_ASPY_RIM_1
61	0	33.8647	32.6743	0	0	0.0091	29.7822	0	3.231	0.0284	0.4102	0	0	100	MR05_ASPY_RIM_2
62	0	49.8001	0	0	0.0214	0	25.4704	0	0	0	0	24.7081	0	100	MR05_CPY_CORE_1
63	0	49.7147	0	0	0.0179	0	25.2772	0	0	0	0	24.9902	0	100	MR05_CPY_RIM_1
64	0	52.8484	0	0	0.0154	0	47.1359	0	0	0	0.0004	0	0	100	MR05_PO_CORE_1
65	0	52.4202	0	0	0.0249	0	47.5549	0	0	0	0	0	0	100	MR05_PO_CORE_2
66	0	53.4133	0	0	0.0354	0	46.4618	0	0.0029	0	0.0866	0	0	100	MR05_PO_RIM_1
67	0	53.443	0	0	0.0407	0	46.3633	0	0	0	0.153	0	0	100	MR05_PO_RIM_2
68	0	33.7195	33.1393	0	0.0047	0.0048	26.6588	0.0514	3.0903	0.0098	3.3213	0	0	100	MR05_ASPY_CORE_3
69	0.0093	33.1831	33.2416	0.0362	0.0515	0.0083	30.6297	0.0438	2.0686	0	0.6832	0.0448	0	100.0001	MR05_ASPY_CORE_4
70	0.0167	33.5965	32.9661	0.0214	0.0281	0.0091	29.5992	0.0202	3.5016	0	0.241	0	0	100	MR05_ASPY_RIM_3
71	0.0027	33.8994	32.7046	0.0075	0	0.0075	30.469	0.0311	2.636	0	0.2422	0	0	100	MR05_ASPY_RIM_4
72	0	52.4377	0	0	0.0435	0	47.4415	0	0.0013	0	0.076	0	0	100	MR05_PO_CORE_3
73	0.015	53.3234	0	0	0.0264	0	46.6209	0	0	0	0.0143	0	0	100	MR05_PO_CORE_4
74	0.0065	52.9083	0	0	0.023	0	46.9972	0	0	0	0.065	0	0	100	MR05_PO_RIM_3
75	0.0137	52.9831	0	0	0.0462	0	46.8047	0	0	0	0.1523	0	0	100	MR05_PO_RIM_4
76	0	0	0	0	0	0	0	0	0	0	0	0	0	0	MR05_PO_RIM_5
77	0.0131	49.6367	0	0	0.0636	0	50.284	0	0.0026	0	0	0	0	100	Pyrr239 ctrl
78	0.0035	49.9555	0	0	0.0403	0	25.1863	0	0	0	0	24.8144	0	100	Cpy ctrl
79	0.0279	35.064	31.0326	0.0178	0	0	33.6024	0	0.1201	0	0.1352	0	0	100	Aspy ctrl
80	0.0221	53.1179	0	0	0.0595	0	46.799	0	0.0015	0	0	0	0	100	MR06_PO_CORE_1
81	0.0006	53.0944	0	0	0.0595	0	46.844	0	0.0016	0	0	0	0	100.0001	MR06_PO_CORE_2

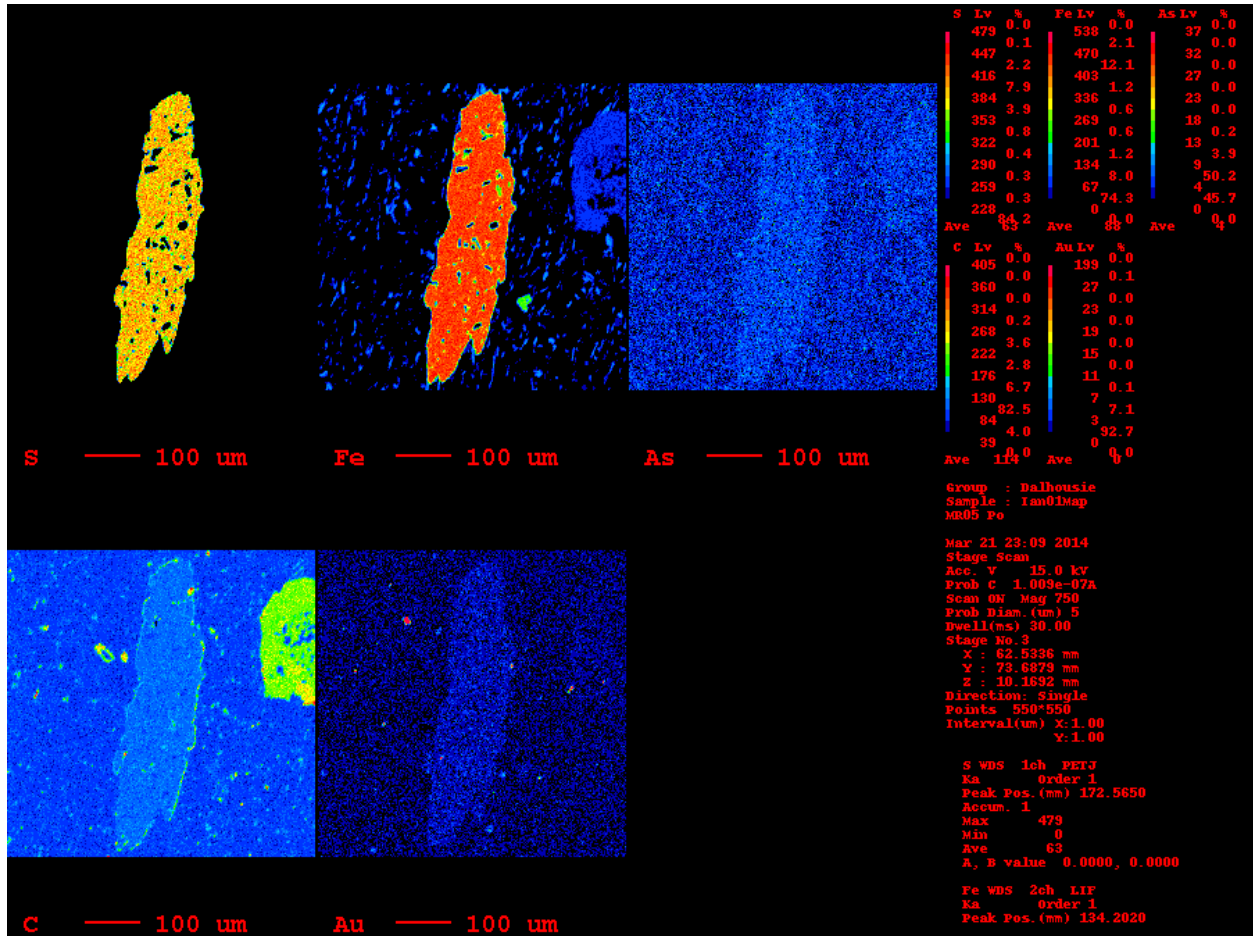| #														Total	Label
82	0.0131	53.0887	0	0	0.0422	0	46.856	0	0	0	0	0	0	100	MR06_PO_RIM_1
83	0.0012	53.1408	0	0	0.0432	0	46.8086	0	0.0059	0	0.0003	0	0	100	MR06_PO_RIM_2
84	0.0035	49.9664	0	0	0.0519	0	25.1166	0	0	0	0	24.8616	0	100	MR06_CPY_CORE_1
85	0.0108	49.8652	0	0	0.0401	0	25.1892	0	0	0	0	24.8947	0	100	MR06_CPY_CORE_2
86	0	49.9921	0	0.0051	0.031	0	25.0294	0	0	0	0	24.9424	0	100	MR06_CPY_RIM_1
87	0.0152	50.3596	0	0.0209	0.0479	0	24.7959	0	0	0	0	24.7604	0	100	MR06_CPY_RIM_2
88	0.0058	53.0677	0	0	0.0434	0	46.8831	0	0	0	0	0	0	100	MR06_PY_CORE_1
89	0	53.1082	0.0111	0.0046	0.0245	0	46.6936	0	0.0674	0	0.0905	0	0	100	MR06_PY_CORE_2
90	0.0142	52.9924	0.0106	0.021	0.0204	0.0094	46.7862	0.0017	0.0612	0	0.0829	0	0	100	MR06_PY_RIM_1
91	0	52.9674	0	0.0164	0.0563	0.013	46.7766	0.0047	0.0556	0	0.1099	0	0	100	MR06_PY_RIM_2
92	0.0031	52.9368	0	0.0023	0.0239	0	46.9145	0	0.0822	0	0.0372	0	0	100	MR06_PY_CORE_3
93	0	53.0601	0	0.0118	0.0486	0.0147	46.6782	0	0.0477	0.0964	0.0426	0	0	100	MR06_PY_CORE_4
94	0	53.1031	0	0.0105	0.0272	0.0133	46.6958	0	0.0572	0	0.093	0	0	100	MR06_PY_RIM_3
95	0.0058	53.2865	0.0061	0.0267	0.0411	0	46.5055	0	0.0438	0	0.0845	0	0	100	MR06_PY_RIM_4
96	0.0088	34.8858	31.1368	0.0638	0.0542	0.0453	33.1842	0.0348	0.1146	0.0426	0.1544	0.1188	0.1559	100	MR04_ASPY_CORE_5
97	0.0197	34.8869	31.2122	0.0675	0.0034	0.0277	33.2474	0.0324	0.1098	0.0504	0.1139	0.1004	0.1284	100.0001	MR04_ASPY_CORE_6
98	0.0081	33.5708	32.5606	0.0891	0	0.0274	32.9577	0.0592	0.1638	0.0503	0.2508	0.1341	0.1281	100	MR04_ASPY_RIM_5
99	0.0246	33.5931	32.6195	0.0765	0	0.0313	32.9854	0.0396	0.176	0.0512	0.1625	0.1028	0.1375	100	MR04_ASPY_RIM_6
100	68.0526	0.5821	0.7923	0.9097	0.2713	15.7421	3.3253	0.5607	1.2222	1.0915	1.8555	2.4276	3.1672	100	MR04_AU1
101	68.0122	0.8212	0.8321	0.9388	0.4262	15.4035	3.3638	0.5966	1.3219	1.0588	1.8784	2.2943	3.0521	100	MR04_AU2
102	0.024	32.7225	33.2599	0.0617	0	0.0227	32.3489	0.0113	0.7644	0.0489	0.5156	0.1092	0.1109	100	MR03_ASPY_CORE_3
103	0	32.8493	33.1127	0.0696	0.0232	0.0249	32.5145	0.013	0.6747	0.0591	0.4044	0.0966	0.158	100	MR03_ASPY_CORE_4
104	0.0091	33.0756	33.2053	0.0723	0.014	0.0293	32.5547	0.0148	0.4016	0.0493	0.3059	0.1326	0.1355	100	MR03_ASPY_RIM_3
105	0.0164	33.3451	32.4699	0.0883	0	0.0176	32.9469	0.0305	0.421	0.0684	0.358	0.1249	0.1131	100	MR03_ASPY_RIM_4
106	0	52.6519	0	0.0185	0.0429	0	47.1725	0	0.0259	0	0.0883	0	0	100	MR03_PO_CORE_1
107	0.0038	52.7681	0	0.0142	0.0206	0.002	47.0541	0	0.0203	0.0052	0.0982	0.0134	0	99.9999	MR03_PO_CORE_2
108	0.0051	52.726	0.0015	0.0129	0.036	0.0147	46.9213	0	0.0347	0	0.2478	0	0	100	MR03_PO_RIM_1
109	0.0001	53.0265	0	0	0.006	0.0032	46.764	0	0.0511	0	0.149	0	0	100	MR03_PO_RIM_2
110	0.0014	49.6505	0.0003	0	0	0.016	50.2376	0.0047	0.054	0	0	0.0354	0	100	Pyrr239 ctrl
111	0.0215	49.7024	0	0.0036	0.0165	0.0011	25.0722	0	0.0204	0	0.0045	25.0721	0.0856	100	Cpy ctrl
112	0.0073	34.8164	31.2447	0.0308	0	0.0333	33.0798	0.0488	0.1838	0.0325	0.2286	0.1372	0.1567	99.9999	Aspy ctrl
Minimum	0	0	0	0	0	0	0	0	0	0	0	0	0	0	
Maximum	68.0526	66.6706	33.824	0.9388	46.9199	15.7421	50.3616	0.5966	4.4756	1.0915	28.0206	25.196	49.341	100.0002	
Average	1.2216	44.2843	12.6156	0.0403	0.6665	0.2872	34.7747	0.0224	0.4674	0.0439	0.4813	3.6487	0.5534	99.1071	
Sigma	9.0493	12.549	15.7853	0.1302	4.9147	2.0706	11.1769	0.0813	0.9722	0.1536	2.662	8.7278	4.6732	9.4491	

Appendix 5

Electron Microprobe Element Maps

MR04 – Arsenopyrite crystal
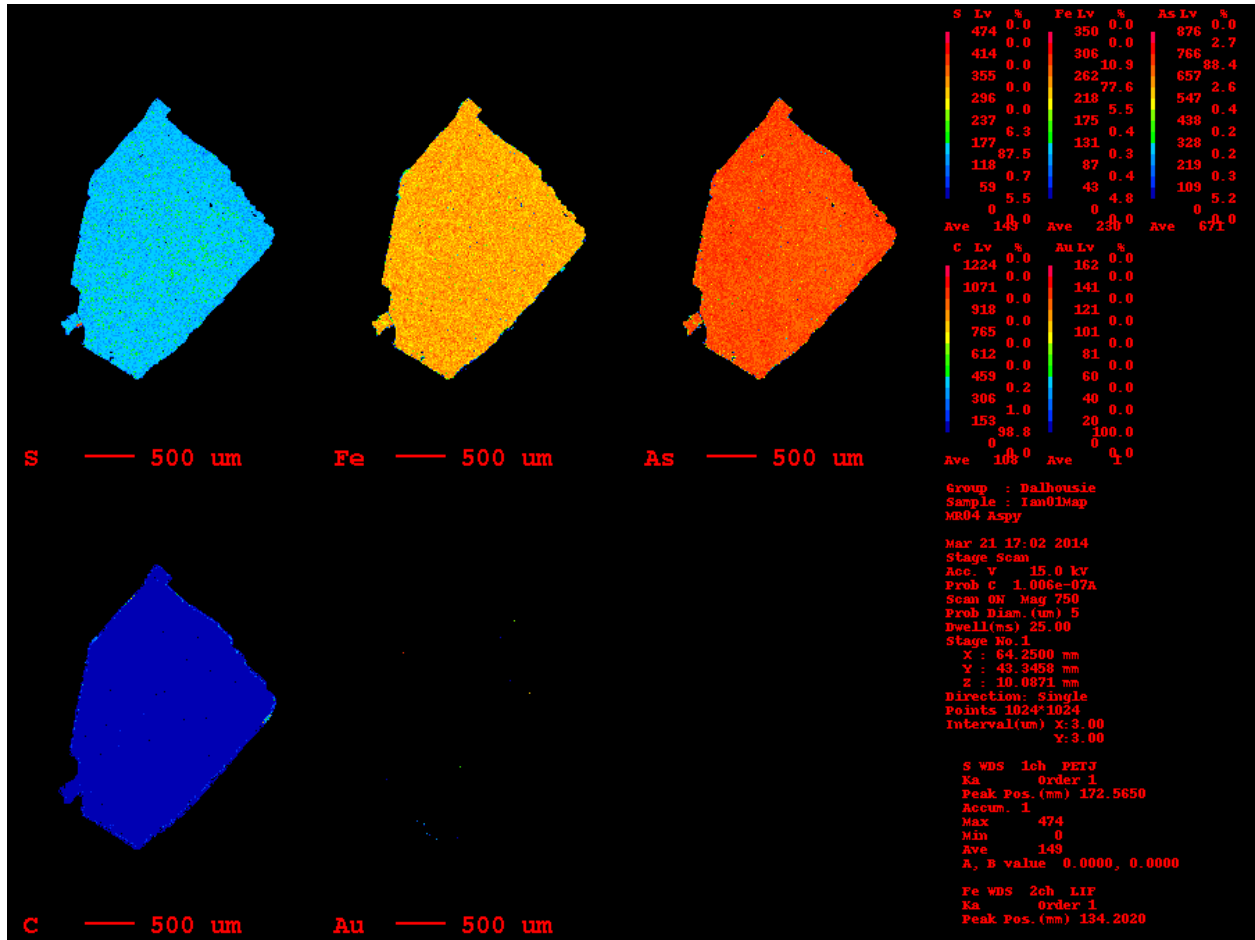
MR05 – Pyrrhotite crystal

MR06 – Pyrite crystal